CO_2 sequestration by mineralisation of coal fly ash in aqueous systems

Long Ji

Department of Environmental Sciences
Faculty of Science and Engineering
Macquarie University, North Ryde

Department of Mineral Processing Technology
School of Chemical and Environmental Engineering
China University of Mining and Technology (Beijing)

This thesis is presented in fulfilment of the
requirement for the degree of
Doctor of Philosophy
undertaken through a
Cotutelle agreement between
Macquarie University and
China University of Mining and Technology (Beijing)

Feb 2019

Table of contents

Statement of Candidate

I certify that the work in this thesis entitled "CO_2 sequestration by mineralisation of coal fly ash in aqueous systems" has not previously been submitted for a degree nor has it been submitted as part of requirements for a degree to any other university or institution other than Macquarie University and China University of Mining and Technology (Beijing).

I also certify that the thesis is an original piece of research and it has been written by me. Any help and assistance that I have received in my research work and the preparation of the thesis itself have been appropriately acknowledged.

In addition, I certify that all information sources and literature used are indicated in the thesis.

Long Ji

8 Feb 2019

Acknowledgements

The five-year Ph.D. study at China University of Mining & Technology (Beijing) and Macquarie University was really a long journey for me. There are so many lovely people who offered their kind help and support throughout the whole period of Ph.D. study, and help me finish the research training. Prof Ming Zeng, my supervisor in China, first encouraged me to go abroad as an exchange student and find a research topic which I really like. Then I would like to thank my supervisor Dr Hai Yu in CSIRO Energy for his guidance and support in the early stage of my study. He always shared his knowledge and provided the best guidance he could to make my research smooth. He also did all he could to create chances for me to attend conferences, seminars and workshops to build my research network and exchange ideas with excellent researchers. I would also like to express my sincere thanks to my supervisors Prof Damian Gore and Dr Shuaifei Zhao in Macquarie University, not only for reviewing my work and offering comments but for inspiring me to improve the impact of my research work and try some fancy things.

My sincere thanks also go to my colleagues at China University of Mining and Technology (Beijing), Macquarie University and CSIRO, and the visitors from Chinese Universities, Prof Jianglong Yu, Prof Rongrong Zhai, Dr Xiaolong Wang, Prof Shuiping Yan, Dr Qi Yang, Dr Mihaela Grigore, Dr David French, Dr Graeme Puxty, Dr Will Conway, Dr Kangkang Li, Dr Kaiqi Jiang, Dr Lichun Li, Dr Qingyao He, Yibin Wei, Bing Yu, Ruijie Zhang, Armin Kavehei, Chathurika Perera, Ruize Lu, Qinhui Ma, Xingchao Zhou and Ying Chen for all their technical support and suggestions, academic contributions and other help during my Ph.D. study.

I would also like to acknowledge the financial support of the China Scholarship Council Scholarship, ‘Creating Outstanding Innovative Talent Project’ from China University of Mining & Technology (Beijing) and Cotutelle-iMQRES scholarship from Macquarie University.

Lastly and most importantly, I give special and sincere thanks to my girl Yu Sui, my father Zhongmin Ji and my mother Chunxia Ning for their love and unconditional support.

Table of acronyms and definitions

Acronyms	Definitions
AMP	2-Amino-2-methyl-1-propanol
BET	Brunauer, Emmett and Teller
BJ	Beijing
Ca	Calcium
CaO	Calcium oxide
$CaCO_3$	Calcium carbonate
CCS	CO_2 capture and storage
CH_3COOH	Acetic acid
CH_3COONH_4	Ammonium acetate
CO_2	Carbon dioxide
CO	Carbon monoxide
DEA	Diethanolamine
EDS	Energy dispersive spectrometry
GHG	Greenhouse gas
H_2	Hydrogen
HTs	Hydrotalcite-like compounds
HW	Hazelwood
IAM	Integrated CO_2 absorption−mineralisation
IGCC	Integrated gasification combined cycle
LDHs	Layered double hydroxides
LY	Loy Yang
MEA	Monoethanolamine
MDEA	N-methyldiethanolamine
Mg	Magnesium
MgO	Magnesium oxide
$MgCO_3$	Magnesium carbonate
Na	Sodium
Na_2CO_3	Sodium carbonate
$NaHCO_3$	Sodium bicarbonate
NaCl	Sodium chloride
NH_4Cl	Ammonium chloride
NH_4NO_3	Ammonium nitrate
PCC	Post-combustion CO_2 capture
PZ	Piperazine
SEM	Scanning electron microscopy
SO_2	Sulfur dioxide
TGA	Thermogravimetric Analysis
TIC	Total inorganic carbon
WH	Wuhai
XRD	X-ray diffraction
XRF	X-ray fluorescence spectrometry
YA	Yallourn

Publications by author

1. L. Ji, H. Yu, Chapter 2 - Carbon dioxide sequestration by direct mineralization of fly ash, in: F. Pacheco-Torgal, C. Shi, A.P. Sanchez (Eds.) Carbon Dioxide Sequestration in Cementitious Construction Materials, Woodhead Publishing 2018, 13-37. **(as Chapter 2)**

2. L. Ji, H. Yu*, R. Zhang, D. French, M. Grigore, B. Yu, X. Wang, J. Yu, S. Zhao. Effects of fly ash properties on carbonation efficiency in CO_2 mineralisation, Fuel Processing Technology, 2019 (Accepted) **(as Chapter 3)**

3. L. Ji, H. Yu, X. Wang, M. Grigore, D. French, Y.M. Gözükara, J. Yu, M. Zeng, CO_2 sequestration by direct mineralisation using fly ash from Chinese Shenfu coal, Fuel Processing Technology, 2017, 156: 429-437. **(as Chapter 4)**

4. L. Ji, H. Yu, B. Yu, R. Zhang, D. French, M. Grigore, X. Wang, Z. Chen, S. Zhao, Insights into carbonation kinetics of fly ash from Victorian Lignite for CO_2 sequestration, Energy & Fuels, 2018, 32: 4569-4578. **(as Chapter 5)**

5. L. Ji, H. Yu, K. Li, B. Yu, M. Grigore, Q. Yang, X. Wang, Z. Chen, M. Zeng, S. Zhao, Integrated absorption-mineralisation for low-energy CO_2 capture and sequestration, Applied Energy, 2018, 225: 356-366. **(as Chapter 6)**

6. L. Ji, H. Yu, B. Yu, K. Jiang, M. Grigore, X. Wang, S. Zhao, K. Li, Integrated absorption–mineralisation for energy-efficient CO_2 sequestration: Reaction mechanism and feasibility of using fly ash as a feedstock, Chemical Engineering Journal, 2018, 352: 151-162. **(as Chapter 7)**

Role of the authors in the publications

Paper No.	Authors	Concept %	Lab work %	Modelling %	Data analysis %	Writing %	Signature and date
1	Long Ji	70	N/A	N/A	N/A	80	Long Ji 22.05.2019
	Hai Yu	30				20	
2	Long Ji	60	70	N/A	70	80	Long Ji 22.05.2019
	Hai Yu	10	0		10	10	
	Ruijie Zhang	0	10		0	0	Ruijie Zhang 22.05.2019
	David French	15	5		5	0	
	Mihaela Grigore	10	5		5	0	
	Bing Yu	0	5		5	0	
	Xiaolong Wang	5	5		0	0	Xiaolong Wang 22.05.2019
	Jianglong Yu	0	0		5	0	18.05.2019
	Shuaifei Zhao	0	0		0	10	Shuaifei Zhao 18.05.2019
3	Long Ji	20	80	N/A	50	55	Long Ji 22.05.2019
	Hai Yu	30	0		30	30	
	Xiaolong Wang	20	5		5	0	Xiaolong Wang 22.05.2019
	Mihaela Grigore	10	5		5	5	
	David French	20	5		5	0	
	Yesim M. Gözükara	0	5		5	0	
	Jianglong Yu	0	0		0	5	22.05.2019
	Ming Zeng	0	0		0	5	18.05.2019
4	Long Ji	70	85	70	70	80	Long Ji 22.05.2019
	Hai Yu	30	0	10	10	5	
	Bing Yu	0	5	10	0	0	
	Ruijie Zhang	0	5	0	0	0	Ruijie Zhang 22.05.2019

	David French	0	0	0	5	0	
	Mihaela Grigore	0	5	0	5	0	
	Xiaolong Wang	0	0	0	5	5	Xiaolong Wang 22.05.2019
	Zuliang Chen	0	0	10	0	5	
	Shuaifei Zhao	0	0	0	5	5	Shuaifei zhao 18.05.2019
5	Long Ji	70	85	40	70	70	Long Ji 22.05.2019
	Hai Yu	15	0	30	10	5	
	Kangkang Li	15	0	30	10	10	
	Bing Yu	0	5	0	0	0	
	Mihaela Grigore	0	5	0	5	0	
	Qi Yang	0	5	0	5	0	
	Xiaolong Wang	0	0	0	0	5	Xiaolong Wang 22.05.2019
	Zuliang Chen	0	0	0	0	3	
	Ming Zeng	0	0	0	0	2	18.05.2019
	Shuaifei Zhao	0	0	0	0	5	Shuaifei zhao 18.05.2019
6	Long Ji	70	90	30	70	70	Long Ji 22.05.2019
	Hai Yu	15	0	20	15	10	
	Bing Yu	0	5	0	5	0	
	Kaiqi Jiang	0	0	20	0	5	
	Mihaela Grigore	0	5	0	5	0	
	Xiaolong Wang	0	0	0	5	0	Xiaolong Wang 22.05.2019
	Shuaifei Zhao	0	0	0	0	5	Shuaifei zhao 18.05.2019
	Kangkang Li	15	0	30	0	10	

Paper No.	Authors	Concept %	Lab work %	Modelling %	Data analysis %	Writing %	Signature and date
1	Long Ji	70	N/A	N/A	N/A	80	
	Hai Yu	30				20	20/5/2019
2	Long Ji	60	70	N/A	70	80	
	Hai Yu	10	0		10	10	20/5/2019
	Ruijie Zhang	0	10		0	0	
	David French	15	5		5	0	
	Mihaela Grigore	10	5		5	0	
	Bing Yu	0	5		5	0	
	Xiaolong Wang	5	5		0	0	
	Jianglong Yu	0	0		5	0	
	Shuaifei Zhao	0	0		0	10	
3	Long Ji	20	80	N/A	50	55	
	Hai Yu	30	0		30	30	20/5/2019
	Xiaolong Wang	20	5		5	0	
	Mihaela Grigore	10	5		5	5	
	David French	20	5		5	0	
	Yesim M. Gözükara	0	5		5	0	
	Jianglong Yu	0	0		0	5	
	Ming Zeng	0	0		0	5	
4	Long Ji	70	85	70	70	80	
	Hai Yu	30	0	10	10	5	20/5/2019
	Bing Yu	0	5	10	0	0	
	Ruijie Zhang	0	5	0	0	0	

	David French	0	0	0	5	0	
	Mihaela Grigore	0	5	0	5	0	
	Xiaolong Wang	0	0	0	5	5	
	Zuliang Chen	0	0	10	0	5	
	Shuaifei Zhao	0	0	0	5	5	
5	Long Ji	70	85	40	70	70	
	Hai Yu	15	0	30	10	5	Hai Yu 2015/2019
	Kangkang Li	15	0	30	10	10	Kangkang Li, 16/05/2019
	Bing Yu	0	5	0	0	0	
	Mihaela Grigore	0	5	0	5	0	
	Qi Yang	0	5	0	5	0	
	Xiaolong Wang	0	0	0	0	5	
	Zuliang Chen	0	0	0	0	3	
	Ming Zeng	0	0	0	0	2	
	Shuaifei Zhao	0	0	0	0	5	
6	Long Ji	70	90	30	70	70	
	Hai Yu	15	0	20	15	10	Hai Yu 2015/2019
	Bing Yu	0	5	0	5	0	
	Kaiqi Jiang	0	0	20	0	5	Kaiqi Jiang 17/05/2019
	Mihaela Grigore	0	5	0	5	0	
	Xiaolong Wang	0	0	0	5	0	
	Shuaifei Zhao	0	0	0	0	5	
	Kangkang Li	15	0	30	0	10	Kangkang Li . 16/05/2019

Paper No.	Authors	Concept %	Lab work %	Modelling %	Data analysis %	Writing %	Signature and date
1	Long Ji	70	N/A	N/A	N/A	80	
	Hai Yu	30				20	
2	Long Ji	60	70	N/A	70	80	
	Hai Yu	10	0		10	10	
	Ruijie Zhang	0	10		0	0	
	David French	15	5		5	0	17/5/19
	Mihaela Grigore	10	5		5	0	16.05.2019
	Bing Yu	0	5		5	0	Bing Yu 19/05/2019
	Xiaolong Wang	5	5		0	0	
	Jianglong Yu	0	0		5	0	
	Shuaifei Zhao	0	0		0	10	
3	Long Ji	20	80	N/A	50	55	
	Hai Yu	30	0		30	30	
	Xiaolong Wang	20	5		5	0	
	Mihaela Grigore	10	5		5	5	16.05.2019
	David French	20	5		5	0	17/5/19
	Yesim M. Gözükara	0	5		5	0	
	Jianglong Yu	0	0		0	5	
	Ming Zeng	0	0		0	5	
4	Long Ji	70	85	70	70	80	
	Hai Yu	30	0	10	10	5	
	Bing Yu	0	5	10	0	0	Bing Yu 19/05/2019
	Ruijie Zhang	0	5	0	0	0	

	David French	0	0	0	5	0	
	Mihaela Grigore	0	5	0	5	0	16.05 2019
	Xiaolong Wang	0	0	0	5	5	
	Zuliang Chen	0	0	10	0	5	
	Shuaifei Zhao	0	0	0	5	5	
5	Long Ji	70	85	40	70	70	
	Hai Yu	15	0	30	10	5	
	Kangkang Li	15	0	30	10	10	
	Bing Yu	0	5	0	0	0	
	Mihaela Grigore	0	5	0	5	0	16.05.2019
	Qi Yang	0	5	0	5	0	
	Xiaolong Wang	0	0	0	0	5	
	Zuliang Chen	0	0	0	0	3	
	Ming Zeng	0	0	0	0	2	
	Shuaifei Zhao	0	0	0	0	5	
6	Long Ji	70	90	30	70	70	
	Hai Yu	15	0	20	15	10	
	Bing Yu	0	5	0	5	0	
	Kaiqi Jiang	0	0	20	0	5	
	Mihaela Grigore	0	5	0	5	0	16.05 2019
	Xiaolong Wang	0	0	0	5	0	
	Shuaifei Zhao	0	0	0	0	5	
	Kangkang Li	15	0	30	0	10	

Abstract

Carbon dioxide (CO_2) mineralisation by industrial wastes can mitigate carbon emissions safely and permanently with low cost. Disadvantages of coal fly ash-based CO_2 mineralisation are low CO_2 removal efficiency, slow reaction kinetics and low capacity, which restrict application of this technology. My research (i) explores mechanisms in coal fly ash-based CO_2 mineralisation; and (ii) develops innovative approaches to enhance carbonation reactions and make them more technically and economically feasible. Five Chinese or Australian coal fly ashes were selected for carbonation experiments to understand fly ash properties affecting CO_2 sequestration capacity and kinetics of carbonation reactions. A Chinese ash with 16 % CaO displayed the fastest kinetics while an Australian ash with 32 % CaO and 29 % MgO exhibited the largest CO_2 capacity. Carbonation experiments investigated effects of temperature (20−220 °C), solid to liquid ratio (50−200 g/L), and additives (Na_2CO_3, $NaHCO_3$ and NaCl) on CO_2 capacity and reaction kinetics, and mechanisms involved in carbonation reactions. Parameter optimization and introduction of additives can improve carbonation efficiency and enhance carbonation reactions between fly ash and CO_2, and the carbonation efficiency could become stable within 1.5 h, but it was still slow for further application. Integrated CO_2 absorption−mineralisation, that integrates amine scrubbing, CO_2 mineralisation and amine regeneration in a single process, was developed. Regeneration of amines by calcium oxide and fly ash was investigated. Results show that after carbonation reactions with calcium oxide and fly ash at 40 ℃ in 15 min, amine solutions can be regenerated to a similar CO_2 loading compared to traditional thermal regeneration method, and that the CO_2 absorbed by amine solutions can be precipitated as calcium carbonate with fast kinetics.

Key Words: fly ash, CO_2 mineralisation, chemical regeneration, IAM, low-energy consumption

Chapter 1 Introduction

1.1 CO_2 capture technologies

CO_2 emissions resulting from human activity are widely accepted as a major greenhouse gas (GHG) contributing to global warming [1-3]. Among the human activities that generate CO_2, fossil fuel combustion is the largest emission source accounting for 37 % of total anthropogenic carbon emissions [4]. Driven by rapid population growth and industrialisation, the average atmospheric CO_2 concentration has increased significantly from 280 ppmv in pre-industrial times to 413 ppmv in January 2019 [5] while the average temperature of the global surface increased by 0.6−1.0 ℃ [6]. Without considerable efforts to reduce GHG emissions, the atmospheric CO_2 concentration will continue to increase to 750−1300 ppmv by 2100 [6] and will lead to a rise of global surface temperature of around 3.7−4.8 °C by 2100 compared to pre-industrial temperatures. To deal with this serious environmental problem, governments and researchers around the world have been making great efforts to reduce the global atmospheric concentration of CO_2.

There are several possible strategies to reduce CO_2 emissions: (i) increasing energy conversion efficiency, (ii) increasing the use of low carbon fuel/renewable energy, and (iii) developing CO_2 capture and storage (CCS) technologies. Of these, CCS technology is a promising route to directly reduce CO_2 emissions in the short to intermediate term. A typical CCS technology consists of three steps: CO_2 separation from the emitters, CO_2 compression and transportation to a storage site, and long-term isolation from the atmosphere. Currently, there are three primary CO_2 capture options suitable for commercial application in the near to medium term: pre-combustion, oxy-fuel combustion and post-combustion [7]. The pre-combustion process is normally implemented in coal-based integrated gasification combined cycle (IGCC) power stations. Feeding coal is pretreated with steam and oxygen/air to generate the synthesized gas which is mainly carbon monoxide (CO) and hydrogen (H_2). The synthesized gas is then reacted with water steam to produce CO_2 and more H_2. The CO_2 concentration of the resulting gas can be more than 20 % [1]. The produced carbon-free energy H_2 is ready to be combusted for heat/power generation. The energy efficiency penalty of coupling a pre-combustion process to an IGCC power station is 7−8 % or more [8]. In oxy-fuel combustion processes, the fuel is combusted in high purity oxygen (O_2) gas (>95 %) instead of air, producing a flue gas with high CO_2 concentration (>80 %) [1]. After combustion, minor components such as sulfur dioxide (SO_2) can be removed from the flue gas by a traditional desulfurization process. The treated flue gas with very high CO_2 concentration can then be compressed to remove moisture, prior to transport for sequestration. Energy consumption

by the oxy-fuel process is mainly from high purity O_2 gas making in an air separation unit, which results in an energy penalty of >7 % [1, 2]. In the post-combustion process, CO_2 is directly separated from the flue gas by adsorbents, absorbents or membranes and then released to produce high purity CO_2 gas (>99 %) for subsequent compression, transportation and sequestration [9]. Compared with the other two technologies, post-combustion CO_2 capture technology (PCC) is easier to apply to existing plants, which require only a few modifications [10]. Although PCC also suffers from a great energy penalty (>7 %) due to CO_2 desorption [11-13], it is the most suitable option for the large-scale removal of CO_2 in existing fossil fuel-based power stations and other industries [14].

1.2 Post-combustion CO_2 capture technologies

The low CO_2 partial pressure in flue gas leads to a limited thermodynamic driving force of CO_2 separation and thus requires a strong interaction between sorbents and CO_2. Various PCC technologies have been developed, including adsorption, absorption, and mineralisation.

Adsorption technology involves CO_2 adsorption and release by solid adsorbents in a non-aqueous system. Adsorbents can be categorized into three kinds by their working temperature: low temperature (<200 °C), intermediate temperature (200−400 °C) and high temperature (>400 °C) [15-17]. Low temperature adsorbents are normally porous materials and amine-grafted porous materials, including carbon materials (e.g. silica, carbon nanotube), zeolites (e.g. X, Y, ZSM), metal organic frameworks, and graphite/graphene [15]. The ability to capture CO_2 can be mainly attributed to their high surface areas and nano-sized pores, but their selectivity towards CO_2 is low. In order to improve their CO_2 capture capacity and selectivity, several approaches have been developed, such as microstructure and morphology control, composition optimization, cation exchange, surface modification, and hybrid materials. Grafting certain types of solid amines onto the porous materials is also a promising approach. Layered double hydroxides (LDHs), also known as hydrotalcite-like compounds (HTs) or anionic clays are typical intermediate-temperature adsorbents [15]. They are layered alkaline solids, in which the high surface area and abundant basic sites on the surface are favorable for CO_2 absorption. These adsorbents display great potential for CO_2 adsorption, but there are still many problems to be solved before commercial use, especially high material cost. Calcium oxide (CaO) is a typical high temperature adsorbent. CO_2 capture occurs in the carbonator to form calcium carbonate ($CaCO_3$), then $CaCO_3$ is passed to a calciner, where the sorbent material is regenerated producing high purity CO_2. This process integrates very well with cement manufacture [2].

In the absorption method, sorbents for CO_2 capture can be amine solutions, ionic liquids, or aqueous ammonium. Amine scrubbing is the leading technology for large-scale CO_2 capture and has been commercially realised in coal-fired power stations, such as the Boundary Dam (Saskatchewan, Canada) and Washington Parish (Texas, USA) power plants [18-20]. It is a continuous, cyclic process involving CO_2 absorption and desorption. The solvent selectively absorbs CO_2 from the flue gas in an absorber at low temperatures (40−80 °C). CO_2 desorption and absorbent regeneration is conducted at elevated temperatures (100−140 °C) to produce high-purity CO_2 and lean-CO_2 loading solvent to re-absorb CO_2. The amino group of amines enable highly efficient removal of CO_2 from flue gas over aqueous ammonium [21]. Compared to ionic liquids, amine solvents have the advantage of much lower material cost. Despite commercial applications, the amine-based technology still suffers from a significant energy penalty and high capital cost. For example, installing the current monoethanolamine (MEA) capture process in a coal-fired power plant would result in a loss of overall thermal efficiency of 25−40 % and a rise in the cost of electricity of 70−100 % [22, 23]. Amine degradation during absorption and desorption is another major challenge involved in amine scrubbing technology [24-26]. For instance, degradation causes a solvent loss rate of 0.35-2.0 kg-MEA/t-CO_2, increasing operating costs [27].

Although adsorption and absorption display high CO_2 removal efficiency from flue gas and produce a high purity CO_2 product, the product needs to be compressed and transferred to a geological storage site, resulting in large additional energy costs [23]. Also, geological CO_2 storage has great uncertainties in terms of quantifying storage potential, monitoring injected CO_2 and engineering challenges to ensure that the injected CO_2 remains in the subsurface for hundreds or thousands of years. Some countries, such as Finland and India, have insufficient storage capacity or lack suitable geological storage formations, and hence cannot sequester CO_2 in this manner [28]. In this case, CO_2 mineralisation is a viable alternative to adsorption/absorption-based CO_2 capture by targeting small and medium emitters (<2.5 Mt-CO_2/a) [28].

CO_2 mineralisation can capture and store CO_2 permanently and safely without long-term monitoring [29]. It is the accelerated process of natural rock weathering, where carbonic acid from the dissolution of CO_2 in rainwater is neutralised with alkaline metal minerals, minerals rich in calcium (Ca) and magnesium (Mg), to form carbonate minerals. CO_2 mineralisation technologies can be categorised into in-situ (below ground) and ex-situ (above ground). In-situ CO_2 mineralisation involves the injection of CO_2 into underground reservoirs to promote reaction between CO_2 and alkaline-minerals present in the geological formation to form carbonates [30]. Considering this route still needs a CO_2 capture step prior to mineralisation, the ex-situ route is

attracting more attention recently. The ex-situ process employs direct reaction between minerals and CO_2/flue gas. It was initially developed to use natural silicate minerals from the serpentine group (e.g. $Mg_3SiO_5(OH)_4$), olivine group (e.g. Mg_2SiO_4) or wollastonite ($CaSiO_3$) as feedstocks to react with CO_2, due to their effectiveness and high world-wide abundance. Natural reserves of calcium and magnesium silicates near Earth's surface are capable of sequestration of the CO_2 that can be produced from recoverable fossil-fuel reserves [28]. But the effectiveness of CO_2 mineralisation using natural minerals has been limited by the slow kinetics of carbonation reactions between CO_2 and silicates [31]. Energy intensive mechanical, chemical, or thermal pre-treatments are normally needed prior to carbonation reaction to increase the feedstock reactivity. Moreover, since the CO_2 emission source and mineral deposit location normally do not coincide, the requirement for additional ore mining and transport increases the energy consumption of CO_2 mineralisation. These drawbacks of mineralisation of natural minerals can be avoided by use of industrial wastes such as fly ash, carbide slag and steel slag as a feedstock [32-35]. They have low material costs, high reactivity, do not require pre-treatment, and are readily available near CO_2 emission sources.

1.3 CO_2 mineralisation by coal fly ash

Coal fly ash is a by-product of coal combustion power plants. The coal fly ash that is rich in CaO/MgO and has high alkalinity is a promising material for CO_2 sequestration, because of its high alkalinity and particularly large volume production worldwide [36]. Specifically, it normally contains alkaline oxides such as CaO and MgO which are ideal feedstocks for CO_2 sequestration because of their high reactivity [37]. Also, fly ash is fine enough with the particles at micron or even submicron size, and grinding is not required prior to carbonation. In 2010, the global generation of coal fly ash was approximately 780 Mt [38]. As a hazardous waste, fly ash without proper disposal can pollute water and soil, disrupt ecological cycles and pose other environmental hazards. Technologies have been developed to recycle this residue and use it as construction materials in cement, reclamation of low-lying areas, roads and embankments, mine filling and agricultural activities, but only 53 % of fly ash was utilised in the world in 2010. The annual generation of fly ash is increasing, with unused fly ash frequently stored in waste piles or landfills [38]. The application of CO_2 mineralisation by fly ash can not only reduce CO_2 emissions, but also increase the stability of fly ash by reducing its alkalinity through carbonation reactions, and thus reduce the potential hazard of fly ash disposal and expand further use.

Extensive studies have been made to investigate the technical feasibility of CO_2 mineral carbonation, as well as the underlying mechanisms [39-69]. Mineral carbonation processes can be

divided into two routes: indirect and direct. Indirect mineral carbonation refers to any mineral carbonation process that takes place in more than one stage. The process is initiated by dissolution of mineral species in an aqueous medium to extract the alkaline-earth metals, mainly Ca and Mg. After liquid-solid separation, the leachate which is rich in alkaline-earth metal cations is subsequently carbonated by CO_2 gas, or by carbonates (e.g. $NaHCO_3$/Na_2CO_3, NH_4HCO_3/$(NH_4)_2CO_3$) obtained from other capture systems. One of the advantages of indirect carbonation is that it allows valuable pure carbonates such as $MgCO_3$ to be produced because impurities, such as silica and iron, can be removed prior to carbonate precipitation. Previous studies on indirect route have investigated the dissolution of fly ash in different leaching agents [39-43]. Sun et al. [39] investigated the extraction of Ca^{2+} and Mg^{2+} from Victorian brown coal fly ash using 6% acetic acid (CH_3COOH) at 20-80 °C and the carbonation of the leachate with pure CO_2 gas. The results also indicated that the CO_2 suquestration capacity of indirect route was ten-folds larger than that of direct route using the same fly ash. Hosseini et al. [40, 41] developed a closed-loop, multistep process to study the leaching and precipitation of Ca^{2+} and Mg^{2+} as carbonates from two Victorian brown coal fly ashes using ammonium chloride (NH_4Cl) as a leaching agent. He et al. [42] compared the extraction effect of NH_4Cl, ammonium nitrate (NH_4NO_3) and ammonium acetate (CH_3COONH_4) on a Chinese lignite-fired fly ash. High dissolution (>80%) and carbonation efficiency (>60%) could be achieved at moderate temperature (<100°C). Hosseini et al. [43] investigated the effect of Mg^{2+}/Ca^{2+} on the kinetics and efficiency of carbonates formation. When Mg^{2+}/Ca^{2+} ratio is 2, carbonation efficiency could be 100% in 30 min. The CO_2 suquestration capacity of indirect route is much larger than that of direct route using the same fly ash, but the difficulty in recycling the leaching agents is hindering the application of this technology on a large scale. In addition, considering Ca^{2+} and Mg^{2+} are already partially present as carbonates in some fly ashes, leaching agents react with these carbonates and release CO_2 before they are re-carbonated.

For direct carbonation, the carbonation reaction takes place in a single reactor. It can be achieved through both gas-solid carbonation route or wet/aqueous carbonation route. The advantages of direct route are the simplicity of process and the minimal use of chemical reagents, which makes it the most promising technology of CO_2 sequestration by fly ash. The direct reaction of gaseous CO_2 with fly ash at suitable temperatures and pressures is the most basic process of direct mineral carbonation. Previous studies confirmed that the gas-solid carbonation of dry fly ash under low pressure conditions was technical viable [44-46]. However, due to the slow reaction kinetics, elevated temperatures and pressures are normally required in gas-solid carbonation. Faster kinetics and higher CO_2 capacity could be achieved in the presence of moisture in the CO_2 gas feeding or

by adding water into the fly ash [46]. For example, for the dry route, 65 % calcium conversion was achieved in a few minutes at 400°C under a 10% CO_2 atmosphere, while for the wet route a similar clacium conversion was obtained at 30°C [44]. The enhanced carbonation was attribute to the fact that the moisture and water could help extract Ca^{2+} and Mg^{2+} ions from the solid matrix of fly ash particles. Thus, the wet/aqueous route proved to be more effective than the gas-solid method. Extensive studies [47-65] investigated the technical feasibility of wet/aqueous route and compared carbonation capacities and efficiencies of different fly ashes at various operating conditions. Montes-Hernandez et al. [50] determined the CO_2 sequestration capacity of a French fly ash under various conditions (25−60 °C, CO_2 gas pressure 1−4 Mpa, solid/liquid ratio 50−150 g/L, stirring rate 450 rpm), and investigated the reaction pathways using scanning electron microscopy and X-ray diffraction (XRD). Back et al. [49, 53] verified the carbonation mechanism of a German lignite fly ash in aqueous system by analysing the variation of pH, electrical conductivity and CO_2 conversion rate during the carbonation reaction. Ukwattage et al. [55, 57] investigated the CO_2 sequestration capacity of three Australian fly ashes in an autoclave reactor under various conditions (20−80 °C, liquid/solid ratio 0.1−1, CO_2 gas pressure 3 Mpa). The results indicated that the carbonation performance of fly ash was significantly affected by operation conditions, such as temperature, CO_2 pressure, solid to liquid ratio, stirring rate, and reaction time. The carbonation capacity and efficiency can be improved by optimisation of experimental parameters. Apart from the operating parameters, carbonation reactions are also affected by solid material properties (particle size, porosity and surface area, and mineralogy) and liquid agent (carbonate concentration or additional Ca^{2+} and Mg^{2+} concentration). Soong et al. [66] investigated the carbonation of fly ash in oil and gas production wastewater rich in metal ions (Mg, Ca, and Na) and claimed that the CO_2 sequestration capacity of the ash-wastewater mixture was higher than that of ash-water slurry and wastewater seperately. Calcium from both the wastewater and fly ash contributed to the formation of calcium carbonate. Likewise, Nyambura et al. [67] suggested that the carbonation conversions of solid wastes were higher in the brine−solid residues system, compared to the water−solid residues. The carbonation efficiency in the fly ash/brine system under a pressure of 4 MPa at 30 °C was 86%, which was superior to the water/brine system (i.e., 68 %). A maximum capture capacity of 283 g CO_2 per kg slag, corresponding to a carbonation conversion of 89%, can be achieved in alkaline wastewater with a reaction time of 120 min at 25 °C and an L/S ratio of 20. Pei et al. [68] found that the leaching concentration of calcium ions in metalworking wastewater was higher than that in deionized water, thereby resulting in a greater carbonation reaction rate and higher CO_2 sequestration capacity. The presence of inorganic ionic species in wastewater, such as sodium and chloride, can promote the dissolution of calcium and magnesium from the matrix of

fly ash particles due to the formation of surface complexes, leading to the reductive (and oxidative) dissolution of minerals.

1.4 Knowledge gaps

Previous studies have discussed the technical feasibility of direct CO_2 mineral carbonation with fly ash via gas-solid and aqueous routes. Mineral carbonation conducted by the aqueous route proved to be more effective than other methods. The carbonation performance of fly ash is significantly affected by operation conditions, such as temperature, CO_2 pressure, solid to liquid ratio, stirring rate, and reaction time, or liquid agents. However, different fly ash samples displayed different optimal conditions. The relationships between fly ash properties and oprating conditions are still not clear. Also, the mechanisms involved in carbonation reactions are not fully understood. Fly ash properties, especially mineralogy, may have considerable effects on carbonation efficiency [69]. Due to different raw coal sources, coal combustion processes, fly ash collection methods, and implementation of environmental hazard mitigation techniques, different fly ashes show different particle size distributions, morphologies, elemental compositions and mineralogies. Even for fly ashes with similar elemental compositions, the distributions of elements in a range of minerals can be very different. Further studies should investigate how fly ash properties affect carbonation performance and to determine optimal conditions for mineralisation. Also, given that the reaction rate of mineralisation is too slow (several hours of reaction duration) for large-scale application under current operating conditions, further studies of the reaction kinetics of carbonation with fly ash are also required to promote carbonation reactions.

1.5 Research structure

Corresponding to the identified problems, this research will explore the mechanisms involved in coal fly ash-based CO_2 mineralisation, and develop innovative approaches to enhance carbonation reactions and make the process more technically and economically feasible. This thesis is presented as a series of six published papers which are in chapters 2 to 7. Descriptions of each chapter are as follows:

Chapter 1: This chapter briefly introduces the current research status of CO_2 mineralisation by coal fly ash and point out critical challenges. The objectives and structure of this thesis will be summarised in this chapter.

Chapter 2: This chapter reviews the literature of CO_2 mineralisation by coal fly ash, including fly ash properties, technical routes and process chemistry. Also, the enhancement of carbonation reactions will be reviewed in detail.

Chapter 3: This chapter investigates fly ash properties affecting CO_2 sequestration capacity and kinetics of carbonation reactions, such as particle size, morphology, elemental and mineralogical compositions. Five coal fly ashes will be selected as exemplar of a range of fly ash compositions for carbonation experiments under various operating conditions.

Chapter 4: In this chapter, the effects of temperature, solid to liquid ratio, gas flow rate, and initial CO_2 pressure on the CO_2 sequestration capacity of ash from Beijing (BJ) will be systematically investigated. Apart from parameter optimization, the effects of additives including Na_2CO_3, $NaHCO_3$ and NaCl for carbonation efficiency will be investigated. The reaction mechanisms involved will also be discussed.

Chapter 5: In this chapter, the CO_2 sequestration capacity and the carbonation kinetics of HW ash will be investigated at various temperatures, stirring rates and initial CO_2 pressures to identify rate-limiting steps. A wide range of kinetic models will be introduced and compared to investigate the effects of various parameters on carbonation rate and efficiency. A selected model will then be used to predict maximum carbonation efficiency. The morphology of fresh and carbonated fly ash will be characterized to promote understanding of carbonation mechanisms.

Chapter 6: This chapter will propose an integrated CO_2 absorption−mineralisation (IAM) process, which integrates amine scrubbing, CO_2 mineralisation and amine regeneration in a single process. The technical feasibility of IAM will be investigated by adding calcium oxide into CO_2-loaded amine solutions, including five commonly used amines: monoethanolamine, diethanolamine, piperazine (PZ), N-methyldiethanolamine and 2-Amino-2-methyl-1-propanol. The performance stability of the optimised amine will be verified in multicycle experiments. The technical feasibility of IAM in practical applications using fly ash as a feedstock for absorbent regeneration will also be conducted with BJ ash.

Chapter 7: This chapter selects the benchmark MEA absorbent to further investigate the technical performance and reaction mechanisms of the IAM process. Given the highly heterogeneous nature and diverse components of the wastes, the reaction-active chemical calcium oxide, sodium hydroxide and calcium chloride will be used to gain insights into carbonation mechanisms and fundamental reaction pathways. The performance of MEA in the IAM process, including cyclic

CO_2-loading and regeneration efficiency, will be systematically investigated at various CO_2-loadings and reaction times. The performance stability of MEA will also be investigated in multicycle IAM experiments. Further experiments will be conducted using fly ash as a feedstock to demonstrate the technical feasibility of IAM in practical applications. Finally, comparison with traditional thermal absorbent regeneration will be conducted to determine the energy and cost savings of IAM.

Chapters 8 and 9: These chapters will discuss (Ch 8) and give the main conclusions (Ch 9) of this research. Recommendations and identification of possible future research directions will be made to further advance CO_2 mineralisation by coal fly ash.

1.6 References

1. MacDowell, N.; Florin, N.; Buchard, A.; Hallett, J.; Galindo, A.; Jackson, G.; Adjiman, C. S.; Williams, C. K.; Shah, N.; Fennell, P., An overview of CO_2 capture technologies. Energy & Environmental Science, 2010, 3(11): 1645-1669.
2. Boot-Handford, M. E.; Abanades, J. C.; Anthony, E. J.; Blunt, M. J.; Brandani, S.; Mac Dowell, N.; Fernández, J. R.; Ferrari, M.-C.; Gross, R.; Hallett, J. P.; Haszeldine, R. S.; Heptonstall, P.; Lyngfelt, A.; Makuch, Z.; Mangano, E.; Porter, R. T. J.; Pourkashanian, M.; Rochelle, G. T.; Shah, N.; Yao, J. G.; Fennell, P. S., Carbon capture and storage update. Energy & Environmental Science, 2014, 7 (1): 130-189.
3. Bui, M.; Adjiman, C. S.; Bardow, A.; Anthony, E. J.; Boston, A.; Brown, S.; Fennell, P. S.; Fuss, S.; Galindo, A.; Hackett, L. A.; Hallett, J. P.; Herzog, H. J.; Jackson, G.; Kemper, J.; Krevor, S.; Maitland, G. C.; Matuszewski, M.; Metcalfe, I. S.; Petit, C.; Puxty, G.; Reimer, J.; Reiner, D. M.; Rubin, E. S.; Scott, S. A.; Shah, N.; Smit, B.; Trusler, J. P. M.; Webley, P.; Wilcox, J.; Mac Dowell, N., Carbon capture and storage (CCS): the way forward. Energy & Environmental Science, 2018, 11 (5): 1062-1176.
4. Creamer, A. E.; Gao., B., Carbon-Based Adsorbents for Postcombustion CO_2 Capture: A Critical Review. Environmental Science & Technology, 2016, 50 (14): 7276-7289.
5. https://www.co2.earth/
6. Pachauri, R.K.; Meyer, L., Climate Change 2014: Synthesis Report, https://www.ipcc.ch/site/assets/uploads/2018/02/SYR_AR5_FINAL_full.pdf, 2014.
7. Tan, Y.; Nookuea, W.; Li, H.; Thorin, E.; Yan, J., Property impacts on Carbon Capture and Storage (CCS) processes: A review. Energy Conversion and Management, 2016, 118: 204-222.

8. Leung, D. Y. C.; Caramanna, G.; Maroto-Valer, M. M., An overview of current status of carbon dioxide capture and storage technologies. Renewable and Sustainable Energy Reviews, 2014, 39: 426-443.

9. Rochelle, G.T., Amine scrubbing for CO_2 capture. Science, 2009. 325: 1652-1654.

10. Hu, B.; Zhai, H., The cost of carbon capture and storage for coal-fired power plants in China. International Journal of Greenhouse Gas Control, 2017, 65: 23-31.

11. Black, J., Cost and performance baseline for fossil energy plants volume 1: Bituminous coal and natural gas to electricity. Final report (2nd edition), National Energy Technology Laboratory (2010 Nov) Report no.: DOE20101397, 2010.

12. Haszeldine, R.S., Carbon capture and storage: how green can black be? Science, 2009, 325: 1647-1652.

13. Goto, K.; Yogo, K.; Higashii, T., A review of efficiency penalty in a coal-fired power plant with post-combustion CO2 capture. Applied Energy, 2013, 111: 710-720.

14. Dave, N., Do, T., Palfreyman, D., Assessing post-combustion capture for coal fired power stations in APP countries. CSIRO Internal Report ET/IR–1083, 2008.

15. Wang, J.; Huang, L.; Yang, R.; Zhang, Z.; Wu, J.; Gao, Y.; Wang, Q.; O'Hare, D.; Zhong, Z., Recent advances in solid sorbents for CO_2 capture and new development trends. Energy & Environmental Science, 2014, 7 (11): 3478-3518.

16. Samanta, A.; Zhao, A.; Shimizu, G. K. H.; Sarkar, P.; Gupta, R., Post-Combustion CO_2 Capture Using Solid Sorbents: A Review. Industrial & Engineering Chemistry Research, 2012, 51 (4): 1438-1463.

17. Ünveren, E. E.; Monkul, B. Ö.; Sarıoğlan, Ş.; Karademir, N.; Alper, E., Solid amine sorbents for CO_2 capture by chemical adsorption: A review. Petroleum, 2017, 3 (1): 37-50.

18. Stéphenne, K., Start-up of world's first commercial post-combustion coal fired CCS project: Contribution of Shell Cansolv to SaskPower Boundary Dam ICCS project, 2013.

19. SaskPower, Boundary Dam Carbon Capture Project. http://www.saskpower.com/our-power-future/carbon-capture-and-storage/boundary-dam-carbon-capture-project/, 2014.

20. Global CCS Institute Projects Database, Petra Nova Carbon Capture. https://www.globalccsinstitute.com/projects/petra-nova-carbon-capture-project, 2017.

21. Shakerian, F.; Kim, K.-H.; Szulejko, J. E.; Park, J.-W., A comparative review between amines and ammonia as sorptive media for post-combustion CO_2 capture. Applied Energy, 2015, 148: 10-22.

22. Li, K.; Leigh, W.; Feron, P.; Yu, H.; Tade, M., Systematic study of aqueous monoethanolamine (MEA)-based CO_2 capture process: Techno-economic assessment of the MEA process and its improvements. Applied Energy, 2016, 165: 648–659.

23. Li, K.; Cousins, A.; Yu, H.; Feron, P.; Tade, M.; Luo, W.; Chen, J., Systematic study of aqueous monoethanolamine-based CO_2 capture process: model development and process improvement. Energy Science & Engineering, 2016, 4(1): 23–39.

24. Gouedard, C.; Picq, D.; Launay, F.; Carrette, P. L., Amine degradation in CO_2 capture. I. A review. International Journal of Greenhouse Gas Control, 2012, 10: 244-270.

25. Lepaumier, H.; Picq, D.; Carrette, P.-L., New Amines for CO_2 Capture. I. Mechanisms of Amine Degradation in the Presence of CO_2. Industrial & Engineering Chemistry Research, 2009, 48: 9061–9067.

26. Bernhardsen, I. M.; Knuutila, H. K., A review of potential amine solvents for CO_2 absorption process: Absorption capacity, cyclic capacity and pKa. International Journal of Greenhouse Gas Control, 2017, 61: 27-48.

27. Bailey, D. and Feron P. H.M., Post-combustion decarbonisation processes. Oil & Gas Science and Technology, 2005, 60: 461-474.

28. Zevenhoven, R.; Fagerlund, J.; Songok, J. K., CO_2 mineral sequestration: developments toward large-scale application. Greenhouse Gases Science and Technology, 2011, 1 (1): 48-57.

29. Sanna, A.; Uibu, M.; Caramanna, G.; Kuusik, R.; Maroto-Valer, M. M., A review of mineral carbonation technologies to sequester CO_2. Chemical Society reviews, 2014, 43 (23): 8049-8080.

30. Olajire, A. A., A review of mineral carbonation technology in sequestration of CO_2. Journal of Petroleum Science and Engineering, 2013, 109: 364-392.

31. Azdarpour, A.; Asadullah, M.; Mohammadian, E.; Hamidi, H.; Junin, R.; Karaei, M. A., A Review on Carbon Dioxide Mineral Carbonation Through pH-swing Process. Chemical Engineering Journal, 2015, 279: 615-630.

32. Sanna, A.; Dri, M.; Hall, M. R.; Maroto-Valer, M., Waste materials for carbon capture and storage by mineralisation (CCSM) – A UK perspective. Applied Energy, 2012, 99: 545-554.

33. Gomes, H. I.; Mayes, W. M.; Rogerson, M.; Stewart, D. I.; Burke, I. T., Alkaline residues and the environment: a review of impacts, management practices and opportunities. Journal of Cleaner Production, 2016, 112: 3571-3582.

34. Kirchofer, A.; Becker, A.; Brandt, A.; Wilcox, J., CO_2 mitigation potential of mineral carbonation with industrial alkalinity sources in the United States. Environmental Science & Technology, 2013, 47 (13): 7548-7554.

35. Bodor, M.; Santos, R. M.; Van Gerven, T.; Vlad, M., Recent developments and perspectives on the treatment of industrial wastes by mineral carbonation − a review. Central European Journal of Engineering, 2013, 3 (4): 566-584.

36. Wee, J.-H., A review on carbon dioxide capture and storage technology using coal fly ash. Applied Energy, 2013, 106: 143-151.

37. Bobicki, E. R.; Liu, Q.; Xu, Z.; Zeng, H., Carbon capture and storage using alkaline industrial wastes. Progress in Energy and Combustion Science, 2012, 38 (2): 302-320.

38. Heidrich, C., Feuerborn., H.J., Weir, A., Coal combustion products: a global perspective. World of Coal Ash (WOCA) Conference, April 22-25, Lexington, KY, America, 2013.

39. Sun, Y.; Parikh, V.; Zhang, L., Sequestration of carbon dioxide by indirect mineralization using Victorian brown coal fly ash. Journal of hazardous materials, 2012, 209-210: 458-466.

40. Hosseini, T.; Selomulya, C.; Haque, N.; Zhang, L., Indirect Carbonation of Victorian Brown Coal Fly Ash for CO_2 Sequestration: Multiple-Cycle Leaching-Carbonation and Magnesium Leaching Kinetic Modeling. Energy & Fuels, 2014, 28: 6481-6493.

41. Hosseini, T.; Haque, N.; Selomulya, C.; Zhang, L., Mineral carbonation of Victorian brown coal fly ash using regenerative ammonium chloride – Process simulation and techno-economic analysis. Applied Energy, 2016, 175: 54-68.

42. He, L.; Yu, D.; Lv, W.; Wu, J.; Xu, M., A novel method for CO_2 sequestration via Indirect carbonation of coal fly ash. Industrial & Engineering Chemistry Research, 2013, 52 (43): 15138-15145.

43. Hosseini, T.; Selomulya, C.; Haque, N.; Zhang, L., Investigating the effect of the Mg^{2+}/Ca^{2+} molar ratio on the carbonate speciation during the mild mineral carbonation process at atmospheric pressure. Energy & Fuels, 2015, 29 (11): 7483-7496.

44. Baciocchi, R.; Costa, G.; Polettini, A.; Pomi, R.; Prigiobbe, V., Comparison of different reaction routes for carbonation of APC residues. Greenhouse Gas Control Technologies, 2009, 1(1): 4851-4858.

45. Sun, J.; Bertos, M.F.; Simons, S.J.R., Kinetic study of accelerated carbonation of municipal solid waste incinerator air pollution control residues for sequestration of flue gas CO_2. Energy & Environmental Science, 2008, 1(3): 370-377.

46. Mazzella, A.; Errico, M.; Spiga, D., CO_2 uptake capacity of coal fly ash: Influence of pressure and temperature on direct gas-solid carbonation. Journal of Environmental Chemical Engineering, 2016, 4(4): 4120-4128.

47. Rendek, E.; Ducom, G.; Germain, P., Carbon dioxide sequestration in municipal solid waste incinerator (MSWI) bottom ash. Journal of hazardous materials, 2006, 128 (1): 73-79.

48. Uliasz-bochenczyk, A.; Mokrzycki, E.; Mazurkiewicz, M.; Piotrowski, Z., Utilization of carbon dioxide in fly ash and water mixtures. Chemical Engineering Research and Design, 2006, 84 (9): 843-846.

49. Back, M.; Kuehn, M.; Stanjek, H.; Peiffer, S., Reactivity of alkaline lignite fly ashes towards CO_2 in water. Environmental Science & Technology, 2008, 42 (12): 4520-4526.

50. Montes-Hernandez, G.; Perez-Lopez, R.; Renard, F.; Nieto, J. M.; Charlet, L., Mineral sequestration of CO_2 by aqueous carbonation of coal combustion fly-ash. Journal of hazardous materials 2009, 161 (2-3): 1347-1354.

51. Uliasz-Bochenczyk, A.; Mokrzycki, E.; Piotrowski, Z.; Pomykala, R., Estimation of CO_2 sequestration potential via mineral carbonation in fly ash from lignite combustion in Poland. Enrgy Procedia, 2009, 1: 4873-4879.

52. Baciocchi, R.; Costa, G.; Lategano, E.; Marini, C.; Polettini, A.; Pomi, R.; Postorino, P.; Rocca, S., Accelerated carbonation of different size fractions of bottom ash from RDF incineration. Waste Management, 2010, 30 (7): 1310-1317.

53. Back, M.; Bauer, M.; Stanjek, H.; Peiffer, S., Sequestration of CO_2 after reaction with alkaline earth metal oxides CaO and MgO. Applied Geochemistry, 2011, 26 (7): 1097-1107.

54. Mayoral, M. C.; Andrés, J. M.; Gimeno, M. P., Optimization of mineral carbonation process for CO_2 sequestration by lime-rich coal ashes. Fuel, 2013, 106: 448-454.

55. Ukwattage, N. L.; Ranjith, P. G.; Wang, S. H., Investigation of the potential of coal combustion fly ash for mineral sequestration of CO_2 by accelerated carbonation. Energy, 2013, 52: 230-236.

56. Uibu, M.; Kuusik, R., Main physicochemical factors affecting the aqueous carbonation of oil shale ash. Minerals Engineering, 2014, 59: 64-70.

57. Ukwattage, N. L.; Ranjith, P. G.; Yellishetty, M.; Bui, H. H.; Xu, T., A laboratory-scale study of the aqueous mineral carbonation of coal fly ash for CO_2 sequestration. Journal of Cleaner Production, 2015, 103: 665-674.

58. Chang, E. E.; Pan, S. Y.; Yang, L.; Chen, Y. H.; Kim, H.; Chiang, P. C., Accelerated carbonation using municipal solid waste incinerator bottom ash and cold-rolling wastewater: Performance evaluation and reaction kinetics. Waste Management, 2015, 43: 283-292.

59. Han, S.-J.; Im, H. J.; Wee, J.-H., Leaching and indirect mineral carbonation performance of coal fly ash-water solution system. Applied Energy, 2015, 142: 274-282.

60. Mursito, A. T.; Yuliyanti, A.; Jakah, Hydrothermal carbonation of K–rich ash, value added energy engineering and CO_2 mineral sequestration. Procedia Chemistry, 2015, 14: 56-65.

61. Jaschik, J.; Jaschik, M.; Warmuziński, K., The utilisation of fly ash in CO_2 mineral carbonation. Chemical and Process Engineering, 2016, 37 (1): 29-39.

62. Pan, S.-Y.; Hung, C.-H.; Chan, Y.-W.; Kim, H.; Li, P.; Chiang, P.-C., Integrated CO_2 fixation, waste stabilization, and product utilization via High-Gravity carbonation process exemplified by circular fluidized bed fly ash. ACS Sustainable Chemistry & Engineering, 2016, 4 (6): 3045-3052.

63. Tamilselvi Dananjayan, R. R.; Kandasamy, P.; Andimuthu, R., Direct mineral carbonation of coal fly ash for CO_2 sequestration. Journal of Cleaner Production, 2016, 112: 4173-4182.

64. Wang, L.; Chen, Q.; Jamro, I. A.; Li, R.; Li, Y.; Li, S.; Luan, J., Geochemical modeling and assessment of leaching from carbonated municipal solid waste incinerator (MSWI) fly ash. Environmental science and pollution research international, 2016, 23 (12): 12107-12119.

65. Uliasz-Bocheńczyk, A.; Pawluk, A.; Pyzalski, M., The mineral sequestration of CO_2 with the use of fly ash from the co-combustion of coal and biomass. Gospodarka Surowcami Mineralnymi 2017, 33 (4): 143-156.

66. Soong, Y.; Fauth, D. L.; Howard, B. H.; Jones, J. R.; Harrison, D. K.; Goodman, A. L.; Gray, M. L.; Frommell, E. A., CO_2 sequestration with brine solution and fly ashes. Energy Conversion and Management, 2006, 47 (13-14): 1676-1685.

67. Nyambura, M. G.; Mugera, G. W.; Felicia, P. L.; Gathura, N. P., Carbonation of brine impacted fractionated coal fly ash: Implications for CO_2 sequestration. Journal of Environmental Management, 2011, 92 (3): 655-664.

68. Pei, S. L.; Pan, S. Y.; Li, Y. M.; Chiang, P. C., Environmental benefit assessment for the carbonation process of petroleum coke fly ash in a rotating packed bed. Environmental Science & Technology, 2017, 51 (18): 10674-10681.

69. Baciocchi, R.; Costa, G.; Di Gianfilippo, M.; Polettini, A.; Pomi, R.; Stramazzo, A., Thin-film versus slurry-phase carbonation of steel slag: CO_2 uptake and effects on mineralogy. Journal of Hazardous Materials, 2015, 283(0): 302-313.

Pages 15-39 of this thesis have been removed as they contain published material. Please refer to the following citation for details of the article contained in these pages.

L. Ji, H. Yu, (2018). Carbon dioxide sequestration by direct mineralization of fly ash. In F. Pacheco-Torgal, C. Shi, A.P. Sanchez (Eds.), *Carbon Dioxide Sequestration in Cementitious Construction Materials* (pp.13-37). Woodhead Publishing.

Pages 40-57 of this thesis have been removed as they contain published material. Please refer to the following citation for details of the article contained in these pages.

Ji, L., Yu, H., Zhang, R., French, D., Grigore, M., Yu, B., Wang, X., Yu, J., & Zhao, S. (2019). Effects of fly ash properties on carbonation efficiency in CO_2 mineralisation. *Fuel Processing Technology*, *188*, 79-88.

DOI: 10.1016/j.fuproc.2019.01.015

Fuel Processing Technology 156 (2017) 429–437

Contents lists available at ScienceDirect

Fuel Processing Technology

journal homepage: www.elsevier.com/locate/fuproc

Research article

CO_2 sequestration by direct mineralisation using fly ash from Chinese Shenfu coal

Long Ji [a,b,f], Hai Yu [b,*], Xiaolong Wang [c,*], Mihaela Grigore [d], David French [d], Yeşim M. Gözükara [e], Jianglong Yu [f], Ming Zeng [a,*]

[a] China University of Mining & Technology Beijing, Beijing, 100083, China
[b] CSIRO Energy, Newcastle, NSW 2304, Australia
[c] Huaneng Clean Energy Research Institute, Beijing 102209, China
[d] CSIRO Energy, North Ryde, NSW 2113, Australia
[e] CSIRO Manufacturing, Clayton, VIC 3169, Australia
[f] University of Newcastle, University Drive, Callaghan, NSW 2308, Australia

ARTICLE INFO

Article history:
Received 2 August 2016
Received in revised form 30 September 2016
Accepted 3 October 2016
Available online 18 October 2016

Keywords:
CO_2 sequestration
Mineral carbonation
Fly ash
Calcium oxide

ABSTRACT

Fly ash is a potential source of highly reactive feedstock for CO_2 mineral carbonation. It does not require pre-treatment, but it has a low carbonation rate and efficiency. To address these issues, we studied the carbonation performance and mechanism of a fly ash from Shenfu coal of China. The effects of temperature, solid to liquid ratio and gas flow rate on the carbonation efficiency of the fly ash were systematically investigated in a direct mineralisation process. Our results indicated that calcium in lime and portlandite had a higher reactivity towards CO_2 than that in other calcium bearing phases either crystalline or amorphous. Solely increasing the temperature did not improve carbonation efficiency. However, experiments in a batch reactor under elevated temperature (140, 180, and 220 °C) and pressure conditions (10 and 20 bar) using recyclable additives showed that a combination of high temperature and pressure significantly improved carbonation efficiency in the presence of 0.5 mol/L Na_2CO_3. Our multiple-cycle experiments showed that Na_2CO_3 facilitated the precipitation of calcium carbonate and was well regenerated in the process.

1. Introduction

CO_2 sequestration by mineralisation is one of the safest and most permanent methods for storing CO_2 emitted by fossil fuel combustion, and could be a viable alternative to CO_2 geological storage [1,2]. It is suitable for small and medium emitters, or wherever geological storage is not possible [3–6]. Comparing to natural minerals, industrial by-products such as fly ash have several advantages to be the feedstock, including low materials cost, high materials reactivity, no pre-treatment requirement, and ease of availability near CO_2 emission sources [4–7]. Specifically, fly ash normally contains alkaline oxides such as CaO and MgO which are seen as the ideal feedstocks for CO_2 sequestration because of their high reactivity. Also, fly ash generally is fine enough with the majority of the particles falling in micron or even submicron scale, and grinding is not required prior to the carbonation process. In addition, fly ash is generated with CO_2 together after combustion in coal-fired power plants, so it does not need any extra cost of transport [8].

By 2015, >580 million tonnes of fly ash were estimated to be generated annually from coal-fired power plants in China, accounting for >50% of global production [9,10]. As a toxic by-product of coal combustion that is generated in such huge amounts, the disposal of fly ash has become a serious problem. Technologies have been developed to utilize this residue in construction materials production [9]. Fly ash normally contains active species, such as CaO and MgO, so that blended cement or concrete containing fly ash could gradually absorb moisture from the air and cause expansion in the product life cycle [11], which is one of important factors stopping fly ash from widespread application in construction industry. Using fly ash to sequester CO_2 can not only reduce the CO_2 emission but also increase fly ash stability thus expanding its utilization in construction material production. However most Chinese fly ashes have a lower CO_2 sequestration capacity [6,9] than other industrial wastes rich in CaO such as steel slag (calcium oxide content is normally 32–52%)[6] because of the low content of these CO_2 reactive species in most Chinese fly ashes (normally <15%) [9]. Despite the low capacity, using fly ash as feedstock for CO_2 mineral carbonation is still attracting wide attention because of the huge volumes of annual production.

Mineral carbonation processes can be divided into two routes: direct and indirect. The indirect route is initiated by dissolution of mineral species in an aqueous medium to extract the alkaline-earth metals. The leachate, rich in alkaline-earth metal cations, is subsequently carbonated by CO_2, or by other carbonates (e.g. $NaHCO_3/Na_2CO_3$) obtained from

* Corresponding authors.
E-mail addresses: hai.yu@csiro.au (H. Yu), wangxiaolong@hnceri.com (X. Wang), marzeng@yeah.net (M. Zeng).

L. Ji, H. Yu, X. Wang, M. Grigore, D. French, Y.M. Gözükara, J. Yu, M. Zeng, CO_2 sequestration by direct mineralisation using fly ash from Chinese Shenfu coal, Fuel Processing Technology, 2017, 156: 429-437. https://doi.org/10.1016/j.apenergy.2018.04.108

other capture systems [7]. Recent studies of indirect route have focused on investigate different leaching agents [4,5,8]. Indirect route can produce more valuable pure carbonates than direct route, because impurities such as silica and iron can be removed prior to carbonate precipitation. However, the difficulty in recycling the leaching agents and the low alkaline-earth metals extraction ratio is hindering the application of this technology on a large scale [12,13]. In addition, calcium and magnesium are already present as carbonates in some fly ashes. Leaching agents could react with these carbonates and release CO_2 before they are re-carbonated [4].

Research on mineral carbonation of CO_2 using coal fly ash has focused mainly on direct aqueous route [14], which involves a direct reaction of fly ash with CO_2 in a single reactor, with water or brine as the reaction medium. The advantages of direct route are its simplicity and the minimal use of chemical reagents, which make it the most promising technology of CO_2 sequestration using fly ash [6,14]. Many recent studies have investigated effect of various parameters, such as temperature, CO_2 pressure, solid to liquid ratio, stirring rate, and reaction time, on the carbonation reaction of various fly ashes in aqueous system [15–24]. Carbonation efficiency and CO_2 sequestration capacity are widely used in these existing studies [15–26] to estimate the carbonation performance of various fly ashes. Some other studies have introduced additives to improve fly ash carbonation [25,26]. For example, Soong et al. [25] developed a process for carbonation of fly ash in brine solution in the presence of NaOH as an additive in an autoclave reactor and claimed that the CO_2 sequestration capacity of the mixture is higher than when using fly ash-water slurry and brine, respectively. Calcium from both the brine and fly ash contribute to the formation of calcium carbonate.

Despite the previous research, there is still knowledge gap on our understanding of the reaction mechanism involved in carbonation reaction. The effect of chemical properties of fly ash on carbonation efficiency is not fully understood either. Carbonation efficiency can be affected by not only the process parameters but also the heterogeneous chemical properties of fly ashes and the proportion of Ca/Mg-bearing mineral phases available for carbonation reaction. Actually, the mineral phases of different fly ashes represent various constitutions. The factors controlling this variation probably include the mineralogy and inorganic geochemistry of the raw coals, as well as the different combustion conditions [27–31]. For example, the principal crystalline phases present in fly ash from black coals are mullite, quartz, magnetite, maghemite, and hematite, while the main crystalline phases in lignite are quartz, lime, anorthite, mullite and anhydrite [27]. During the cooling stage after combustion, the lime can react with CO_2, H_2O and SO_2 from the flue gas, and was converted into $Ca(OH)_2$, $CaCO_3$, and $CaSO_4$ [28], or combined with amorphous phase. Thus, the mineral phases of various fly ashes involved in carbonation reaction can be very different. It is important to understand the effect of mineral phases on carbonation reaction because it can help improve our understanding of carbonation mechanism and develop more effective methods to promote carbonation reaction. Especially given the large volume of fly ash produced in China, it is important to understand more about the characteristics of Chinese fly ash in carbonation process, for which very limited published data is available.

In this study, the aim was to investigate the sequestration potential of a fly ash from Chinese Shenfu coal [32] in direct aqueous mineralisation process, to improve the understanding of the effect of various operating parameters on carbonation performance, to verify the mineral phase changes of fly ash before and after carbonation, and thus develop a method to further improve carbonation efficiency. We also investigated the role of additives such as Na_2CO_3, $NaHCO_3$ and NaCl in carbonation reaction using fly ash. The carbonation experiments were first carried out at moderate temperature and ambient pressure in a semi-batch reactor, in which CO_2 gas was bubbled through fly ash and water slurry. The changes in the mineral phases of the fly ash before and after carbonation were determined by quantitative XRD analysis to study the carbonation behaviour of different Ca-bearing mineral phases. Carbonation experiments were also conducted in a closed reactor under elevated conditions (higher temperature and pressure) and in the presence of additives including Na_2CO_3, $NaHCO_3$ and NaCl. We also performed a multiple-cycle carbonation process to investigate the regeneration and recycling of Na_2CO_3, the most effective additive investigated in this work.

2. Materials and methods

2.1. Materials

The fly ash used in this study was collected from the fifth stage of electrostatic precipitators of Huaneng Gaobeidian power plant in Beijing, which is based on Chinese black coal from Shenfu, Shanxi province. Na_2CO_3 (≥99.5%), $NaHCO_3$ (≥99.7%), and NaCl (≥99%) chemicals were purchased from Sigma-Aldrich. All of the fly ash samples were dried overnight prior to any test. The elemental composition of the fresh samples was determined by X-ray fluorescence spectroscopy (XRF), while the crystalline phases present in fresh and carbonated samples were determined by XRD analyses. The XRD analyses were run on an Empyrean Panalytical X-Ray Diffractometer using CuKα radiation at 40 kV and 40 mA. Step scans were undertaken from 2 to 90° 2θ, with a step interval of 0.02° 2θ. The phase identification was performed using the Bruker Eva software package. The quantitative phase analysis was done using Siroquant™, which uses the Rietveld method to perform full profile matching [33–35]. The amount of amorphous matter in the ash was determined using an observed (hkl) file of an amorphous clay material, which was experimentally determined [33]. An inferred chemical composition for the amorphous fraction was calculated by subtracting the elements' percentage of crystalline phases from the bulk chemical composition [33,34]. The detailed description and validation of the method for calculation of chemical composition of amorphous phase in fly ash was published previously [33,34]. Total inorganic carbon (TIC) was determined by a Shimadzu TOC-L CPH C-analyser.

The calcium carbonate content of fresh and carbonated samples, expressed in terms of CO_2, was determined by a Netzsch STA 449 F1 Jupiter system coupled to a Pfeiffer Thermostar mass spectrometer. Mass changes as a function of temperature were measured by TGA, and evolved gases during thermal decomposition of materials were identified and monitored by the mass spectrometer. For each test, samples (10–20 mg) were heated in aluminium oxide ceramic cups under a nitrogen atmosphere at 10°/min from 30 to 950 °C. The temperature was held for 15 min at 105 °C and 600 °C, respectively, and then for 30 min at 950 °C. The mass spectrometer simultaneously analysed the evolved gases, including CO_2 and H_2O and confirmed that the weight loss at 30–105 °C, 105–600 °C and 600–950 °C was caused by evaporation of water, thermal decomposition of hydroxide, and thermal decomposition of carbonates, respectively [26,35–36] (Fig. 1). The amount of CO_2 in the fresh sample Eq. (1) was defined on the basis of its dry weight at 105 °C ($m_{105\ °C,\ 0}$, [g]) and its weight loss between 600 and 950 °C ($\Delta m_{600-950\ °C,\ 0}$, [g]) which is indicated in Fig. 1.

$$CO_{2,0}[wt\%] = \frac{\Delta m_{600-950\ °C,0}[g]}{m_{105\ °C,0}[g]} \times 100 \quad (1)$$

The weight loss of CO_2 in carbonated sample was from two parts: the decomposition of $CaCO_3$ contained in the fresh sample and the decomposition of $CaCO_3$ formed in the carbonation process. The CO_2 weight loss of the former part ($\Delta m'_{600-950\ °C}$, [g]) was calculated by Eq. (2):

$$\Delta m'_{600-950\ °C}[g] = \frac{m_{105\ °C}[g] - \Delta m_{600-950\ °C}[g]}{m_{105\ °C,0}[g] - \Delta m_{600-950\ °C,0}[g]} \times \Delta m_{600-950\ °C,0}[g] \quad (2)$$

where $m_{105\ °C}$ [g] is the dry weight of the carbonated sample at 105 °C, and $\Delta m_{600-950\ °C}$ [g] is the weight loss between 600 °C and 950 °C for the

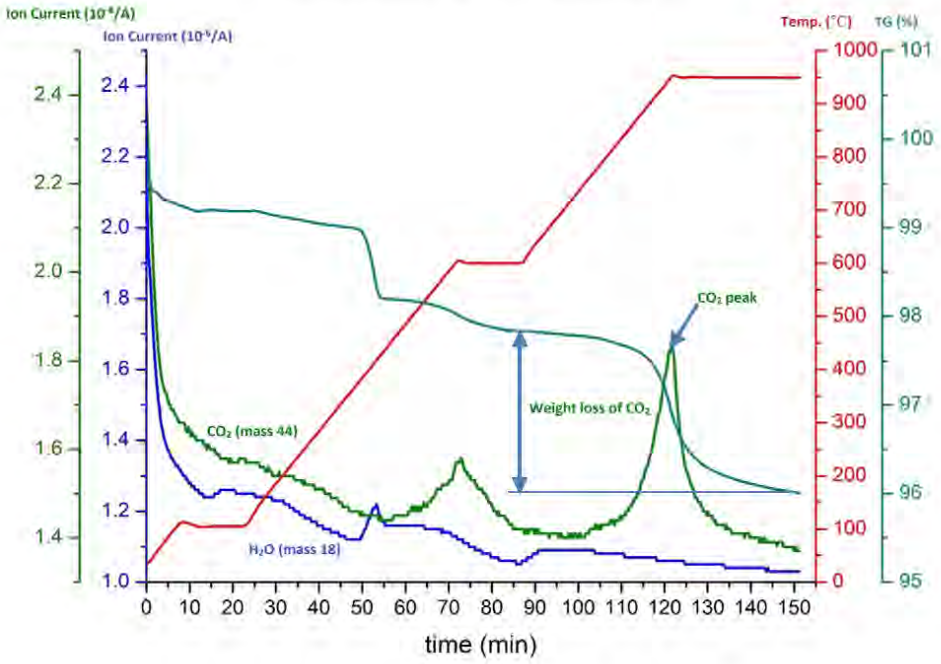

Fig. 1. Thermal gravimetrical analysis–mass spectrometry curve of fly ash.

carbonated sample. The amount of CO_2 in the carbonated sample due to the carbonation process was calculated by Eq. (3):

$$CO_2[wt\%] = \frac{\Delta m_{600-950\,^\circ C}[g] - \Delta m'_{600-950\,^\circ C}[g]}{m_{105\,^\circ C}[g]} \times 100 \quad (3)$$

The total calcium content (Ca_{total}, [wt, %]) and the carbonation efficiency (ζ_{Ca}, [%]) were calculated by Eqs. (4), and (5), respectively [23, 36]. The carbonation efficiency was then used to estimate the extent of the carbonation reaction.

$$Ca_{total}[wt\%] \quad \frac{\frac{(100-CO_2[wt\%])}{100} \times m_{105\,^\circ C}[g] \times \frac{CaO[wt\%]}{100} \times \frac{M_{Ca}[g/mol]}{M_{CaO}[g/mol]}}{m_{105\,^\circ C}[g]} \times 100 \quad (4)$$

$$\zeta_{Ca}[\%] = \frac{CO_2[wt\%] \times M_{Ca}[g/mol]}{Ca_{total}[wt\%] \times M_{CO_2}[g/mol]} \times 100 \quad (5)$$

where CaO [wt%] is the CaO content in fly ash obtained from XRF results; M_{Ca}, M_{CaO} and M_{CO_2} are the molecular weight of Ca, CaO and CO_2, respectively. Every test was repeated twice and the average value of the two results was calculated.

2.2. Carbonation experiments in a semi-batch reactor

For each carbonation experiment, 200 mL of high-purity water with electrical resistivity of 18.2 MΩ cm was poured into a 400-mL glass flask reactor and then heated to the specific temperature (60, 70, 80 and 90 °C) by a temperature-controlled silicone oil bath. Subsequently, a certain quality of fly ash was added to achieve a certain solid/liquid ratio (50, 100 and 200 g/L). At the same time, the mixture of 15% CO_2 (99.5% from BOC) and 85% nitrogen (99.9% from BOC) was introduced to the flask and bubbled through the slurry with a certain gas flow rate (60, 150, 250 and 350 mL/min). The solid sample was well mixed with the water and CO_2 gas was well dispersed using a magnetic stirrer at 500 rpm [17,23,36]. Pressure in the flask remained almost constant at atmospheric level throughout the experiment, and temperature was maintained at the set point. Slurry samples (5 mL) were sampled using a syringe at given interval times (5, 10, 15, 30 and 60 min). After 90 min reaction, the gas flow was stopped. The flask was removed from the heating system and quenched in cold water until the temperature decreased to room temperature. The slurry samples obtained at different time were immediately filtered through 0.2-μm syringe filter units respectively. The filter cakes were dried overnight in an oven at 105 °C and then tested by TGA to determine the carbonation efficiency of the reaction. The mineral phases of some samples were determined by quantitative XRD analyses.

2.3. Accelerated carbonation experiments in a batch reactor

The accelerated carbonation reactions were carried out in an autoclave Parr reactor made of Hastelloy alloy with an internal volume of 300 mL. For each carbonation experiment, 200 mL of high-purity water, a certain amount of additives (Na_2CO_3, $NaHCO_3$, and a mixture of Na_2CO_3 and NaCl) and 20 g fly ash were added into the autoclave. The fly ash particles were immediately dispersed by mechanical stirring (500 rpm). The slurry was then heated to the required temperature (60, 140, 230 and 275 °C) using an oven specifically adapted to the reactor. Subsequently, pure CO_2 gas was introduced into the reactor from the gas cylinder until a pre-determined CO_2 pressure was reached (10 and 20 bar). The temperature was kept at the set point by removing the reaction heat. After 2 h, the autoclave was cooled using cold water and depressurised. The suspension was immediately filtered by a 0.2-μm membrane filter and a vacuum pump. The solid was dried overnight in an oven at 105 °C and then analysed by TGA. The method to determine carbonation efficiency was same as that used in carbonation experiments in a semi-batch reactor. The concentration of TIC in the filtrate was then quantified.

2.4. Multiple-cycle carbonation experiments

To clarify the carbonation pathway in the presence of Na_2CO_3, we designed and conducted multiple-cycle carbonation experiments. The experiments involved six steps (as shown in Fig. 2).

The first experiment was carried out in the 300-mL autoclave Parr reactor, into which 200 mL of 0.5 mol/L Na_2CO_3 and 20 g fly ash were added. The system was heated to 275 °C and held there for 2 h with 500 rpm stirring rate. After carbonation, the suspension was immediately filtered through a 0.2-μm membrane filter and a vacuum

pump. The solid was dried and tested by TGA to determine carbonation efficiency. The filtrate was analysed by TIC and then saved for the second carbonation. In the second carbonation, 150 mL of the filtrate from the first carbonation and 15 g fresh fly ash were added to the autoclave. The carbonation conditions were same to the first carbonation. These two carbonation experiments aimed to investigate the effect of CO_3^{2-} consumption on the carbonation efficiency. In the first Na_2CO_3 regeneration, the filtrate from the second carbonation step was collected and poured into the three-necked flask reactor. CO_2 was then directly bubbled into the three-necked flask for 3 h to make sure N_2CO_3 was fully regenerated. After regeneration, the carbon-rich solution was analysed for TIC and then used for the third carbonation experiment followed by the second regeneration and the fourth carbonation. It should be mentioned that the condition setting used for in the multiple-cycle experiments were not optimised. Selection of the carbonation reaction conditions were based on those used in Section 2.3 to achieve a high carbonation efficiency. For the regeneration step, the conditions were selected to ensure N_2CO_3 was fully regenerated.

3. Results and discussion

3.1. Reaction mechanism of carbonation

Previous studies of fly ash carbonation suggest a simple reaction mechanism for CO_2 mineral sequestration [14,38]. The carbonation process can be described by Eqs. (6)–(12) as follows:

$$CO_2(g) + H_2O \rightarrow H_2CO_3(aq) \quad (6)$$

H_2CO_3 dissociation:

$$H_2CO_3(aq) \leftrightarrow HCO_3^- + H^+ \quad (7)$$

HCO_3^- dissociation:

$$HCO_3^- \leftrightarrow H^+ + CO_3^{2-} \quad (8)$$

The irreversible hydration of calcium oxide or lime:

$$CaO(s) + H_2O \rightarrow Ca(OH)_2 \quad (9)$$

The simultaneous dissolution of $Ca(OH)_2$ and ionization:

$$Ca(OH)_2(s) \rightarrow Ca^{2+} + 2OH^- \quad (10)$$

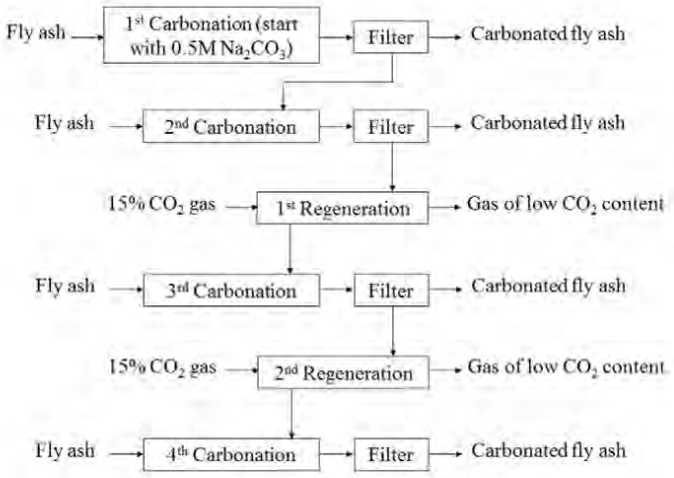

Fig. 2. Flow diagram of multiple-cycle experiments.

Table 1
Elemental quantification of fly ash determined by X-ray fluorescence spectroscopy.

Composition (wt.%)							
SiO_2	Al_2O_3	Fe_2O_3	CaO	MgO	Na_2O	K_2O	SO_3
42.80	19.15	9.06	16.41	1.23	1.68	1.50	1.9

The formation and precipitation of calcium carbonate:

$$Ca^{2+} + CO_3^{2-} \rightarrow CaCO_3(nuclei) \quad (11)$$

Crystal growth occurs spontaneously until equilibrium between calcite and the solution is reached [14]:

$$CaCO_3(nuclei) \rightarrow CaCO_3(calcite) \quad (12)$$

3.2. Chemical composition and mineralogy analysis

The chemical composition of the fly ash is given in Table 1. SiO_2 is the major constituent (42.80%), followed by Al_2O_3 (19.15%), CaO (16.41%) and Fe_2O_3 (9.06%). Ca and Mg are the ideal feedstock for CO_2 mineral carbonation [19]. Although the content of MgO is very low (1.23%), this fly ash is still suitable for mineral CO_2 sequestration because of its high Ca content and high alkalinity (pH = 12.0). Assuming that all of Ca is available for carbonation, the theoretical maximal CO_2 sequestration capacity is 0.1289 kg CO_2/kg fly ash.

The crystalline phases and concentrations are given in Fig. 3 and Table 2. Lime (CaO), portlandite ($Ca(OH)_2$), anhydrite ($CaSO_4$) and brownmillerite ($Ca_2(Al, Fe)_2O_5$) are the crystalline calcium-bearing phases identified in the fresh ash, along with quartz (SiO_2), mullite ($Al_2Si_6O_{13}$), hematite (Fe_2O_3) and magnetite (Fe_3O_4). A significant percentage (84.6%) of the ash is amorphous and may consist of one or several phases. Calcium distribution (shown in Table 3) in the crystalline and amorphous phases can be calculated using the mineralogical compositions (Table 2) of the fresh and carbonated samples and the chemical composition (Table 1) of the fresh fly ash. Specifically, the calcium content in the amorphous phase was calculated by subtracting the calcium content of crystalline phases from the total calcium content of the ash given by XRF analysis.

Table 3 shows that only a small portion of calcium occurs in crystalline phases of the fresh sample. The concentrations of calcium in the calcium-bearing phases of lime, portlandite, anhydrite and brownmillerite are 1.89, 0.86, 0.62, and 0.17%, respectively. Most calcium (8.35%) is

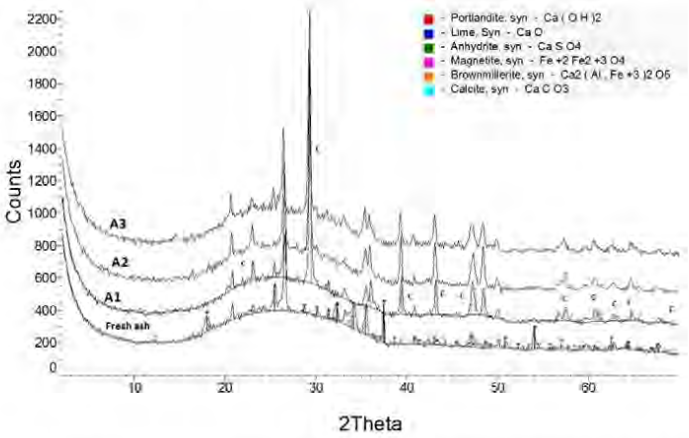

Fig. 3. X-ray diffraction patterns of fresh ash and corresponding carbonated ashes: A1 (solid/liquid ratio, 200 g/L; temperature, 80 °C; gas flow rate, 250 mL/min; reaction time, 1.5 h), A2 (solid/liquid ratio, 50 g/L; temperature, 80 °C; gas flow rate, 250 mL/min; reaction time, 1.5 h) and A3 (solid/liquid ratio, 50 g/L; temperature, 80 °C; gas flow rate, 250 mL/min; reaction time, 1 h).

Table 2
Relative concentrations (wt.%) of phases identified in fly ash samples.

Id.	Chemical formula	Fresh ash	A1[a]	A2[b]	A3[c]
Quartz	SiO_2	3.3	3.5	3.6	3.2
Mullite	$Al_6Si_2O_{13}$	1.4	1.4	1.4	1.7
Hematite	Fe_2O_3	1.4	0.8	0.6	1.1
Magnetite	Fe_3O_4	1.8	1.1	1.7	1.5
Brownmillerite	$Ca_2(Al, Fe)_2O_5$	0.7	0.3	0.3	0.6
Anhydrite	$CaSO_4$	2.1	1.3	0.7	1.5
Portlandite	$Ca(OH)_2$	3.5	–	–	–
Lime	CaO	1.2	–	–	–
Calcite	$CaCO_3$	–	11.2	11.8	10.0
Amorphous	–	84.6	80.4	79.9	80.4

[a] Carbonated sample after carbonation (conditions: solid/liquid ratio, 200 g/L; temperature, 80 °C; CO_2 flow rate, 250 mL/min; reaction time, 1.5 h).
[b] Carbonated sample after carbonation (conditions: solid/liquid ratio, 50 g/L; temperature, 80 °C; CO_2 flow rate, 250 mL/min; reaction time, 1.5 h).
[c] Carbonated sample after carbonation (conditions: solid/liquid ratio, 50 g/L; temperature, 80 °C; CO_2 flow rate, 250 mL/min; reaction time, 1 h).

present in the amorphous phase. No lime or portlandite can be detected in the carbonated sample, which indicates that they reacted with CO_2 and produced calcite during carbonation reaction. In addition, some of the anhydrite, brownmillerite and amorphous phase also reacted with CO_2. The concentrations of anhydrite, brownmillerite and amorphous phase are smaller in the carbonated ashes than in the fresh ash. The reactivity of lime and portlandite with CO_2 is greater than that of anhydrite, brownmillerite and amorphous species [37]. No Magnesium mineral was found in any crystalline phase, which indicates all of Mg was contained in amorphous phase. No magnesite ($MgCO_3$) was formed after carbonation reaction, which shows that the amorphous magnesium-bearing phases in the ash do not react with CO_2 under the conditions used in these carbonation tests. Calcite was the only crystalline carbonate detected by XRD in the carbonated ashes.

The experimental results of our work are consistent with the theory listed in Section 3.1. The main reactants are lime and portlandite. Calcite was the only crystalline carbonate detected. The novel finding in this study is that the anhydrite, brownmillerite and amorphous phase also reacted with CO_2 in carbonation process.

3.3. Carbonation experiments in a semi batch reactor

The effects of three operational parameters that may influence the carbonation process in the semi-batch system are discussed below.

3.3.1. Effect of solid/liquid ratio

Carbonation experiments were conducted in a semi-batch system at various solid/liquid ratios (50, 100 and 200 g/L), ambient pressure and temperature of 80 °C for a reaction time of 1.5 h. Fig. 4 shows the effect of solid/liquid ratio on carbonation efficiency at various carbonation times. For 50 g/L, the carbonation efficiency increased rapidly in the first 30 min and became stable at 33.1% after 30 min reaction. Similar trends were observed at solid/liquid ratios of 100 and 200 g/L; the carbonation efficiency increased dramatically initially, and then stabilised at a similar value. The only difference between the different solid/liquid ratios was that the higher the ratio, the longer the time required to reach the same value of carbonation efficiency. Our results indicate that it takes less time for the carbonation reaction to reach a limit at which the system becomes more diluted. Higher solid/liquid ratios mean that more reactants are available, which results in a longer carbonation reaction. To achieve a higher carbonation efficiency within a relatively short reaction time the solid/liquid ratio needs to be reduced. Our data are consistent with the data reported by previous studies [19, 39].

3.3.2. Effect of gas flow rate

The effect of gas flow rate on the carbonation process was studied at a solid/liquid ratio of 100 g/L, ambient pressure and temperature of 80 °C for a given reaction time of 1.5 h (Fig. 5). The average carbonation rate within 30 min at different gas flow rates decreases in the following order: 350 mL/min ≈ 250 mL/min > 150 mL/min > 60 mL/min. The carbonation rate was defined as:

$$r = \frac{d\xi_{Ca}[\%]}{dt} \tag{13}$$

At a lower gas flow rate, such as 60 mL/min, the gas flow is less turbulent and the CO_2 mass transfer rate from the liquid to the gas–liquid interface is lower. Therefore, less CO_2 is available in the liquid phase and the carbonation rate is also lower. With an increase in the gas flow rate, the difference of CO_2 mass transfer rate between lower gas flow rate and increased gas flow rate becomes much smaller. After the gas flow rate increases to 250 mL/min, any further increases have little impact on carbonation rate and efficiency, suggesting that the gas phase is well mixed and the reaction in the slurry is the limiting step in the carbonation process, which is consistent with the finding of previous paper [20]. Fig. 5 also shows that after a 90-min reaction, carbonation efficiency is similar at different gas flow rates, which indicates the carbonation has reached its limit. As expected, the gas flow rate does not affect the carbonation equilibrium from a thermodynamic point of view, but it does affects the mass transfer of gaseous CO_2 into liquid and thus the kinetics of the carbonation process [40,41].

3.3.3. Effect of carbonation temperature

Fig. 6 shows that the carbonation efficiency is similar at different temperatures (60, 70, 80 and 90 °C) throughout the duration of the carbonation reaction. This is due to two opposing effects of temperature on the carbonation process. From a kinetic point of view, increased temperature increases the reaction rate by improving the mass transfer rate, promoting the thermal motion of molecules and increasing their average kinetic energy. However, raising the reaction temperature also reduces the solubility of carbon dioxide in the liquid, which leads to low concentrations of carbonate ions. The equilibrium concentration of free CO_2 in liquid follows Henry's law:

$$[CO_2] = k_H \times P_{CO_2} \tag{14}$$

where P_{CO_2} is the CO_2 partial pressure, which is kept constant in this semi-batch experiment; and k_H is the Henry's law constant, which decreases with increased temperature [39,42]. Higher temperatures also reduce the solubility of $Ca(OH)_2$ and its concentration in solution [18, 20], while low concentrations of carbonate ion and Ca^{2+} in the solution hinder the formation and precipitation of $CaCO_3$. Moreover, since the carbonation reaction is exothermic, the equilibrium moves to the

Table 3
Calcium distribution of fresh and carbonated samples in different phases.

Calcium content (wt.%)[a]							
Sample	Lime (CaO)	Portlandite ($Ca(OH)_2$)	Anhydrite ($CaSO_4$)	Brownmillerite ($Ca_2(Al, Fe)_2O_5$)	Amorphous	Calcite ($CaCO_3$)	Total
Fresh ash	1.89	0.86	0.62	0.17	8.35	0.00	11.72
A1	0.00	0.00	0.22	0.07	6.51	4.92	11.72

[a] Refers to 100 g fresh ash for both fresh ash and A1 samples.

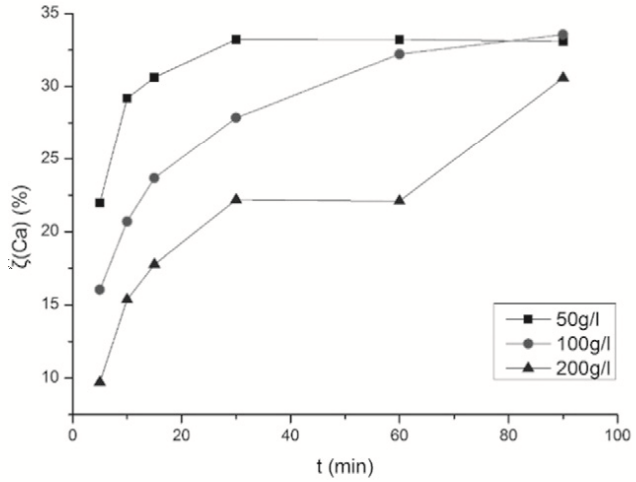

Fig. 4. Effect of solid/liquid ratio of slurry on carbonation reaction (80 °C, 250 mL/min gas flow rate).

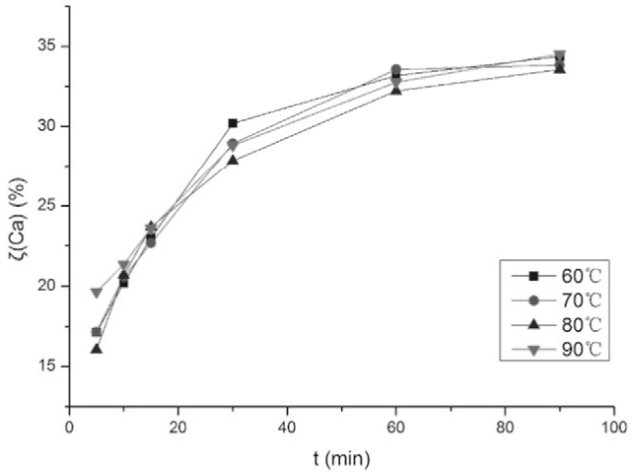

Fig. 6. Effect of temperature on carbonation reaction (250 mL/min gas flow rate, 100 g/L solid/liquid ratio).

negative direction as temperature increases. Therefore, increasing temperature alone cannot effectively improve carbonation efficiency. A balance is required between the positive and negative effect of the temperature-related increase in carbonation.

As shown in Figs. 4–6, the carbonation rate decreased as the reaction time elapsed. In the first 30 min, carbonation efficiency increased rapidly and reached a maximum value after 90 min. Similar results were observed in the literature [40,41]. Our XRD results showed that after 90 min, no lime or portlandite were detected in the carbonated ash, which means that they reacted with CO_2 and produced calcite. Similar results were reported by previous studies which showed the dissolution of lime and portlandite occurred very fast and it was not the rate limiting step of the carbonation process [17,20]. Our XRD results also showed anhydrite, brownmillerite and the amorphous phase partially reacted with CO_2 to form calcite during the carbonation reaction. Here, we define calcium from lime and portlandite as reactive calcium at ambient conditions, whereas calcium from anhydrite, brownmillerite and the amorphous phase, which haven't completely reacted with CO_2, is defined as unreactive calcium at ambient conditions. Since the reactivity of anhydrite, brownmillerite and amorphous phase with CO_2 is much lower than that of lime and portlandite [37,43–44], the limited carbonation efficiency value is due to the consumption of reactive calcium available at moderate temperatures and ambient pressure conditions.

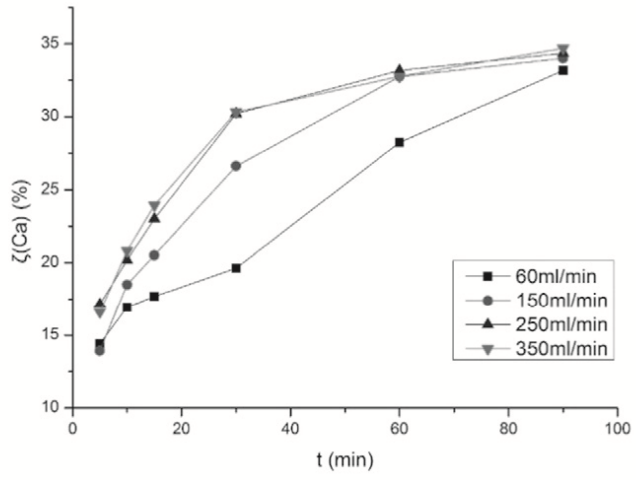

Fig. 5. Effect of gas flow rate on carbonation reaction (80 °C, 100 g/L solid/liquid ratio).

To further increase carbonation efficiency, it is necessary to raise the carbonation temperature to activate the unreactive calcium and produce more Ca^{2+} and to increase concentration of CO_3^{2-} to precipitate $CaCO_3$. However, as discussed above, elevated temperatures hinder the carbonation reaction by reducing the solubility of CO_2 in the liquid phase and the solubility of $Ca(OH)_2$. Therefore, in the following accelerated carbonation experiments, we used elevated initial CO_2 pressure and additives such $NaHCO_3$ and Na_2CO_3 to maintain the CO_2 or CO_3^{2-} concentration in the liquid phase while increasing the temperature. NaCl was also selected, because it is reported to increase the solubility of $Ca(OH)_2$ in the liquid phase [42,45].

3.4. Carbonation experiments under accelerated conditions

To further increase carbonation efficiency, we analysed the effect of initial CO_2 pressure, temperature and additives in a series of accelerated carbonation experiments.

3.4.1. Effect of initial CO_2 pressure at various temperatures

The results of carbonation experiments in the semi-batch reactor showed that increasing temperature alone cannot effectively improve carbonation efficiency. To evaluate the effect of initial CO_2 pressure and temperature on the carbonation reaction, we conducted several experiments at initial CO_2 pressures of 10 and 20 bar, at various temperatures. Fig. 7 show that the carbonation efficiency increases with temperature at 10 bar and 20 bar initial CO_2 pressure respectively, and that the carbonation efficiency at 20 bar was higher than that at 10 bar at the same temperature. According to Henry's law Eq. (14), CO_2 pressure plays a critical role in the mass transfer of CO_2 molecules from gas into water. At high pressures, the amount of CO_2 molecules dissolved into the water increases, leading to more carbonate ions available for carbonation [41]. Although increasing temperature decreases CO_2 solubility in water, carbonation efficiency can be improved through the combined effect of increased temperature and initial CO_2 pressure.

3.4.2. Effect of carbonation temperature with Na_2CO_3 as an additive

Carbonation experiments were conducted in the batch reactor with 0.5 mol/L Na_2CO_3 as an additive at different temperatures (60, 140, 230 and 275 °C) for a reaction time of 2 h and an initial CO_2 pressure of 20 bar. Fig. 8 shows that increasing the reaction temperature substantially increased carbonation efficiency. This trend is similar to that observed in the absence of additive (Fig. 7), but carbonation efficiency in the presence of Na_2CO_3 was much higher than in its absence. The effect of carbonation temperature and addition of Na_2CO_3 on carbonation

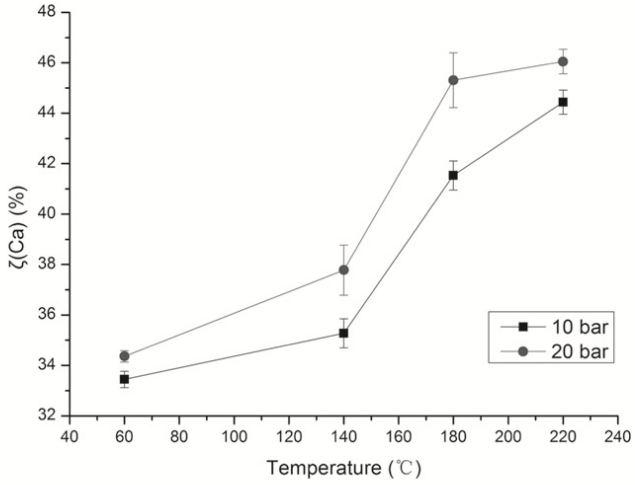

Fig. 7. Effect of initial pressure on carbonation reaction at various temperature (500 rpm stirring rate, 100 g/L solid/liquid ratio).

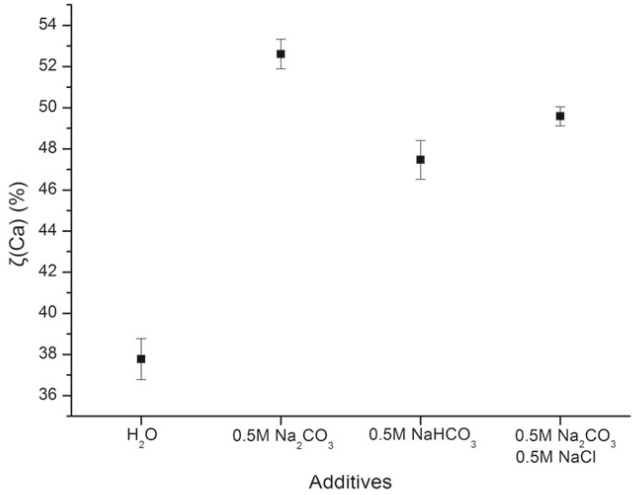

Fig. 9. Effect of different additives on carbonation reaction (140 °C, 100 g/L solid/liquid ratio, 500 rpm stirring rate, 20 bar initial CO_2 pressure).

efficiency can be explained using the solubility product constant of calcite, K_{sp}:

$$K_{sp} = \left[Ca^{2+}\right] \times \left[CO_3^{2-}\right] \quad (15)$$

where $[Ca^{2+}]$ is the concentration of calcium ions, and $[CO_3^{2-}]$ is the concentration of carbonate ions. Although elevated temperatures significantly reduce the concentration of carbonate ions by decreasing the solubility of CO_2 in the liquid phase, adding 0.5 mol/L Na_2CO_3 can effectively maintain CO_3^{2-} concentration in the liquid phase not only by its ionization to release CO_3^{2-} but also by dissolving more CO_2 from gas phase because of its high pH [42]. Based on the discussion in Section 3.2, we believe that the increased carbonation efficiency is mainly contributed by the conversion of calcium from the amorphous phase. Elevated temperatures can effectively make more unreactive calcium available for carbonation, and a high concentration of calcium and carbonate ions benefits the precipitation of calcium carbonate. Carbonation efficiency can therefore be significantly improved by the combination of increased temperature and Na_2CO_3. Similar results were obtained in the study carried out by Chen et al. [42] who found out that the increased concentration of carbonate ions improved the precipitation of extracted Mg^{2+}, therefore increasing the carbonation efficiency of serpentine.

3.4.3. Effect of different additives

Carbonation experiments were conducted in the batch reactor in the presence of various additives at 140 °C and initial CO_2 pressure of 20 bar for a reaction time of 2 h. Fig. 9 shows that carbonation efficiency of carbonation reactions with different additives decreases in the following order: 0.5 mol/L Na_2CO_3 > 0.5 mol/L Na_2CO_3 & 0.5 mol/L NaCl > 0.5 mol/L $NaHCO_3$ > H_2O. Both Na_2CO_3 and $NaHCO_3$ can help maintain the CO_3^{2-} concentration in the liquid phase as the temperature rises. Since the pH of $NaHCO_3$ is lower than that of Na_2CO_3, Na_2CO_3 can provide more CO_3^{2-} by absorbing more CO_2 than $NaHCO_3$, which results in higher carbonation efficiency within the same reaction time. Adding NaCl can improve the carbonation of natural minerals such as serpentine and olivine, because it improves the solubility of magnesium silicate, and helps leach the magnesium ions from the silicate matrix [42]. However, adding NaCl also increases the solubility of magnetite, which would be counter-productive [41]. In the case of fly ash, carbonation efficiency in the presence of 0.5 mol/L Na_2CO_3 is higher than that in the presence of a mixture of 0.5 mol/L Na_2CO_3 & 0.5 mol/L NaCl. This is because even though adding NaCl can increase the solubility of $Ca(OH)_2$ and help leach Ca from fly ash to the liquid phase, it also increases the solubility of $CaCO_3$ in the liquid phase, which hinders the precipitation of $CaCO_3$ [42].

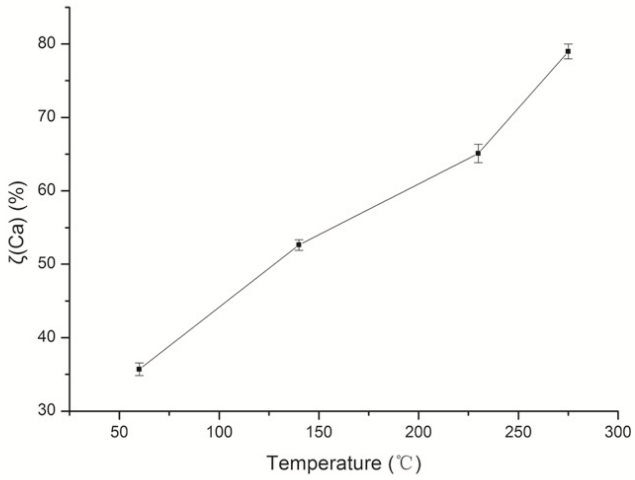

Fig. 8. Effect of temperature on carbonation reaction with 0.5 mol/L Na_2CO_3 (500 rpm stirring rate, 100 g/L solid/liquid ratio, 20 bar initial CO_2 pressure).

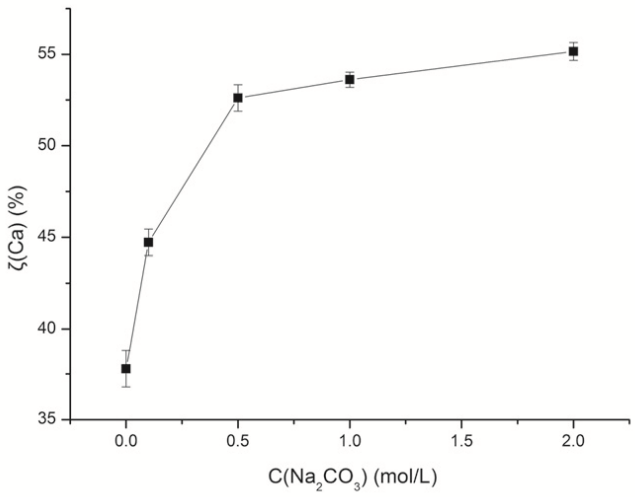

Fig. 10. Effect of Na_2CO_3 concentration on carbonation reaction (140 °C, 100 g/L solid/liquid ratio, 500 rpm stirring rate, 20 bar initial CO_2 pressure).

Table 4
Total inorganic carbon (TIC) results of multiple-cycle experiments.

Step	Experimental steps	Conditions	TIC (ppm)	ζ_{Ca} (%)
0	–	250 mL 0.5 mol/L Na_2CO_3	5590	–
1	First carbonation	20 g fresh ash, no CO_2 gas, 200 mL 0.5 mol/L Na_2CO_3, 275 °C, 2 h	4728	80.53
2	Second carbonation	15 g fresh ash, no CO_2 gas, 150 mL filtrate from Step 1, 275 °C, 2 h	3340	68.26
3	First regeneration of Na_2CO_3	15% CO_2 gas, 135 mL filtrate from Step 2, 25 °C, 3 h	8145	–
4	Third carbonation	13.5 g fresh ash, no CO_2 gas, 135 mL filtrate from Step 3, 275 °C, 2 h	4740	79.06
5	Second regeneration of Na_2CO_3	15% CO_2 gas, filtrate from Step 4, 25 °C, 3 h	8412	–
6	Fourth carbonation	11 g fresh ash, no CO_2 gas, 110 mL filtrate from Step 5, 275 °C, 2 h	5040	78.69

3.4.4. Effect of Na_2CO_3 concentration

Carbonation experiments were conducted in the batch reactor using different concentrations of Na_2CO_3 at 140 °C and initial CO_2 pressure of 20 bar for a reaction time of 2 h. The carbonation efficiency increased remarkably when the concentration of Na_2CO_3 increased from 0 to 0.5 mol/L (Fig. 10). However, once Na_2CO_3 concentration reached 0.5 mol/L, further increases had very little influence on carbonation efficiency. The effect of Na_2CO_3 concentration on carbonation efficiency can be explained using the solubility product constant of calcite, K_{sp} (shown in Eq. (15)). High concentration of Na_2CO_3 provides more carbonate ions which enhances the precipitation of calcium carbonate. In addition, the pH value of Na_2CO_3 solution also affects carbonation efficiency. The pH values of Na_2CO_3 solution at different concentration (0.1, 0.5, 1.0, and 2.0 mol/L) and room temperature are 11.29, 11.37, 11.40, and 11.58 respectively which increase with an increase in concentration. High pH value enhances CO_2 transfer from the gas phase to the aqueous phase and then promotes the precipitation of $CaCO_3$. This is in good agreement with published results [45,46] in which the carbonation reaction was favourable at high pH values.

3.5. Multiple-cycle experiments

Table 4 shows the results of our multiple-cycle experiments which consists of six steps, as described in experimental section. Since no CO_2 gas was injected to the slurry during the first two carbonation reaction steps, the carbon sources for carbonation reaction was from Na_2CO_3 through reaction

$$Na_2CO_3 \leftrightarrow CO_3^{2-} + 2Na^+ \quad (16)$$

The concentration of TIC in the aqueous solution dropped from 5590 to 4728 ppm after the first carbonation reaction and then to 3340 ppm after the second carbonation reaction. OH^- concentrations was expected to increase through reaction Eqs. (10) and (11) [47]. The carbonation efficiency in the first carbonation step reached 80.5%, which was similar to the maximum valued obtained at high CO_2 pressure and in the presence of the same concentration of Na_2CO_3 (Fig. 8). With CO_3^{2-} concentration decreasing in the second concentration, the carbonation efficiency dropped to 68.3%. The results of the first and second carbonation steps further indicated that CO_3^{2-} concentration can significantly affect carbonation efficiency.

The results of Step 3 in Table 4 showed that the TIC concentration rose to 8145 ppm after one regeneration step, which indicates the makeup of the consumed CO_3^{2-} (regeneration of Na_2CO_3) was achieved via

$$CO_2(g) + OH^- \leftrightarrow HCO_3^- \quad (17)$$

and reaction Eq. (8) as well as CO_2 dissolution Eqs. (6)–(7). The results of Step 4 in Table 4 showed the carbonation efficiency increased back to about 80% by carbonation with the regenerated Na_2CO_3 solution. However, the TIC concentration in Step 3 (8145 ppm) was much higher than that in the initial Na_2CO_3 solution of Step 1, which suggested that a significant amount of HCO_3^- was present in the solution (production of $NaHCO_3$) [47]. The decrease of TIC concentration from Step 3 to Step 4 was larger than that from Step 0 to Step, which was due to carbon loss to the gas phase by decomposition of H_2CO_3 and $NaHCO_3$. The results of Steps 3–6 in Table 4 showed that Na_2CO_3 can be regenerated in multi-cycle.

3.6. Comparison of the carbonation efficiency of this work and previous work

Reported carbonation efficiencies vary from 10% to 80% for different processes as shown in Table 5. Given the relatively short reaction times of 2 h, a considerable carbonation efficiency (79%) was achieved in the batch reactor in this study, which is much higher than some of the results obtained in previous work [20,22–23,39]. Some other studies [17,19], however, required substantially longer reaction durations (> 4.5 h) to reach such high values. The results of this study reveal that CO_2 sequestration by aqueous mineralisation using Shenfu coal ash could be an attractive method to reduce the CO_2 emission from the power plant. The maximum CO_2 sequestration capacity could reach 0.102 kg/kg fly ash. This capacity seems smaller compared to that of some other industrial wastes such as steel slag. However, the annually generated volume of fly ash from Shenfu coal is very huge. Shenfu-

Table 5
Comparison of the experimental parameters and maximum carbonation efficiency of this work and previous work.

Paper	[19] (2008)	[17] (2009)	[20] (2011)	[22] (2012)	[22] (2012)	[23] (2014)	[39] (2016)	This work	This work
Reactor type	Semi-batch	Batch	Semi-batch	Column	Column	Batch	Batch	Semi batch	Batch
Ca content (%)	8.2	2.9	28.4	5.1	5.1	17.7	4.8	11.7	11.7
Temperature (°C)	25–75	25–60	25–80	~30	~30	20–80	~30	60–90	60–275
Solid/liquid ratio (g/L)	25–75	50–150	8333	100–330	100–330	1000–10,000	50–500	5–200	100
Initial CO_2 pressure (bar)	0.1–0.3	40	0.1–0.2	0.15	0.15	30	2–10	0.15	10–20
Gas flow rate (L/min)	1	–	3	0.02–0.08	0.02–0.08	–	–	60–350	–
Stirring ratio (rpm)	300–600	450	1500	–	–	60	900	500	500
Time (hour)	2–4.5	18	2	18	18	10	0.25–4	1.5	2
Maximum CO_2 storage capacity (kg/kg fly ash)	0.23	0.026	0.211	0.023	0.020	0.027	0.050	0.045	0.102
Maximum carbonation efficiency (%)	75	81.4	52.8	34.3	29.2	13.6	67.9	34.7	79
Additive	–	–	–	1 M NH_4Cl	Seawater	–			0.5 M Na_2CO_3

Dongsheng Coalfield is one of the eight largest coalfields in the world and the largest coalfield in China, and its annual output of coal reached 205 million tonnes in 2010.

4. Conclusions

This paper demonstrates the feasibility of using one Chinese fly ash for CO_2 mineral sequestration via aqueous carbonation. Semi-batch reactor carbonation experiments indicate that carbonation efficiency increases very quickly in the first 30 min of the reaction, and reaches a limit after 90 min. Gas flow rate and solid/liquid ratio have very small influence on carbonation efficiency, and it cannot be improved by increasing temperature alone, due to poor CO_2 solubility in the liquid phase at high temperatures. No lime or portlandite can be detected in carbonated sample, indicating that they reacted with CO_2 to produce calcite during the carbonation reaction. Calcium from anhydrite, brownmillerite and the amorphous phase partially reacted with CO_2 to form calcite during the carbonation reaction, but the reactivity of the Ca-bearing amorphous phase is much lower than that of lime and portlandite. Batch reactor carbonation experiments indicate that elevated temperature can effectively increase the amount of calcium available for carbonation, by diffusing calcium from the amorphous phase to the solution. A high concentration of CO_3^{2-} also increases calcium carbonate precipitation. Increasing temperature in the presence of Na_2CO_3 significantly improves carbonation efficiency, mainly via conversion of calcium from the Ca-bearing amorphous phase. The Na_2CO_3 is regenerated in the multiple-cycle process at ambient pressure and room temperature, making the reaction an efficient process.

Acknowledgment

Long Ji is grateful to China Scholarship Council for supporting his PhD studies in CSIRO under grant number 201406430029, to China University of Mining & Technology (Beijing) for funding from the 'Creating Outstanding Innovative Talent Project', and to Huaneng Clean Energy Research Institute for the opportunity to work in their laboratory.

References

[1] W. Seifritz, CO_2 disposal by means of silicates, Nature 345 (1990) 486.
[2] K.S. Lackner, C.H. Wendt, D. Butt, E. Joyce Jr., D. Sharp, Carbon dioxide disposal in carbonate minerals, Energy 20 (1995) 1153–1170.
[3] A. Sanna, A. Lacinska, M. Style, M.M. Maroto-Valer, Silicate rock dissolution by ammonium bisulphate for pH swing mineral CO_2 sequestration, Fuel Process. Technol. 120 (2014) 128–135.
[4] T. Hosseini, C. Selomulya, N. Haque, L. Zhang, Indirect carbonation of Victorian brown coal fly ash for CO_2 sequestration: multiple-cycle leaching-carbonation and magnesium leaching kinetic modeling, Energy Fuel 28 (2014) 6481–6493.
[5] L. He, D. Yu, W. Lv, J. Wu, M. Xu, A novel method for CO_2 sequestration via indirect carbonation of coal fly ash, Ind. Eng. Chem. Res. 52 (2013) 15138–15145.
[6] E.R. Bobicki, Q. Liu, Z. Xu, H. Zeng, Carbon capture and storage using alkaline industrial wastes, Prog. Energy Combust. Sci. 38 (2012) 302–320.
[7] X. Wang, M.M. Maroto-Valer, Dissolution of serpentine using recyclable ammonium salts for CO_2 mineral carbonation, Fuel 90 (2011) 1229–1237.
[8] Y. Sun, V. Parikh, L. Zhang, Sequestration of carbon dioxide by indirect mineralization using Victorian brown coal fly ash, J. Hazard. Mater. 209–210 (2012) 458–466.
[9] Z. Yao, X. Ji, P. Sarker, J. Tang, L. Ge, M. Xia, Y. Xi, A comprehensive review on the applications of coal fly ash, Earth Sci. Rev. 141 (2015) 105–121.
[10] Z. Yao, M. Xia, P. Sarker, T. Chen, A review of the alumina recovery from coal fly ash, with a focus in China, Fuel 120 (2014) 74–85.
[11] S. Pan, C. Hung, Y. Chan, H. Kim, P. Li, P. Chiang, Integrated CO_2 fixation, waste stabilization, and product utilization via high-gravity carbonation process exemplified by circular fluidized bed fly ash, ACS Sustain. Chem. Eng. 4 (2016) 3045–3052.
[12] M. Werner, S. Hariharan, A.V. Bortolan, D. Zingaretti, R. Baciocchi, M. Mazzotti, Carbonation of activated serpentine for direct flue gas mineralization, Energy Procedia 37 (2013) 5929–5937.
[13] M. Werner, S. Hariharan, D. Zingaretti, R. Baciocchi, M. Mazzotti, Dissolution of dehydroxylated lizardite at flue gas conditions: I. Experimental study, Chem. Eng. J. 241 (2014) 301–313.
[14] J.-H. Wee, A review on carbon dioxide capture and storage technology using coal fly ash, Appl. Energy 106 (2013) 143–151.
[15] A. Uliasz-Bochenczyk, E. Mokrzycki, Z. Piotrowski, R. Pomykala, Estimation of CO_2 sequestration potential via mineral carbonation in fly ash from lignite combustion in Poland, Greenh. Gas Control Technol. 1 (2009) 4873–4879.
[16] A. Uliasz-bochenczyk, E. Mokrzycki, M. Mazurkiewicz, Z. Piotrowski, Utilization of carbon dioxide in fly ash and water mixtures, Chem. Eng. Res. Des. 84 (2006) 843–846.
[17] G. Montes-Hernandez, R. Perez-Lopez, F. Renard, J.M. Nieto, L. Charlet, Mineral sequestration of CO_2 by aqueous carbonation of coal combustion fly-ash, J. Hazard. Mater. 161 (2009) 1347–1354.
[18] M. Back, M. Bauer, H. Stanjek, S. Peiffer, Sequestration of CO_2 after reaction with alkaline earth metal oxides CaO and MgO, Appl. Geochem. 26 (2011) 1097–1107.
[19] M. Back, M. Kuahn, H. Stanjek, S. Peiffer, Reactivity of alkaline lignite fly ashes towards CO_2 in water, Environ. Sci. Technol. 42 (2008) 4520–4526.
[20] M. Bauer, N. Gassen, H. Stanjek, S. Peiffer, Carbonation of lignite fly ash at ambient T and P in a semi-dry reaction system for CO_2 sequestration, Appl. Geochem. 26 (2011) 1502–1512.
[21] H.Y. Jo, J.H. Kim, Y.J. Lee, M. Lee, S.J. Choh, Evaluation of factors affecting mineral carbonation of CO_2 using coal fly ash in aqueous solutions under ambient conditions, Chem. Eng. J. 183 (2012) 77–87.
[22] H.Y. Jo, J.H. Ahn, H. Jo, Evaluation of the CO_2 sequestration capacity for coal fly ash using a flow-through column reactor under ambient conditions, J. Hazard. Mater. 241–242 (2012) 127–136.
[23] N.L. Ukwattage, P.G. Ranjith, M. Yellishetty, H.H. Bui, T. Xu, A laboratory-scale study of the aqueous mineral carbonation of coal fly ash for CO_2 sequestration, J. Clean. Prod. 103 (2015) 665–674.
[24] N.L. Ukwattage, P.G. Ranjith, S.H. Wang, Investigation of the potential of coal combustion fly ash for mineral sequestration of CO_2 by accelerated carbonation, Energy 52 (2013) 230–236.
[25] Y. Soong, D.L. Fauth, B.H. Howard, J.R. Jones, D.K. Harrison, A.L. Goodman, M.L. Gray, E.A. Frommell, CO_2 sequestration with brine solution and fly ashes, Energy Convers. Manag. 47 (2006) 1676–1685.
[26] M.G. Nyambura, G.W. Mugera, P.L. Felicia, N.P. Gathura, Carbonation of brine impacted fractionated coal fly ash: implications for CO_2 sequestration, J. Environ. Manag. 92 (2011) 655–664.
[27] R. Mark, K.T.S. Towler, P. Mooney, R.G. Hill, N. Moreno, X. Querol, Modelling of the glass phase in fly ashes using network connectivity theory, Chem. Eng. Technol. (2002).
[28] S. Vassilev, R. Menendez, D. Alvarez, M. Diaz-Somoano, M. Martinez-Tarazona, Phase-mineral and chemical composition of coal fly ashes as a basis for their multicomponent utilization. 1. Characterization of feed coals and fly ashes, Fuel 82 (2003) 1793–1811.
[29] S. Vassilev, R. Menendez, M. Diaz-Somoano, M. Martinez-Tarazona, Phase-mineral and chemical composition of coal fly ashes as a basis for their multicomponent utilization. 2. Characterization of ceramic cenosphere and salt concentrates, Fuel 83 (2004) 585–603.
[30] S. Vassilev, R. Menendez, A. Borrego, M. Diaz-Somoano, M. Martinez-Tarazona, Phase-mineral and chemical composition of coal fly ashes as a basis for their multicomponent utilization. 3. Characterization of magnetic and char concentrates, Fuel 83 (2004) 1563–1583.
[31] S. Vassilev, R. Menendez, Phase-mineral and chemical composition of coal fly ashes as a basis for their multicomponent utilization. 4. Characterization of heavy concentrates and improved fly ash residues, Fuel 84 (2005) 973–991.
[32] J. Han, An energy conglomerate incorporating coal mining, power generation and coal liquefaction, Proceedings of the 5th International Symposium on Mining Science and Technology, 20–22 October 2004 Xuzhou, Jiangsu, China.
[33] C. Ward, D. French, Determination of glass content and estimation of glass composition in fly ash using quantitative X-ray diffractometry, Fuel 85 (2006) 2268–2277.
[34] C. Ward, D. French, Relation between coal and fly ash mineralogy based on quantitative X-Ray diffraction methods, 2005 World of Coal Ash, 11–15 April, 2005 Lexington, Kentucky, United States.
[35] T. Hosseini, C. Selomulya, N. Haque, L. Zhang, Investigating the effect of the Mg^{2+}/Ca^{2+} molar ratio on the carbonate speciation during the mild mineral carbonation process at atmospheric pressure, Energy Fuel 29 (2015) 7483–7496.
[36] W. Huijgen, G. Witkamp, R. Comans, Mechanisms of aqueous wollastonite carbonation as a possible CO_2 sequestration process, Chem. Eng. Sci. 61 (2006) 4242–4251.
[37] W. Wang, Z. Luo, Z. Shi, K. Cen, Thermodynamic analysis of ash mineral phases in combustion of high-sulfur coal with lime, Ind. Eng. Chem. Res. 50 (2011) 3064–3070.
[38] O. Velts, M. Uibu, J. Kallas, R. Kuusik, Waste oil shale ash as a novel source of calcium for precipitated calcium carbonate: carbonation mechanism, modeling, and product characterization, J. Hazard. Mater. 195 (2011) 139–146.
[39] R. Dananjayan, P. Kandasamy, R. Andimuthu, Direct mineral carbonation of coal fly ash for CO_2 sequestration, J. Clean. Prod. 112 (2016) 4173–4182.
[40] E. Chang, S. Pan, L. Yang, Y. Chen, H. Kim, P. Chiang, Accelerated carbonation using municipal solid waste incinerator bottom ash and cold-rolling wastewater: performance evaluation and reaction kinetics, Waste Manag. 43 (2015) 283–292.
[41] E. Rendek, G. Ducom, P. Germain, Carbon dioxide sequestration in municipal solid waste incinerator (MSWI) bottom ash, J. Hazard. Mater. 128 (2006) 73–79.
[42] Z. Chen, W. O'Connor, S. Gerdemann, Chemistry of aqueous mineral carbonation for carbon sequestration and explanation of experimental results, Environ. Prog. 25 (2006) 161–166.
[43] Y. Wu, P. Xu, J. Chen, L. Li, M. Li, Effect of temperature on phase and alumina extraction efficiency of the product from sintering coal fly ash with ammonium sulfate, Chin. J. Chem. Eng. 22 (2014) 1363–1367.
[44] H. Li, J. Hui, C. Wang, W. Bao, Z. Sun, Extraction of alumina from coal fly ash by mixed-alkaline hydrothermal method, Hydrometallurgy 147–148 (2014) 183–187.
[45] X. Wang, M.M. Maroto-Valer, Optimization of carbon dioxide capture and storage with mineralisation using recyclable ammonium salts, Energy 51 (2013) 431–438.
[46] X. Wang, M.M. Maroto-Valer, Integration of CO_2 capture and mineral carbonation by using recyclable ammonium salts, ChemSusChem 4 (2011) 1291–1300.
[47] H. Konno, Y. Nanri, M. Kitamura, Crystallization of aragonite in the causticizing reaction, Powder Technol. 123 (2002) 33–39.

Pages 67-80 of this thesis have been removed as they contain published material. Please refer to the following citation for details of the article contained in these pages.

Ji, L., Yu, H., Yu, B., Zhang, R., French, D., Grigore, M., Wang, X., Chen, Z., & Zhao, S. (2018). Insights into carbonation kinetics of fly ash from Victorian lignite for CO_2 sequestration. *Energy and Fuels*, *32*(4), 4569-4578.

DOI: 10.1021/acs.energyfuels.7b03137

Applied Energy 225 (2018) 356–366

Contents lists available at ScienceDirect

Applied Energy

journal homepage: www.elsevier.com/locate/apenergy

Integrated absorption-mineralisation for low-energy CO_2 capture and sequestration

Long Ji[a,b,c], Hai Yu[c,*], Kangkang Li[c], Bing Yu[c], Mihaela Grigore[d], Qi Yang[e], Xiaolong Wang[f], Zuliang Chen[g], Ming Zeng[a], Shuaifei Zhao[b,*]

[a] School of Chemical & Environmental Engineering, China University of Mining & Technology (Beijing), Beijing 100083, China
[b] Department of Environmental Sciences, Macquarie University, Sydney, NSW 2109, Australia
[c] CSIRO Energy, Newcastle, NSW 2304, Australia
[d] CSIRO Energy, North Ryde, NSW 2113, Australia
[e] CSIRO Manufacturing, Clayton, VIC 3169, Australia
[f] Huaneng Clean Energy Research Institute, Beijing 102209, China
[g] Fujian Key Laboratory of Pollution Control and Resource Reuse, School of Environmental Science and Engineering, Fujian Normal University, Fuzhou 350007, China

HIGHLIGHTS

- The application of fly ash in chemical regeneration of amine absorbents for CO_2 capture and sequestration.
- Large CO_2 cyclic capacity and solvent regeneration efficiency.
- Low energy penalty and cost.
- Novel process without thermal regeneration, CO_2 compression, or geological storage.

ARTICLE INFO

Keywords:
CO_2 capture
Chemical regeneration
Carbonation
Piperazine
Multicycle
Fly ash

ABSTRACT

The high energy penalty of absorbent regeneration remains the most critical challenge hindering the large-scale application of amine-based carbon dioxide (CO_2) capture. To overcome this challenge, we developed an integrated CO_2 absorption-mineralisation (IAM) process in which the amine sorbent can be regenerated by a chemical method rather than the traditional thermal method. We investigated the technical feasibility of IAM and the associated mechanisms by adding calcium oxide or fly ash into CO_2-loaded amine solutions, including the five commonly used amines: monoethanolamine, diethanolamine, piperazine (PZ), N-methyldiethanolamine and 2-amino-2-methy-1-propanol. The performance stability of the optimised amine was verified in multicycle experiments. We also investigated the technical feasibility of IAM in practical applications using fly ash as a feedstock for absorbent regeneration. The CO_2 absorption and mineralisation experiments were performed in a bubble column and a stirred reactor respectively. Acid titration was used to measure the CO_2-loading of solid and liquid sample. FT-IR spectroscopy was used to analyse the species changes in the amine solutions during regeneration. The crystalline phases present in fresh and carbonated fly ash samples were determined by X-ray diffraction analysis. The results indicate that CO_2 absorbed by the five amine solutions was sequestered into carbonate precipitates at a moderate temperature (40 °C) and the amine absorbents were regenerated after carbonation reactions. PZ exhibited the largest cyclic loading (0.72 mol/mol) and regeneration efficiency (91%) among the five amines. PZ also achieved stable cyclic loading, regeneration efficiency and kinetic performance over five cycles of IAM experiments. When the industrial waste, fly ash was used, PZ displayed a cyclic loading of 4.2 mol/mol, lower than that of CaO but still 1.1 times higher than that of the thermal regeneration-based process. Compared with the traditional thermal regeneration-based CO_2 capture, the IAM process has great advantages in energy reduction and capital savings due to a larger cyclic CO_2 capacity, a requirement for less energy for amine regeneration and no need for CO_2 compression and pipeline transport. This technology has great potential for industrial applications, particularly with CaO-containing wastes, such as fly ash and other alkaline wastes.

* Corresponding authors.
E mail addresses: hai.yu@csiro.au (H. Yu), shuaifei.zhao@mq.edu.au (S. Zhao).

https://doi.org/10.1016/j.apenergy.2018.04.108
Received 22 February 2018; Received in revised form 21 April 2018; Accepted 30 April 2018
Available online 15 May 2018

Ji, L., Yu, H., Li, K., Yu, B., Grigore, M., Yang, Q., Wang, X., Chen, Z., Zeng, M., & Zhao, S. (2018). Integrated absorption-mineralisation for low-energy CO_2 capture and sequestration. Applied Energy, 225, 356-366. https://doi.org/10.1016/j.apenergy.2018.04.108

1. Introduction

Carbon dioxide (CO_2) is the major greenhouse gas contributing to global warming [1]. Post-combustion CO_2 capture (PCC) from large, stationary, fossil-fuel-based power plants, steel mills and other industrial sectors is a direct and effective option to mitigate CO_2 emissions in the near and middle term [2]. A number of PCC technologies have been developed, including amine scrubbing [3–8], membrane separation [1,2], solid adsorption [9,10] and mineralisation [11–16]. Of these, amine scrubbing is considered to be the leading technology for large-scale CO_2 capture and has been commercially realised in coal-fired power stations, such as the Boundary Dam and WA Parish power plants [17,18].

Amine-based scrubbing is a continuous, cyclic process involving CO_2 absorption and desorption. The solvent selectively absorbs CO_2 from the flue gas in an absorber at low temperatures (40–80 °C). CO_2 releasing and absorbent regeneration is conducted at elevated temperatures (100–140 °C) [1,2]. This method enables highly efficient removal of CO_2 from flue gas and the production of high-purity CO_2. Despite commercial applications, the amine-based technology still suffers from a significant energy penalty and high capital cost. For example, installing the current monoethanolamine (MEA) capture process in a coal-fired power plant would result in a loss of the overall thermal efficiency of 25–40% and a rise in the cost of electricity of 70–100% [19]. In general, the energy penalty mainly arises from the amine regeneration stage using high-temperature thermal heat, while the main capital cost comes from the columns and the rich/lean heat exchanger, which are significantly affected by the absorption rate and cyclic loading of the amine solution [19].

Extensive research has been carried out to reduce both the energy consumption of solvent regeneration and its capital cost by improving solvent performance [20,21] and implementing process improvements [22–25]. Since no single amine can include all desirable chemical and physical properties for CO_2 capture, the blended amine solvents are usually used to combine the optimum properties of individual amines such as high absorption capacity, fast absorption rate, low heat of absorption, low degradation and corrosion [26]. A widely-used absorbent formula is to combine primary or secondary amines that have fast absorption rates with tertiary amines that have high CO_2 absorption capacities and low heat requirements for CO_2 regeneration [27]. For instance, the regeneration heat of blended solvents can be reduced by the amines with low CO_2 regeneration heat. However, this approach also introduces the drawbacks of the individual amines in the solvent formulation. Besides the blended amines, recent studies indicated that metal additives such as copper can reduce the energy consumption of MEA regeneration by 13.2–24% by enhancing the regeneration rate and enlarging the cyclic CO_2 capacity [28]. Introducing catalysts into the solvents can also result in lower energy consumption for solvent regeneration by reducing the regeneration temperature [29–31]. As for process improvements, various advanced configurations have been proposed to reduce the absorbent regeneration duty, such as absorber inter-cooling, rich-split and stripper inter-heating. The most recent advanced process can reduce the overall energy consumption of the MEA process by 8–20% compared with the conventional configuration [19]. Using an inert, immiscible organic component as the purging gas in the regeneration process can allow a lower regeneration temperature (70–100 °C) and reduce the energy consumption by 38% compared with the traditional steam-based regeneration process [32].

Although the CO_2 capture performance has been largely improved by advanced absorbent performance and process configuration modifications, the energy penalty from thermal regeneration, accounting for more than 50% of total PCC energy consumption [19], is still too high for commercial applications. The environmental concerns of amine volatilisation and degradation and equipment corrosion resulting from the high regeneration temperatures also remain. Moreover, the CO_2 product needs to be compressed and transferred to a geological storage site, which results in further energy costs. To deal with these problems, new technologies of amine regeneration have been developed to reduce the large energy consumption in traditional thermal regeneration [33–36].

CO_2 mineralisation captures and stores CO_2 permanently and safely without long-term monitoring [16]. It is the accelerated process of natural rock weathering, where carbonic acid from the dissolution of CO_2 in rainwater is neutralised with alkaline metal minerals to form carbonate minerals [11]. The process was initially developed to use natural silicates as feedstocks, including serpentine, olivine and wollastonite, due to their high worldwide abundance [13,14]. The alkaline industrial wastes such as fly ash, carbide slag and steel slag can also be used as a feedstock for CO_2 mineralisation. These raw materials have low material costs, high reactivity, and are readily available near CO_2 emission sources without further pre-treatment [12,15]. However, CO_2 mineralisation is confronted by several challenges, the most critical of which being its slow reaction kinetics.

Considering the fast CO_2 absorption by aqueous amine and the low energy consumption of CO_2 mineralisation, a number of studies have been devoted to combining the amine scrubbing technology with CO_2 mineralisation to make use of the dual benefits of the two technologies and achieve energy-efficient CO_2 sequestration. Arti et al. [33] reported a chemical regeneration process to release CO_2 from the absorbent by conducting carbonation reactions between calcium chloride ($CaCl_2$) and CO_2-loaded amine solutions, in which the CO_2 absorbed by the amines was converted to carbonate solid without additional energy input. However, amine regeneration was not performed in their study. Kang et al. [36] improved the chemical regeneration process by conducting a carbonation reaction between calcium oxide (CaO) and a 2-amino-2-methy-1-propanol (AMP) solution, in which the CO_2 was released from AMP solutions and AMP was recovered in the carbonation reaction without thermal energy consumption. Li et al. [35] reported carbonation reactions between a CO_2-loaded MEA solution and wollastonite ($CaSiO_3$), in which MEA can be regenerated after carbonation reactions. Despite this previous research, there are still knowledge gaps to be filled before we can achieve amine-based CO_2 absorption and regeneration by a mineralisation process. The technical feasibility of the integrated process has not been confirmed by investigating the key performance indicators, such as amine regeneration efficiency, CO_2 cyclic loading and cyclic stability. The effect of various amine absorbents on the CO_2 mineralisation performance is unclear. The mechanisms involved in the amine regeneration by mineralisation, especially the reaction pathways between CO_2–amine mixtures and alkaline metal oxide, are not fully understood. Previous studies using chemicals ($CaCl_2$ and CaO) rather than real materials as the feedstock for solvent regeneration would be hindered by the high cost of the un-recyclable chemicals. New feedstocks should be found to reduce the material costs and promote the practical application of this process.

The present study developed an integrated absorption-mineralisation (IAM) process for CO_2 sequestration from flue gas that integrates amine scrubbing, CO_2 mineralisation and amine regeneration in a single process. We investigated the technical feasibility of IAM and the associated mechanisms by adding CaO or fly ash into CO_2-loaded amine solutions, including the five commonly used amines: MEA, diethanolamine (DEA), piperazine (PZ), N-methyldiethanolamine (MDEA) and AMP. Amine-screening was also conducted through a thorough comparison of their performance in CO_2 absorption and chemical regeneration by mineralisation. The important parameters that characterise the performance of amines in PCC process were systematically investigated, such as CO_2 absorption capacity, cyclic capacity, and regeneration efficiency. The target material of this technology is the industrial waste that contains CaO, such as fly ash, to reduce the material costs. Considering the highly heterogeneous nature and diverse components of the wastes, we first selected the reaction-active CaO chemicals to gain insights into the carbonation mechanisms involved and the fundamental reaction pathways. The performance stability of the

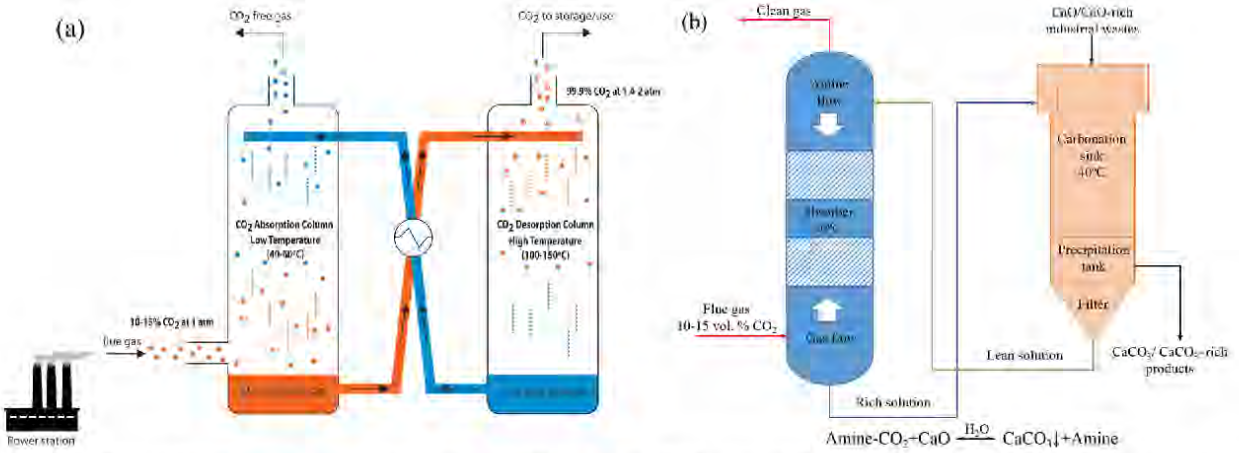

Fig. 1. (a) Process flow sheet of a conventional amine-scrubbing process, (b) Concept of the integrated absorption-mineralisation process.

optimised amine was verified in multicycle experiments. Then further experiments were conducted using fly ash as a feedstock to confirm the technical feasibility of IAM for commercial applications. The mineral changes of the fly ash before and after carbonation were characterised by X-ray diffraction (XRD) to provide a deeper understanding of the reaction mechanisms. Finally, we compared the IAM process with the traditional thermal regeneration to investigate potential energy savings.

The originality and novelty of the present work include (i) development of the IAM process and confirming its technical feasibility with various amines; (ii) investigation of the mechanisms of various amines in the IAM process; (iii) identification of the amine absorbent with best performance in IAM and exploring its performance stability in cyclic CO_2 absorption and chemical regeneration; (iv) the utilisation of fly ash for amine regeneration and CO_2 sequestration in one step.

2. Process description and chemistry

2.1. Process concept description

Fig. 1a shows the process flow sheet of a conventional, thermally regenerative CO_2 capture process and Fig. 1b shows the concept of amine-based CO_2 capture and chemical regeneration of absorbent by mineralisation. In Fig. 1b, CO_2 is first captured by an amine solvent in a CO_2 absorber, resulting in a CO_2-rich solution. Then the CO_2-loaded solution is transferred to the carbonation sink, where CaO or CaO-rich industrial wastes are added. Carbonation reactions occur between CaO and the CO_2-loaded solution, from which CO_2 is precipitated as $CaCO_3$, and the amine solvent is regenerated and sent back to the top of the absorber for continuous CO_2 capture. In such a cyclic process, CO_2 is sequestrated in the form of $CaCO_3$ and the amine is chemically regenerated through a pH swing instead of a temperature swing as is used in a conventional amine scrubbing process.

2.2. Process chemistry

The reaction pathways of CO_2 absorption-mineralisation involve three steps: CO_2 absorption, CO_2 mineralisation and absorbent regeneration. The most commonly used amine absorbents can be divided into two groups by their CO_2 absorption mechanisms. One group is carbamate-formation amines, including primary (e.g. MEA) and secondary (e.g. DEA) amines. The other group is bicarbonate-formation amines, including sterically hindered (e.g. AMP) and tertiary (e.g. MDEA) amines.

Firstly, in the CO_2 absorption step, carbamate-formation amines react with dissolved CO_2 to form a zwitterion (R_2R_2NCOOH) by reaction (1).

$$R_1R_2NH + CO_2(aq) \leftrightarrow R_1R_2NH^+COO^- \quad (1)$$

The unstable zwitterion subsequently deprotonates to the carbamate by giving a proton to a second amine molecule through reaction (2) [37].

$$R_1R_2NH^+COO^- + R_1R_2NH \leftrightarrow R_1R_2NCOO^- + R_1R_2NH_2^+ \quad (2)$$

This pathway leads to a maximum absorption capacity of 0.5 mol CO_2 per mole monoamines. The major benefit of this pathway is the rapid reaction rate, while the drawback is the high energy required to release CO_2 from the stable carbamate. At high CO_2-loading, since the pH value of the solution is decreased significantly, carbamate would react with a proton ion to form bicarbonate (HCO_3^-) through reaction (3) [38]

$$R_1R_2NCOO^- + H_2O \xleftrightarrow{K_{cm}} R_1R_2NH + HCO_3^- \quad (3)$$

where K_{cm} is the carbamate stability constant [39]. Steric hindrance can increase the conversion of carbamates to HCO_3^- and release amine to capture more CO_2, resulting in a higher CO_2 capture capacity [37]. Thus, sterically hindered (e.g. AMP) amines form HCO_3^- rather than carbamate after CO_2 absorption. Tertiary (e.g. MDEA) amines do not form carbamates. They act as bases to accept protons from the slow reaction of CO_2 with H_2O [37] through reactions (4) and (5).

$$H_2O + CO_2(aq) \leftrightarrow H^+ + HCO_3^- \quad (4)$$

$$R_1R_2R_3N + H^+ \leftrightarrow R_1R_2R_3NH^+ \quad (5)$$

This pathway significantly increases the capture capacity of the amines and reduces the energy required for CO_2 release, but suffers from a slow reaction rate. Thus, tertiary and sterically hindered amines typically have higher CO_2-loadings than primary and secondary amines and require a lower energy consumption for amine regeneration. The thermal regeneration reaction can be treated as the reverse of the absorption reaction. Specifically, for the carbamate formation amines, the thermal regeneration includes the decomposition of carbamate and deprotonation of the protonated amines. Regeneration of the HCO_3^- formation amines includes deprotonation of the protonated amines and decomposition of the HCO_3^-.

Secondly, in the mineralisation step, once CaO is added into the CO_2-loaded amine solution, the carbonation reactions occur. One mole of CaO introduced into the amine-CO_2–H_2O system can provide one mole of calcium ions (Ca^{2+}) and two moles of hydroxide ions (OH^-) through reaction (6).

$$CaO(s) + H_2O \rightarrow Ca^{2+} + 2OH^- \quad (6)$$

For the bicarbonate-formation amines, the Ca^{2+} and OH^- can react with HCO_3^- directly to precipitate as calcium carbonate ($CaCO_3$) through reactions (7) and (8) [40].

$$HCO_3^- + OH^- \leftrightarrow CO_3^{2-} + H_2O \quad (7)$$

$$Ca^{2+} + CO_3^{2-} \leftrightarrow CaCO_3 \downarrow \quad (8)$$

For the carbamate-formation amines, the process is more complex. The carbonation reactions between Ca^{2+} and (OH^-) can consume HCO_3^- in the solution through reactions (7) and (8), which would shift the equilibrium of reaction (3) forward to release more HCO_3^-.

In the absorbent regeneration step, the OH^- released by CaO can neutralize the protonated amines and convert them into fresh amines via reactions (9) and (10) for bicarbonate-formation amines and carbamate-formation amines, respectively [8].

$$R_1R_2R_3NH^+ + OH^- \leftrightarrow R_1R_2R_3\ N + H_2O \quad (9)$$

$$R_1R_2NH_2^+ + OH^- \leftrightarrow R_1R_2NH + H_2O \quad (10)$$

3. Materials and method

3.1. Materials

The reagents MEA (≥99%), DEA (≥98%), PZ (≥99%), AMP (≥95%), MDEA (≥99%), calcium carbonate ($CaCO_3$, reagent grade) and CaO (reagent grade) were purchased from Sigma-Aldrich. All amines were used without further purification. Amine solutions were prepared by dissolving the amines in deionised water. Carbon dioxide (CO_2, 99.5%) and nitrogen gases (N_2, 99.99%) were purchased from BOC Gases Australia.

The fly ash (FA) used in this study was collected from the fifth stage of electrostatic precipitators of the Huaneng Gaobeidian power plant in Beijing, which is run on Chinese black coal from Shenfu, Shanxi province. This raw material has been identified to be a suitable fly ash for CO_2 mineralization [41]. More detailed information on this fly ash can be found in our previous study [41]. The chemical composition of the fly ash is given in Table 1.

The theoretical CO_2 sequestration capacity of the fly ash can be calculated by Eq. (E1) [42].

$$Thm_{CO_2} = \frac{44}{56}\left(m_{CaO} - \frac{56}{100} \times m_{CaCO_3} - \frac{56}{80} \times m_{SO_3}\right) + \frac{44}{40} m_{MgO} \quad (E1)$$

where Thm_{CO_2} (g CO_2/g FA) is the theoretical CO_2 sequestration capacity, m_{CaO} (g CaO/g FA), m_{SO_3} (g SO_3/g FA), and m_{MgO} (g MgO/g FA) are the weight fractions of CaO, SO_3 and MgO, respectively in fresh samples and were calculated from XRF results [41]. m_{CaCO_3} (g $CaCO_3$/g FA) is the weight fraction of $CaCO_3$ in the fresh fly ash determined by acid titration. The theoretical CO_2 sequestration capacity of this fly ash is 97.5 g CO_2/kg fly ash.

3.2. Single absorption-mineralisation experiment

The bubble column system was used for CO_2 absorption (Fig. 2a). CO_2 (99.8% purity) and N_2 (99.9% purity) gases were mixed as a feed gas, with the flow rate controlled by Bronkhorst mass flow controllers. The mixed gas with 9% CO_2 in N_2 was humidified and bubbled through 200 mL aqueous amine solution (2 mol/L) in the bubble column with a flow rate of 1.7 L/min to obtain CO_2-rich solutions. The temperature of the column was maintained by a circulating water bath at 40 °C during CO_2 absorption. The CO_2 concentrations in the gas phase were recorded every 15 s using a Horiba VA-3000 gas analyser with a measurement range of 0–10 vol% CO_2. The CO_2 bubbling in the amine solution stopped when the CO_2 inlet concentration equalled the CO_2 outlet concentration.

Table 1
Elemental quantification of the fly ash used in this study, as determined by X-ray fluorescence spectroscopy.

Composition (wt.%)							
SiO_2	Al_2O_3	Fe_2O_3	CaO	MgO	Na_2O	K_2O	SO_3
42.80	19.15	9.06	16.41	1.23	1.68	1.50	1.9

The prepared solution was then transferred into a three-necked flask system (Fig. 2b) with a certain amount of CaO or fly ash added for amine regeneration by mineralisation. The CaO dosages (mol/mol) were defined as molar amount of CaO per mole of CO_2, while fly ash dosages (g/L) were defined as grams of fly ash added per litre of CO_2-rich amine solution. The solid sample was well mixed with the rich solution by a magnetic stirrer at 500 rpm. The pressure in the flask remained constant at atmospheric pressure throughout the experiment, and the temperature was maintained at 40 °C using a water bath. During the reaction, slurry samples (10 mL) were extracted with a syringe at 5, 10, 15, 20, 30 and 60 min. The extracted suspension was immediately filtered through a 0.2-μm nylon syringe filter. The filter cake was washed and then dried overnight in an oven at 40 °C, and then tested by acid titration to determine the volume of CO_2 carbonated in the solid powders. The filtrate was measured using a pH meter and acid titration to determine its pH value and CO_2-loading, respectively. 40 °C was selected in the CO_2 absorption and mineralisation because it has been widely accepted as the typical CO_2 absorption temperature for most liquid absorbents including those studied in this work. This temperature is close to the temperature of flue gas after flue gas desulphurisation and relatively high CO_2 absorption performance/loading and low energy consumption can be achieved at this temperature. Fourier transform infrared spectroscopy (FT-IR) was used to investigate chemical species in the filtrate. CO_2-loading of solid samples was defined as the molar amount of CO_2 captured per mole of calcium, while CO_2-loading of the amine solutions was defined as the molar amount of CO_2 captured per mole of amine absorbent. The cyclic loading and regeneration efficiencies were calculated by Eqs. (E2) and (E3).

$$Cyclic\ loading\ (\text{mol/mol}) = CO_2\ rich\ loading - CO_2\ lean\ loading \quad (E2)$$

$$Regeneration\ efficiency\ (\%) = \frac{CO_2\ rich\ loading - CO_2\ lean\ loading}{CO_2\ rich\ loading} \times 100\% \quad (E3)$$

3.3. Multicycle experiment

The process stability of absorption-mineralisation is very important. To investigate amine performance stability upon recycling, the best candidate among the five amines was selected for five cycles of CO_2 absorption and absorbent regeneration experiments, as shown in Fig. 3. Firstly, 200 mL of a CO_2-rich amine solution (2 mol/L) was prepared following the same procedures and conditions used in Section 3.2. CaO was then added to the rich solution with a 1.0 mol CaO/mol CO_2 dosage for amine regeneration. After a 15-min reaction, the suspension was immediately filtered through a 0.2-μm nylon filter to obtain the CO_2-lean solution. FT-IR was used to investigate chemical species in the lean solution. The overall gas phase mass transfer coefficient (K_G) of the CO_2-lean solution was measured using a wetted-wall column (WWC) [43]. The lean solution was then reused for four successive cycles of CO_2 absorption and regeneration experiments.

3.4. Characterisation

The acid titration for CO_2-loading measurement followed the standard method described by previous studies [44,45]. This method involved acidifying a precisely measured quantity of the liquid and solid samples by adding an excess nitric acid (HNO_3, 1 mol/L) aqueous solution. The volume of CO_2 released from the sample (V_{CO_2}) was measured at constant atmospheric pressure using two burettes, which was then used to calculate the CO_2-loading of the solid and liquid samples [44,45]. Reagent-grade calcium carbonate ($CaCO_3$) was used to assess the accuracy of this analytical method. Our results show that the

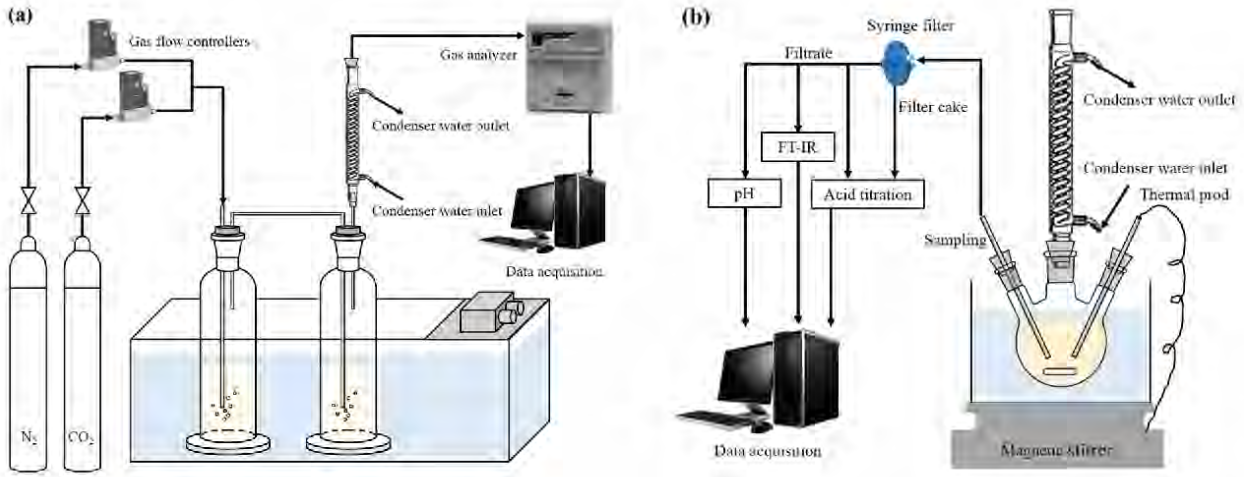

Fig. 2. Schematic diagram of CO_2 absorption (a) and regeneration (b) experiments.

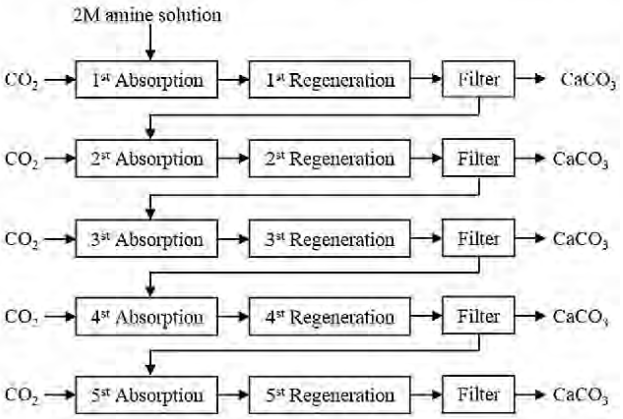

Fig. 3. Flow diagram of multicycle experiments.

average error of this method was ± 3%, indicating its validity for CO_2-loading measurements. FT-IR spectroscopy (VERTEX 70, Bruker Co. Ltd.) was used to analyse the species changes in the amine solutions during regeneration.

WWC was operated at 40 °C using circulating water from a thermostatic bath. A stainless steel column with effective height and external diameter of 8.21 cm and 1.27 cm, respectively, was used. The absorbent was pumped into the column at an appropriate flow rate to form a stable, thin film on the surface of the steel tube. The total flow rate of N_2 and CO_2 was fixed at 3.0 L/min and the partial pressure of CO_2 in the gas flow varied from 1 to 7 kPa. The concentration of CO_2 escaping from the WWC was measured by the gas analyser used to calculate the mass transfer coefficients. The calculation method was reported in previous work [43,46].

The crystalline phases present in fresh and carbonated fly ash samples were determined by XRD analysis. Fly ash samples were ground in an agate mortar and pestle and then packed into an aluminium holder. All samples were run on an Empyrean PANalytical X-ray Diffractometer using CuKα radiation at 40 kV and 40 mA. Step scans were conducted from 2 to 90° 2θ, with a step interval of 0.02° 2θ. Mineral phase identification was performed by the Bruker Eva software package.

4. Results and discussion

4.1. Chemical regeneration of five amines by CaO

The performance of five amines for CO_2 absorption and carbonation was assessed with the process indicator of the cyclic CO_2-loading and amine regeneration efficiency. Fig. 4a–e shows the pH values and CO_2-loading of the liquid and solid phases of the five amines as a function of reaction time, while Fig. 4f–j show the FT-IR spectra of the five amine solutions as a function of reaction time. Among the five amines, PZ exhibited the highest CO_2-loading of the rich solutions (0.79 mol/mol), followed by AMP, DEA, MEA and MDEA (0.74, 0.53, 0.51 and 0.44 mol/mol, respectively). When the CaO was added into the CO_2-rich amine solutions, the CO_2-loading of the solid phases increased while CO_2-loading of the five amine solutions decreased, during which CO_2 was transferred into the solid phases together with a rise in the solution pH. This observation is consistent with the hypothesised mechanism in Section 2.2. The dissolved CaO provided Ca^{2+} and OH^- via reaction (6). The released OH^- by CaO would react with protonated amine molecules via reactions (9) and (10), and thereby increase the pH value in the solution and regenerate fresh amine. The increased pH value then shifts the reaction (7) forward to produce CO_3^{2-}. The formation and precipitation of $CaCO_3$ occurred via reaction (8) which led to the increased CO_2-loading in the solid phase and the decreased CO_2-loading in the liquid phase. Carbamates can also participate in this process by producing HCO_3^- via reaction (3). In this way, the absorbed CO_2 in the form of carbamate and HCO_3^- can be transferred from the liquid phase into the solid phase, resulting in amine absorbent regeneration and CO_2 sequestration. The phenomenon was also demonstrated by the FT-IR results in Fig. 4f–j, which show an obvious increase in the peak intensity of fresh amine as a function of time. (The detailed peak assignment can be seen in the Supporting Information.) This confirmed that the amines were regenerated during the carbonation reactions. Fig. 4f–j also show a decline in the peak intensity of carbamates, CO_3^{2-}/HCO_3^-, and protonated amines as a function of reaction time. This confirms a reduction in CO_2-loading of the amine solutions during the regeneration process. More specifically, for the amines with bicarbonate-formation, Fig. 4i–j show a clear decrease in the intensity of the HCO_3^- and protonated amines peak as a function of time, confirming the CO_2-loading decline in MDEA and AMP solutions and the amine regeneration occurred via reactions (7)–(9). For the carbamate-formation amines (MEA, DEA and PZ), Fig. 4f–h show a decrease in peak intensity of the carbamates, CO_3^{2-}/HCO_3^-, and protonated amines, which demonstrated that both CO_3^{2-}/HCO_3^- and carbamate participated in the carbonation reactions.

Fig. 4a–e also show that the CO_2-loading of the five amine solutions decreased rapidly in the first 5 min of regeneration, which indicates that the carbonation reactions can be completed in a short time. This result is confirmed by a rapid decrease in the peak intensity of the carbamates, CO_3^{2-}/HCO_3^- and protonated amines during the initial 5 min of the carbonation reaction observed in Fig. 4f–j. Specifically, the CO_2-loading in PZ decreased by 0.53 mol/mol, followed by 0.30 mol/

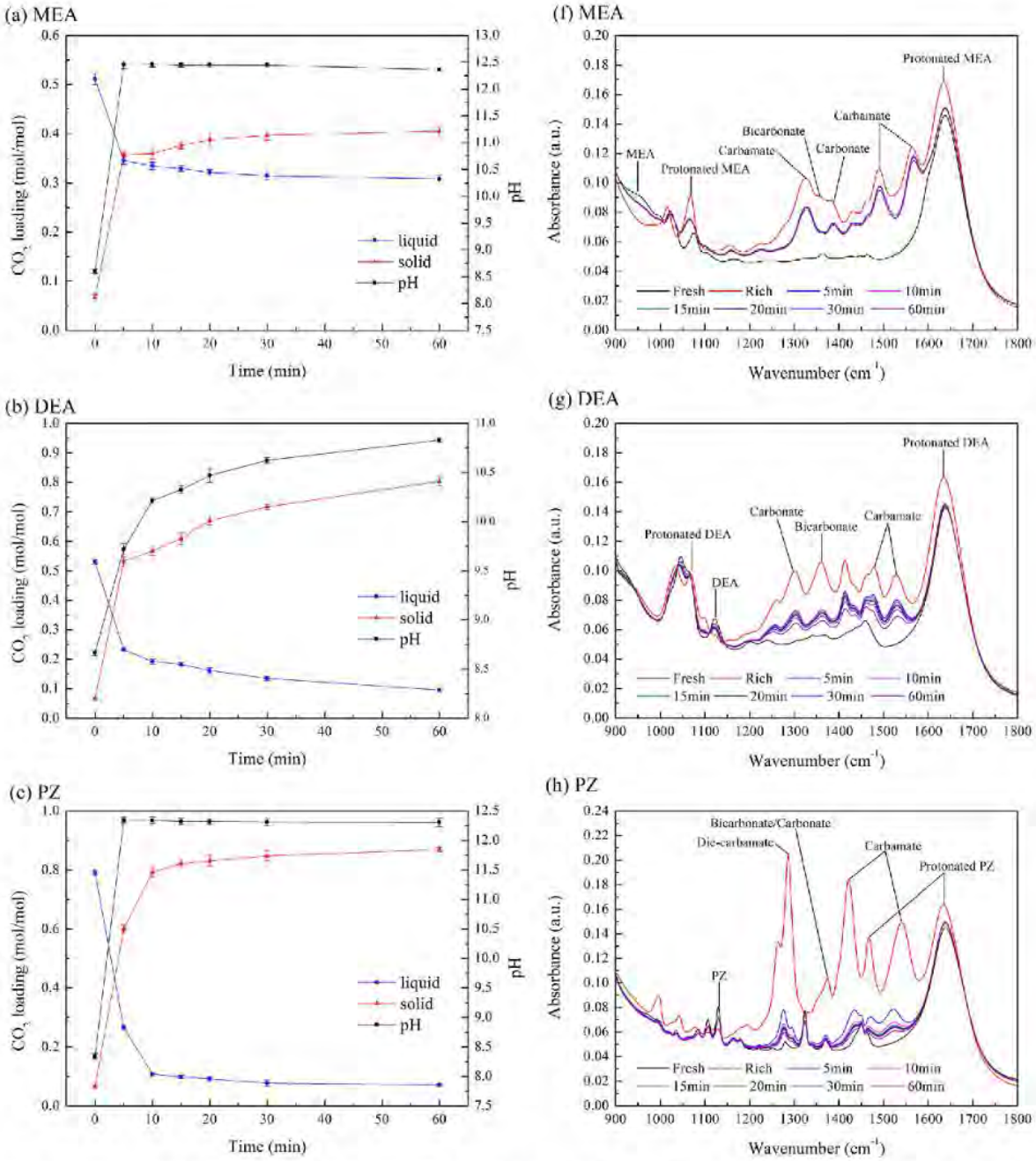

Fig. 4. Time profile of pH values and CO_2-loading of the liquid and solid phases in carbonation reactions with 2 mol/L MEA (a), DEA (b), PZ, (c), MDEA (d) and AMP (e) solutions with a 1.0 mol/mol-CO_2 CaO dosage; and the FT-IR spectra of the liquid phases for MEA (f), DEA (g), PZ (h), MDEA (i) and AMP (j) solutions in the carbonation reaction. The detailed peak assignments can be seen in the Supporting Information.

mol in DEA, 0.22 mol/mol in AMP, 0.17 mol/mol in MEA, and MDEA 0.12 mol/mol in MDEA. Carbonation reactions between CO_2-rich solutions and CaO are very complex and can be affected by many factors. For PZ, DEA and MEA, since they formed carbamate after CO_2 absorption, the carbamate might not directly participate in the carbonation reaction. Previous studies [8,39] suggest that steric hindrance can reduce the stability of primary and secondary amine carbamates and enhance their conversion into HCO_3^- through reaction (3). Lower carbamate stability can favour the formation of a higher HCO_3^- concentration in an amine solution and result in a deeper regeneration of amines. As shown in Table 2, the carbamate stability constant ($-\log_{10}K_{cm}$) decreased in the following order: $MEACO_2^-$ (1.76) > $PZCO_2^-$ (1.49) > $DEACO_2^-$ (0.92) > $PZ(CO_2^-)CO_2^-$ (0.34). The CO_2-loading decrease of DEA was significantly higher than MEA, even considering their similar initial CO_2-loading. This is likely to be due to the lower carbamate stability of DEA. As a diamine, PZ can form monocarbamate as well as dicarbamate after CO_2 absorption [47]. Although the PZ monocarbamate was more stable than DEA carbamate, PZ dicarbamate was far less stable than DEA carbamate, which promoted the formation of bicarbonate in the PZ solution and thereby led to a higher regeneration. The highest initial CO_2-loading in the PZ solution may also contribute to the fastest decrease in CO_2-loading at this early stage of the carbonation reaction compared with the other four amines. As for AMP and MDEA, they formed HCO_3^- rather than carbamate after CO_2 absorption. HCO_3^- can react with CaO directly in the solutions via reactions (7) and (8). Although MDEA and MEA displayed similar CO_2-loadings before regeneration, the CO_2-loading decrease of MDEA at 5 min was much lower than MEA, mainly because of the lower pH value of MDEA at 5 min compared with MEA, as shown in Table 2. A previous study [48] indicated that low pH values could shift the

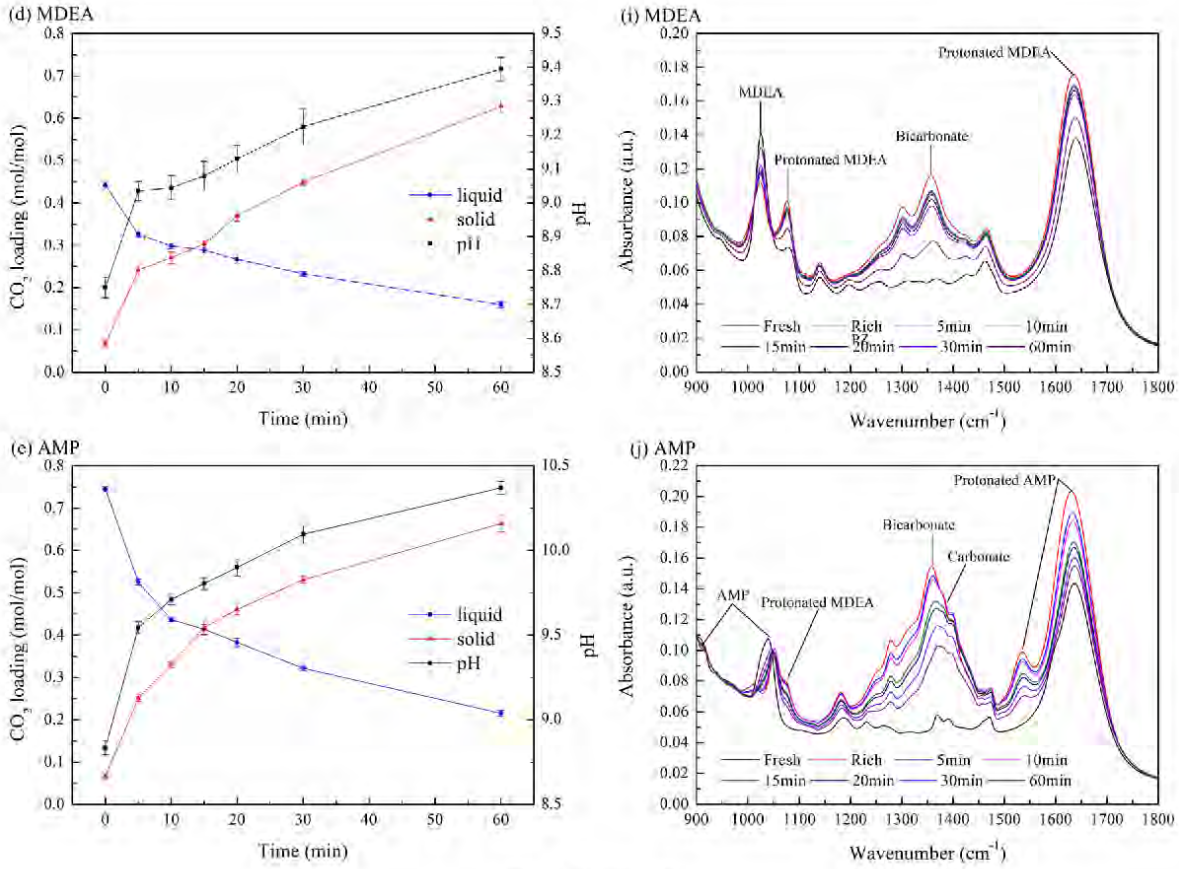

Fig. 4. (*continued*)

Table 2
Comparison of various amines in the carbonation reactions with various 2 mol/L amine solutions with a 1.0 mol/mol-CO_2 CaO dosage.

Parameter	Unit	MEA	DEA	PZ	MDEA	AMP
pH of fresh solution	–	12.2	11.6	12.2	11.3	12.3
pH of CO_2 rich solution	–	8.6	8.7	8.3	8.8	8.8
pH of CO_2 lean solution	–	12.4	10.8	12.3	9.4	10.4
CO_2-rich loading/absorption capacity	mol/mol	0.51	0.53	0.79	0.44	0.74
CO_2-lean loading (60 min)	mol/mol	0.31	0.10	0.07	0.16	0.22
Cyclic loading	mol/mol	0.20	0.44	0.72	0.28	0.53
Regeneration efficiency (5 min)	%	33	56	67	26	29
Regeneration efficiency (60 min)	%	40	82	91	64	71
Carbamate stability ($-\log_{10}K_{cm}$) [39]	–	1.76	0.92	1.49	–	–
Dicarbamate stability ($-\log_{10}K_{cm}$) [47]	–	–	–	0.34	–	–

equilibrium of reaction (3) backwards and thereby hinder the formation of CO_3^{2-}. The low pH value of MDEA led to a low concentration of CO_3^{2-} which hindered the precipitation of $CaCO_3$.

After 5 min, the CO_2-loading of the five amine solutions decreased slightly. Specifically, after 20 min of carbonation, the CO_2-loading of the PZ and MEA solutions stabilised at about 0.08 mol/mol and 0.31 mol/mol, respectively, with 91% and 40% regeneration efficiency achieved, respectively. This suggests that there was not much CO_2 transferred from the liquid to solid phase during this stable stage, though the CO_2-loading of the MEA solution was still high. The large MEA carbamate peak intensity after 20 min, as shown in Fig. 4f, confirms that a large amount of carbamate still existed in the solution and was not regenerated after carbonation reactions, mainly because of the high stability of the MEA carbamate. The rapid increase in pH value might also hinder the conversion of MEA carbamate into HCO_3^- because the increased OH^- would shift reaction (3) backwards. Unlike MEA, the less stable PZ carbamates underwent a deeper regeneration after carbonation reactions. The CO_2-loadings of the DEA, MDEA and AMP solutions continuously decreased after 5 min and decreased to 0.10, 0.16, and 0.22 mol/mol at 60 min, with regeneration efficiencies of 82, 64 and 71%, respectively. It should be noted that the carbonation reactions in these amine solutions can still continue slowly beyond 60 min.

Overall, PZ exhibited the highest cyclic loading (0.72 mol/mol) and largest regeneration efficiency (91%) in the IAM process than the other four amines in this study. Also, the regeneration of the PZ solution can be very fast and completed in a short time (15 min), which is beneficial for reducing the size of the carbonation reactor. These properties position PZ as an attractive solvent in the IAM process.

4.2. *Multicycle absorption-mineralisation performance of PZ*

In the continuous and cyclic absorption-mineralisation process, the absorbent is supposed to be operated steadily at a high absorption rate, cyclic loading and regeneration efficiency. Regeneration by mineralisation should take place quickly to permit short reaction times and thereby reduce capital costs. Multicycle experiments were carried out with 2 mol/L PZ to investigate the technical performance of the absorption and regeneration process, including the amine's reactivity with CO_2 and capability of CO_2 absorption. Fig. 5a presents the pH values and CO_2-loading of PZ solutions in five cycles of absorption-mineralisation. The results indicate that PZ has stable performance, and there is no obvious decline in cyclic loading and regeneration efficiency over the five cycles, with an average cyclic loading of 0.69 mol/mol. The average pH of the five lean solutions is 12.3, which is very close to the fresh PZ solution (12.2, Table 2), also confirming that there is not much decline in the absorption capacity of the absorbent as the number of regeneration cycles increased [38]. FT-IR spectroscopy (Fig. S1) also confirms that CO_2 was effectively removed from the amine solutions,

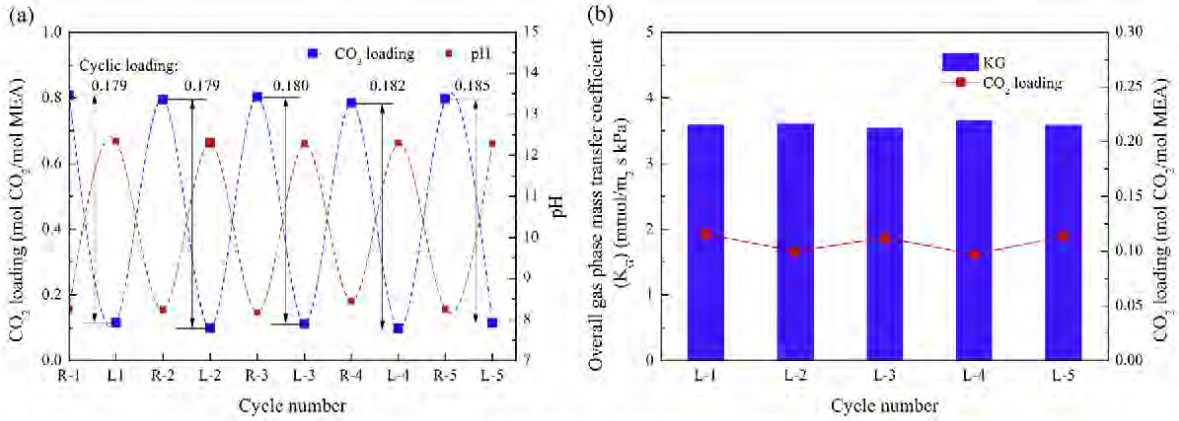

Fig. 5. (a) CO_2-loading and pH values of a 2 mol/L PZ solution in five cycles of CO_2 absorption-mineralisation at a 1.0 mol/mol-CO_2 CaO dosage (R-i: rich solution of cycle i; L-i: lean solution of cycle i), (b) K_G of a 2 mol/L PZ lean solution in five cycles of CO_2 absorption-chemical regeneration at a 1.0 mol/mol-CO_2 CaO dosage.

and that the amine solutions can be well regenerated in the regeneration of every cycle. Only slight changes in chemical species occurred in the rich and lean solution over five cycles.

Since the regeneration efficiency was not 100% in the experiments, some CaO remained in the slurry after the carbonation and before the filtration. The concentration of Ca^{2+} in the regenerated amine solutions can be calculated from thermodynamics. The concentration can be calculated by Eq. (E4).

$$[Ca^{2+}] = \frac{K_{sp}}{[OH^-]} = \frac{K_{sp}}{10^{pH-14}} = 1.3 \times 10^{-4}\ \text{mol/L} \quad \text{(E4)}$$

where the K_{sp} of calcium hydroxide at 40 °C is 6.64×10^{-6} [49], and the average pH of the lean solution in multicycle experiments was 12.3 (Fig. 5a). The concentration of Ca^{2+} after the carbonation reaction relied greatly on the pH value of the lean solution. Fig. 5a in the present paper shows that the pH values of the lean solutions over the five cycles were very stable, indicating that the concentration of Ca^{2+} in the lean solutions were also similar. Thus, calcium ions did not accumulate in multiple cycles.

The overall mass transfer coefficient (K_G) was measured to evaluate the CO_2 absorption kinetics of the amines. Fig. 5b shows the K_G of 2 mol/L PZ solution in five successive cycles of absorption and regeneration. There was only a very slight change in K_G, and no obvious loss of the kinetic performance of the PZ solution in CO_2 capture over the five cycles.

4.3. Regeneration of PZ by mineralisation of fly ash

To confirm the technical feasibility of IAM for commercial applications, further experiments were conducted using fly ash as a feedstock. Fig. 6a–b shows the CO_2-loading and pH values of PZ solutions as a function of reaction time at three levels of fly ash dosages (the weight of fly ash added per litre of solution). Before regeneration, the PZ solution had a CO_2-loading of 0.79 mol/mol. After the fly ash was added into the PZ solutions, CO_2-loading of the PZ solutions decreased, while the pH value of the solution increased. The FTIR results in Fig. S2 show that the intensity of PZ carbamate peaks (1524, 1432, 1276 and 1294 cm^{-1}), the protonated PZ (1475 cm^{-1}) peak, the bicarbonate (1360 cm^{-1}) peak and the carbonate (1388 cm^{-1}) peak decreased during the carbonation reaction. The results confirm that PZ carbamates and CO_3^{2-}/HCO_3^- would take part in the carbonation reactions with fly ash, and that the PZ can be regenerated after carbonation reactions. Fig. 6a also shows that the CO_2 loading of the PZ solution decreased rapidly in the first 5 min of the carbonation reaction (from the initial 0.79 mol/mol to 0.4 mol/mol) and became stable thereafter. The results indicate that the CaO-containing fly ash behaves in a similar way to CaO and was able to regenerate the CO_2 loaded solutions quickly at mild conditions (temperature of 40 °C and atmospheric pressure). However, Fig. 6a and Table 3 clearly show that the regeneration efficiency and solution pH of the PZ solution with fly ash dosages was lower than that with aCaO dosage even when the actual calcium dosages were similar. This observation results from the highly heterogeneous nature and low reactivity of fly ash.

Fly ash is a highly heterogeneous mixture of minerals, and generally consists of three types of components: crystalline minerals, unburnt carbon particles, and non-crystalline aluminosilicate glass. The XRD results of the fresh fly ash (Fig. 7a) shows that the calcium in this fly ash is present as several crystalline phases including lime (CaO), portlandite

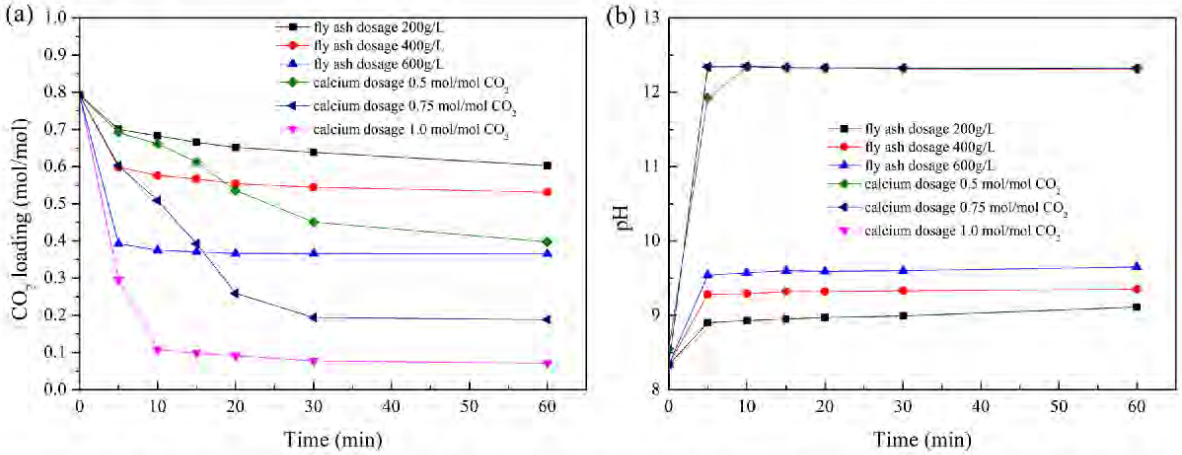

Fig. 6. Time profile of CO_2-loading (a) and pH values (b) of a 2 M PZ solution during chemical amine regeneration at different fly ash or CaO dosages.

Table 3
Comparison of the performance of fly ash with CaO.

Parameter	Fly ash dosage (g/L)			Calcium dosage (mol/mol)		
	200	400	600	0.5	0.75	1.0
Rich loading (mol/mol)	0.79	0.79	0.79	0.79	0.79	0.79
Lean loading (mol/mol)	0.60	0.53	0.37	0.40	0.19	0.07
Regeneration efficiency (%)	0.24	0.33	0.53	0.49	0.76	0.91
Actual calcium dosage (mol Ca/mol CO_2)	0.44	0.88	1.33	0.50	0.75	1.00

($Ca(OH)_2$), calcium sulfate ($CaSO_4$) and gypsum ($CaSO_4{\cdot}H_2O$). Our previous work [41] reported that the calcium is also present in an amorphous phase. After carbonation, most of the lime and portlandite disappeared as shown in Fig. 7b, while the peak of calcium carbonate increased significantly. This result confirms that these phases were converted into calcium carbonate in the carbonation reactions. Also, calcium sulfate, gypsum and amorphous phases may only partially take part in carbonation reactions due to their low reactivity [34]. Thus, to assess the performance of fly ash, it is very important to calculate the active calcium of this fly ash available for carbonation reactions. Given that the theoretical CO_2 sequestration capacity of the fly ash is 97.5 g CO_2/kg fly ash, the actual calcium dosage of fly ash can be calculated based on the theoretical CO_2 sequestration capacity of this fly ash (Table 3). The highly heterogeneous nature of fly ash leads to a low theoretical CO_2 sequestration capacity. The actual calcium dosage reflects the amount of calcium available for carbonation reactions in the CO_2-rich PZ solution. As shown in Fig. 6a, a larger fly ash dosage is likely to lead to a higher PZ regeneration efficiency. The extent of the solvent regeneration depends on the CaO content, chemical-physical properties of the alkaline waste, dosages and many other factors. To achieve a high PZ regeneration efficiency, a high fly ash dosage is preferred. Although the high fly ash dosage leads to the problem of stirring and liquid–solid separation, the fly ash-based IAM is still a promising technology to effectively reduce the energy penalty of amine regeneration.

4.4. Comparison of regeneration methods

The IAM process has significant advantages over conventional amine scrubbing (Table 4). Specifically, it greatly reduces energy consumption, particularly for absorbent regeneration and CO_2 compression. A conventional amine scrubbing process would result in a 25–40% decrease in thermal efficiency and a 70–100% rise in the cost of electricity in coal-fired power stations [19]. In contrast, the IAM involves negligible energy cost, since the CO_2 carbonation reaction takes place at a low temperature of 40 °C, which is the same as the absorption temperature. Instead of energy consumption, it is anticipated that the heat released in the mineral carbonation reaction could be reused, as CO_2 carbonation is exothermic. Particularly, considering that the stripper

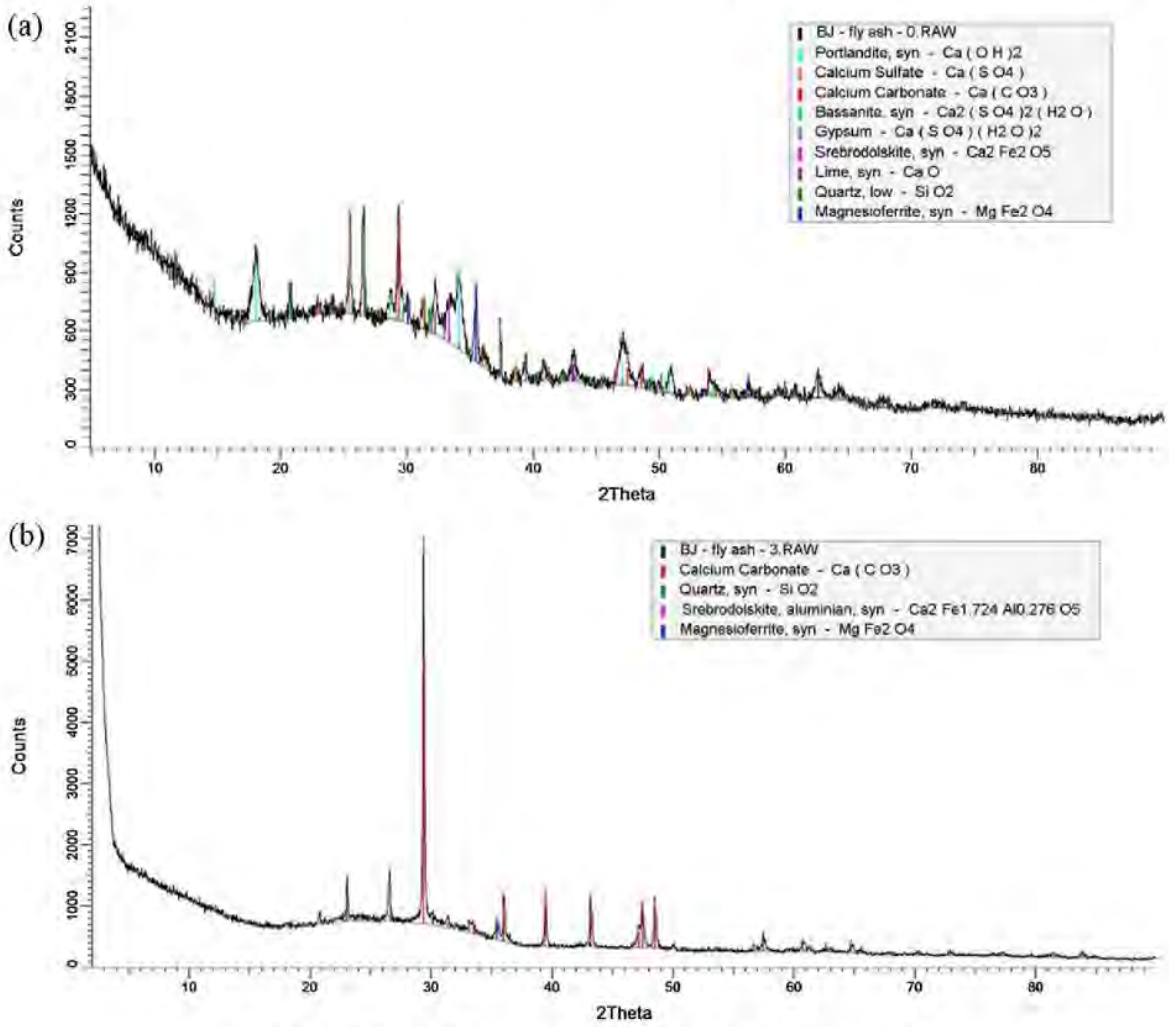

Fig. 7. X-ray diffraction patterns of (a) fresh fly ash and (b) carbonated ash.

Table 4
Comparison of the chemical regeneration process with the conventional PZ process.

CO2 capture technology	IAM (CaO)	IAM (fly ash)	Conventional amine scrubbing[a]	Advanced amine scrubbing [50]
	Experimental/simulation conditions			
Solvent concentration, mol/L	2	2	2	4.7
Flue gas CO_2, kPa	9	9	9	12
Absorption temperature, °C	40	40	40	40
Regeneration pressure, atm	1	1	2	8.2
Temperature approach of heat exchanger, K	–	–	10	5
	Experimental/simulation results			
CO_2-loading after absorption, mol/mol	0.79	0.79	0.79	0.80
CO_2-loading after regeneration, mol/mol	0.07	0.37	0.07	0.60
Cyclic CO_2-loading, mol/mol	0.72	0.42	0.72	0.20
Regeneration temperature, °C	40	40	121	150
Regeneration duty, MJ/kg CO_2	0	0	4.3	2.1
Product	$CaCO_3$	Fly ash rich with $CaCO_3$	CO_2	CO_2

[a] Results were obtained from the Aspen plus process simulation[24,51].

reboiler duty and the CO_2 compression duty were the two largest power consumers, accounting for ~55% and ~30% of the total energy consumption, respectively, the IAM can significantly reduce the energy consumption compared with conventional amine scrubbing. Without thermal regeneration, potential environmental issues resulting from amine volatilisation and degradation at the high regeneration temperature of the conventional process would also be avoided.

IAM also enables deeper amine regeneration. The CO_2-loading of the PZ solution decreases from 0.79 to 0.07 mol/mol after the carbonation reaction with CaO, providing a cyclic loading 3.6 times higher than that of advanced amine scrubbing using PZ (Table 4). If the industrial waste, fly ash, is used, the CO_2-loading of the PZ solution decreases from 0.79 to 0.37 mol/mol after carbonation, providing a cyclic loading of 4.2 mol/mol – still 1.1 times higher than that of advanced amine scrubbing using PZ (Table 4). The CO_2-leaner solvent and larger cyclic CO_2 capacity can greatly improve CO_2 absorption performance and reduce the size of the CO_2 absorber.

In addition, the IAM process simplifies the chain of CO_2 capture and storage. Compared with the traditional amine process, chemical regeneration does not require the stripper, heat exchanger, CO_2 compressor and the geological CO_2 storage site, which significantly saves capital and operational costs. The product obtained from CO_2 carbonation can be used as a value-added material in other industries. Overall, the IAM process shows its competitiveness over current thermal regeneration and its great potential for industrial applications.

4.5. *Industrial wastes for IAM and potential utilisation of the product*

The present study has confirmed the technical feasibility of the fly ash-based IAM process in absorbent regeneration and CO_2 sequestration. Fly ash behaves in a similar way to CaO, indicating that IAM can be used in a CO_2 emission site that produces alkaline wastes. Industrial waste-based IAM process can be applied worldwide. In 2010, the global production of coal fly ash was approximately 780 million metric tons (MT) [52]. The specific coal fly ash production by country was 395 Mt in China, 118 Mt in North America, 105 Mt in India, 52.6 Mt in Europe and 31.1 Mt in Africa [52]. Technologies have been developed to utilise this residue in construction material production, but only 53% of the fly ash was used for this purpose in 2010. The unused fly ash is frequently stored in waste piles or landfills and can be a potential environmental hazard. The application of the IAM process can help to improve the utilisation of this fly ash. Besides fly ash, other alkaline wastes rich in CaO are also suitable for the IAM process, including carbide slag, steel slag and kiln dust, with worldwide productions being 25 Mt, 400 Mt and 150 Mt, respectively.

The IAM process can not only reduce the CO_2 emissions, but can also increase the stability of industrial wastes, thus expanding their utilisation in the production of construction materials. For example, fly ash normally contains active species, such as CaO and MgO, meaning that blended cement or concrete containing fly ash could gradually absorb moisture from the air and cause expansion during the product's life cycle. Heavy metals, such as Hg, Pb, Cr, and Cd ions, leaching from fly ash-containing materials might result in negative impacts on the environment and human health. After the carbonation reaction, the potential for heavy metal leaching and uncontrollable expansion can be reduced or even eliminated. The CaO, $Ca(OH)_2$ and $CaSO_4$ contents significantly decrease and are converted into carbonates. The changes in the physico-chemical properties of carbonated fly ash were found to be beneficial for subsequent use in cement and concrete. Other potential applications for the carbonated products include reclamation of low lying areas, roads and embankments, mine filling, building materials and agricultural activities.

5. Conclusion

This study investigated the technical feasibility of the chemical regeneration of amine-based absorbents by CO_2 mineralisation. The regeneration process involves the reaction of the CO_2-rich amine solutions with CaO or CaO rich fly ash and the transfer of CO_2 from the rich amine solutions to the calcium carbonate precipitates to achieve the solvent regeneration. Five typical amines (MEA, DEA, PZ, AMP and MDEA) were selected for absorption and chemical regeneration experiments. All of them were regenerated to a different extent after a carbonation reaction with CaO at 40 °C, and the absorbed CO_2 was precipitated effectively. PZ exhibited the largest cyclic loading (0.72 mol/mol) and regeneration efficiency (91%) among the five amines. Five cycles of absorption-chemical regeneration also confirmed that PZ achieved stable cyclic loading, regeneration efficiency and kinetic performance. If the industrial waste, fly ash, is used, PZ displayed a lower cyclic loading of 4.2 mol/mol, which is still 1.1 times higher than that of the advanced PZ based scrubbing process which uses thermal regeneration. A comparison of the chemical regeneration we show in this work with conventional amine processes shows that chemical regeneration can greatly reduce the energy penalty of amine-based CO_2 capture and have a potential for a significant reduction in CO_2 capture costs.

While the chemical regeneration process is a promising alternative technology for the reduction in the energy penalty of amine-based CO_2 capture, more detailed studies should be conducted to investigate any potential problems. The leaching and accumulation of various metals from fly ash may affect the CO_2 absorption performance and are likely to require a new amine-CO_2 contactor instead of a packing column. The dissolved metals may lead to amine degradation even though the operating temperature is low (40 °C). Future work will focus on the investigation of the leaching behaviours of the metals from fly ash and

their effect on amine degradation.

Acknowledgments

The views expressed herein are not necessarily the views of the Commonwealth, and the Commonwealth does not accept responsibility for any information or advice contained herein. Long Ji is grateful to Macquarie University for the Cotutelle-iMQRES scholarship, to China University of Mining & Technology (Beijing) for funding from the 'Creating Outstanding Innovative Talent Project', and to CSIRO Energy for the opportunity to work in their laboratories and access their resources.

Appendix A. Supplementary material

Supplementary data associated with this article can be found, in the online version, at http://dx.doi.org/10.1016/j.apenergy.2018.04.108.

References

[1] Boot-Handford ME, et al. Carbon capture and storage update. Energy Environ Sci 2014;7(1):130.
[2] Goto K, Yogo K, Higashii T. A review of efficiency penalty in a coal-fired power plant with post-combustion CO_2 capture. Appl Energy 2013;111:710–20.
[3] Rochelle GT. Amine scrubbing for CO_2 capture. Science 2009;325:1652–4.
[4] Yang N, et al., Aqueous ammonia (NH3) based post combustion CO2 capture: A review. Oil Gas Sci Technol-Rev IFP Energies Nouvelles, 2014;69(5):931–45.
[5] Yang X, et al. Computational modeling and simulation of CO_2 capture by aqueous amines. Chem Rev 2017;117(14):9524–93.
[6] Narku-Tetteh J, et al. Selection of components for formulation of amine blends for post combustion CO_2 capture based on the side chain structure of primary, secondary and tertiary amines. Chem Eng Sci 2017;170:542–60.
[7] Conway W, et al. Toward the understanding of chemical absorption processes for post-combustion capture of carbon dioxide: electronic and steric considerations from the kinetics of reactions of CO_2(aq) with sterically hindered amines. Environ Sci Technol 2013;47(2):1163–9.
[8] Muchan P, et al. Screening tests of aqueous alkanolamine solutions based on primary, secondary, and tertiary structure for blended aqueous amine solution selection in post combustion CO_2 capture. Chem Eng Sci 2017;170:574–82.
[9] Creamer AE, Gao B. Carbon-based adsorbents for postcombustion CO_2 capture: A critical review. Environ Sci Technol 2016;50(14):7276–89.
[10] Lee J, Han S-J, Wee J-H. Synthesis of dry sorbents for carbon dioxide capture using coal fly ash and its performance. Appl Energy 2014;131:40–7.
[11] Bobicki ER, et al. Carbon capture and storage using alkaline industrial wastes. Prog Energy Combust Sci 2012;38(2):302–20.
[12] Wang T, et al. Accelerated mineral carbonation curing of cement paste for CO_2 sequestration and enhanced properties of blended calcium silicate. Chem Eng J 2017;323:320–9.
[13] Wang X, Maroto-Valer MM. Integration of CO_2 capture and mineral carbonation by using recyclable ammonium salts. ChemSusChem 2011;4(9):1291–300.
[14] Wang X, Maroto-Valer MM. Optimization of carbon dioxide capture and storage with mineralisation using recyclable ammonium salts. Energy 2013;51:431–8.
[15] Wee J-H. A review on carbon dioxide capture and storage technology using coal fly ash. Appl Energy 2013;106:143–51.
[16] Zevenhoven R, Fagerlund J, Songok JK. CO_2 mineral sequestration: developments toward large-scale application. Greenhouse Gases-Sci Technol 2011;1(1):48–57.
[17] SaskPower, Boundary Dam Carbon Capture Project. http://www.saskpower.com/our-power-future/carbon-capture-and-storage/boundary-dam-carbon-capture-project/, 2014.
[18] Global CCS Institute Projects Database, Petra Nova Carbon Capture. https://www.globalccsinstitute.com/projects/petra-nova-carbon-capture-project, 2017.
[19] Li K, et al. Systematic study of aqueous monoethanolamine (MEA)-based CO_2 capture process: Techno-economic assessment of the MEA process and its improvements. Appl Energy 2016;165:648–59.
[20] Conway W, et al. Rapid CO_2 absorption into aqueous benzylamine (BZA) solutions and its formulations with monoethanolamine (MEA), and 2-amino-2-methyl-1-propanol (AMP) as components for post combustion capture processes. Chem Eng J 2015;264:954–61.
[21] Conway W, et al. CO_2 absorption into aqueous amine blended solutions containing monoethanolamine (MEA), N, N-dimethylethanolamine (DMEA), N, N-diethylethanolamine (DEEA) and 2-amino-2-methyl-1-propanol (AMP) for post-combustion capture processes. Chem Eng Sci 2015;126:446–54.
[22] Wang M, et al. Process intensification for post-combustion CO_2 capture with chemical absorption: A critical review. Appl Energy 2015;158:275–91.
[23] Li K, et al. Rate-based modelling of combined SO_2 removal and NH_3 recycling integrated with an aqueous NH_3-based CO_2 capture process. Appl Energy 2015;148:66–77.
[24] Li K, et al. Systematic study of aqueous monoethanolamine-based CO_2 capture process: model development and process improvement. Energy Sci Eng 2016;4(1):23–39.
[25] Jiang K, et al. Advancement of ammonia based post-combustion CO_2 capture using the advanced flash stripper process. Appl Energy 2017;202:496–506.
[26] El Hadri N, et al. Aqueous amine solution characterization for post-combustion CO_2 capture process. Appl Energy 2016;185:1433–49.
[27] Xiao M, et al. A study of structure–activity relationships of commercial tertiary amines for post-combustion CO_2 capture. Appl Energy 2016;184:219–29.
[28] Cheng C-H, et al., Amine-based post-combustion CO2 capture mediated by metal ions: Advancement of CO2 desorption using copper ions. Appl Energy, 2018;211:1030–38.
[29] Zhang X, et al. Reduction of energy requirement of CO_2 desorption from a rich CO_2-loaded MEA solution by using solid acid catalysts. Appl Energy 2017;202:673–84.
[30] Oh S-Y, et al. Energy minimization of MEA-based CO_2 capture process. Appl Energy 2016;169:353–62.
[31] Zhao B, et al. Enhancing the energetic efficiency of MDEA/PZ-based CO_2 capture technology for a 650MW power plant: Process improvement. Appl Energy 2017;185:362–75.
[32] Wang T, et al., Solvent regeneration by novel direct non-aqueous gas stripping process for post-combustion CO2 capture. Appl Energy 2017;205:23–32.
[33] Arti M, et al. Single process for CO_2 capture and mineralization in various alkanolamines using calcium chloride. Energy Fuels 2017;31(1):763–9.
[34] Li Y, et al. Dual alkali solvent system for CO_2 capture from flue gas. Environ Sci Technol 2017;51(15):8824–31.
[35] Li Q, et al. A novel strategy for carbon capture and sequestration by rHLPD processing. Front Energy Res 2016;3:53.
[36] Kang JM, et al. Energy-efficient chemical regeneration of AMP using calcium hydroxide for operating carbon dioxide capture process. Chem Eng J 2018;335:338–44.
[37] Yang Q, et al. Toward intelligent CO_2 capture solvent design through experimental solvent development and amine synthesis. Energy Fuels 2016;30(9):7503–10.
[38] Lv B, et al. Mechanisms of CO_2 capture into monoethanolamine solution with different CO_2 loading during the absorption/desorption processes. Environ Sci Technol 2015;49(17):10728–35.
[39] Fernandes D, et al. Investigations of primary and secondary amine carbamate stability by 1H NMR spectroscopy for post combustion capture of carbon dioxide. J Chem Thermodyn 2012;54:183–91.
[40] McGurk SJ, et al. Microwave swing regeneration of aqueous monoethanolamine for post-combustion CO_2 capture. Appl Energy 2017;192:126–33.
[41] Ji L, et al. CO_2 sequestration by direct mineralisation using fly ash from Chinese Shenfu coal. Fuel Process Technol 2017;156:429–37.
[42] Ji L, et al. Insights into Carbonation kinetics of fly ash from Victorian lignite for CO_2 sequestration. Energy Fuels 2018.
[43] Yu H, et al. Promoted CO_2 absorption in aqueous ammonia. Greenhouse Gases Sci Technol 2012;2(3):200–8.
[44] Yan S, et al. Regeneration of CO_2 from CO_2-rich alkanolamines solution by using reduced thickness and vacuum technology: Regeneration feasibility and characteristic of thin-layer solvent. Chem Eng Process Process Intensif 2009;48(1):515–23.
[45] Aroonwilas A, Tontiwachwuthikul P. Mass transfer coefficients and correlation for CO_2 absorption into 2-amine-2-methyl-1-propanol (AMP) using structured packing. Ind Eng Chem Res 1998;37:569–75.
[46] Yu B, et al. Characterisation and kinetic study of carbon dioxide absorption by an aqueous diamine solution. Appl Energy 2017;208:1308–17.
[47] Conway W, et al. Reactions of CO_2 with aqueous piperazine solutions: formation and decomposition of mono- and dicarbamic acids/carbamates of piperazine at 25.0 degrees C. J Phys Chem A 2013;117(5):806–13.
[48] Pan S-Y. CO_2 Capture by accelerated carbonation of alkaline wastes: a review on its principles and applications. Aerosol Air Qual Res 2012;12(5):770–91.
[49] Greenberg SA, et al. The thermodynamic functions for the solution of calcium hydroxide in water. J Phys Chem 1960;64(8):1057–9.
[50] Lin Y-J, Madan T, Rochelle GT. Regeneration with rich bypass of aqueous piperazine and monoethanolamine for CO_2 capture. Ind Eng Chem Res 2014;53(10):4067–74.
[51] Li K, et al. Techno-economic assessment of stripping modifications in an ammonia-based post-combustion capture process. Int J Greenhouse Gas Control 2016;53:319–27.
[52] Yao ZT, et al. A comprehensive review on the applications of coal fly ash. Earth Sci Rev 2015;141:105–21.

Supporting Information

Integrated absorption-mineralisation for low-energy CO_2 capture and sequestration

Long Ji[1,2,3], Hai Yu[3*], Kangkang Li[3], Bing Yu[3], Mihaela Grigore[4], Qi Yang[5], Xiaolong Wang[6], Zuliang Chen[7], Ming Zeng[1], Shuaifei Zhao[2**]

[1] School of Chemical & Environmental Engineering, China University of Mining & Technology (Beijing), Beijing 100083, China

[2] Department of Environmental Sciences, Macquarie University, Sydney, NSW 2109, Australia

[3] CSIRO Energy, Newcastle, NSW 2304, Australia

[4] CSIRO Energy, North Ryde, NSW 2113, Australia

[5] CSIRO Manufacturing, Clayton, VIC 3169, Australia

[6] Huaneng Clean Energy Research Institute, Beijing, 102209

[7] Fujian Key Laboratory of Pollution Control and Resource Reuse, School of Environmental Science and Engineering, Fujian Normal University, Fuzhou 350007, China

*Corresponding author Ph: +61-2-4960-6201 Email: hai.yu@csiro.au

**Corresponding author Ph: +61 2 9850-9672 Email: shuaifei.zhao@mq.edu.au;

Detailed infrared spectral analysis

The hypothesised reaction mechanism of the carbonation reactions demonstrated in Section 2.2 and the observation shown in Figure 4a–e can be confirmed by analysing samples at different carbonation times using FT-IR. The infrared spectra of the five amine solutions at different times in the carbonation reactions were measured and recorded (Figure 4f–j). Several peaks appear or shift due to the formation of carbamate and bicarbonate, the protonation of the amine group and the dissolution of molecular CO_2.

Figure 4f shows that the distinct absorbance peak at 1645 cm^{-1} corresponds to N–H rocking in the fresh MEA solution, while the peak at 955 cm^{-1} reflects the characteristic peak of C–N–H out-of-plane wagging and C–NH_2 twisting [1-4]. When the MEA solution was loaded with CO_2, the peaks corresponding to N–H rocking disappeared, and the peak at 1645 cm^{-1} shifted to 1634 cm^{-1} [1]. Four new signals appeared resulting from the chemical reactions between the primary amino group and the CO_2 molecule. Newly formed peaks of COO^- asymmetric stretching at 1568 cm^{-1}, symmetric stretching at 1486 cm^{-1} and N–COO^- stretching vibration at 1322 cm^{-1} were assigned to MEA carbamate [1, 2]. A typical absorption peak at 1388 cm^{-1} corresponding to doubly degenerate stretching was assigned to carbonate. The bicarbonate peaks were assigned to $-COO^-$ symmetric stretching at 1360 cm^{-1}. The weak bicarbonate band at 1000 cm^{-1} was likely due to C–OH stretching. The specific band of the protonated amine at 1643 cm^{-1} was attributed to asymmetric NH_3^+ scissoring. C–N and C–O stretching shift from 1076 to 1069 cm^{-1} and from 1024 to 1013 cm^{-1}, respectively, occurred as the protonated MEA [1]. Figure 4f also clearly shows the peak intensity change of carbamate, carbonate/bicarbonate and MEA/$MEAH^+$ during the CO_2 absorption and carbonation reactions. During the initial 5 min of the carbonation reaction, the peak intensity of carbamate (1568, 1486, and 1322 cm^{-1}), carbonate (1388 cm^{-1}), and bicarbonate (1360 cm^{-1}) decreased rapidly, reflecting the reduced number of these ions in the solution. This result was consistent with the decline of CO_2-loading in the liquid phase, as seen in Figure 4, and thus confirmed the hypothesised reaction pathways in Section 2.2 that species such as primary carbamate and bicarbonate would participate in the carbonation reaction. The MEA peak at 955 cm^{-1} was also enlarged, while the

protonated MEA ($MEAH^+$) peak at 1069 cm^{-1} decreased and 1634 cm^{-1} shifted back to 1645 cm^{-1}, indicating that MEA was regenerated in the carbonation reaction. As carbonation continued from 5 to 60 min, no further change in peak intensity was observed, though the peak intensity of carbamate is still larger than the fresh MEA. This indicates that the carbonation reaction became stable due to the high stability of MEA carbamate, consistent with the CO_2-loading observation in Figure 4a. The stable carbamate attributes MEA a higher lean CO_2-loading and lower cyclic loading than other four amines.

For fresh DEA, Figure 4g shows that there are C–O and C–N stretching modes at 1048 cm^{-1} and 1123 cm^{-1}, respectively. The shoulder at 1069 cm^{-1} is probably due to the second C–N stretching mode. Fresh DEA also shows an N–H bend about 1630–1650 cm^{-1} but this is strongly overlapping with the H_2O spectrum. The band at 1460 cm^{-1} is likely to be out-of-plane C–H vibration (wagging, twisting). After CO_2 absorption, the peaks corresponding to N–H rocking disappeared, and the peak at about 1640 cm^{-1} shifted to 1630 cm^{-1} which is due to the appearance asymmetric NH_3^+ scissoring [1]. Four new signals appeared, resulting from the chemical reactions between the primary amino group and the CO_2 molecule. Newly formed peaks of COO^- asymmetric stretching at 1533 cm^{-1} (asymmetric stretching of COO^-), 1481 cm^{-1} (symmetric stretching of COO^-) and 1296 cm^{-1} (stretching of $NCOO^-$) were assigned to DEA carbamate [1-2]. The peak at 1414 cm^{-1} is also likely to be carbamate. A typical absorption peak at 1360 cm^{-1} was assigned to bicarbonate. The specific band of the protonated amine at 1630 cm^{-1} was attributed to asymmetric NH_3^+ scissoring. C–N and C–O stretching modes shifted from 1123 to 1097 cm^{-1} and from 1048 to 1033 cm^{-1}, respectively, occurring as the protonated DEA [1]. Figure 4g also shows that the peaks of carbamate (1533, 1481, and 1296 cm^{-1}), bicarbonate (1388 cm^{-1}), and bicarbonate (1360 cm^{-1}) displayed a rapid decrease during the initial 5 min carbonation reaction, reflecting the reduced number of these ions in the solution and thus the reduced CO_2-loading in the solution. This result was consistent with the trend of CO_2-loading of the DEA solution as observed in Figure 4b, and thus confirmed the hypothesised reaction pathways in Section 2.2 that species such as secondary carbamate and bicarbonate would participate in carbonation reactions. The DEA peak at 1123 cm^{-1} was also

enlarged during the carbonation reaction, while the protonated DEA ($DEAH^+$) peak at 1069 cm^{-1} decreased and 1634 cm^{-1} shifted back to 1645 cm^{-1}, indicating that DEA was regenerated. As carbonation continued from 5 to 60 min, a slow but continuous decrease in DEA carbamate and carbonate/bicarbonate peaks was observed. This indicates that the carbonation reaction continuously occurred during this period, consistent with the CO_2-loading observation in Figure 4b. The low stability of DEA carbamate attributes DEA a lower lean CO_2-loading and high cyclic loading than MEA.

The partial FT-IR spectrum (900−1800 cm^{-1}) in Figure 4h collected during carbonation reactions of the PZ solution (2 mol/L) shows that five major FT-IR peaks appeared after CO_2 absorption. The carbamate $NCOO^-$ derivatives of heterocyclic monoamines have been identified as giving rise to several strong absorbance bands in the 1260−1600 cm^{-1} region, including the asymmetric and symmetric vibrations of the COO^- moiety at 1546 cm^{-1} and 1425 cm^{-1}, respectively, and the $N-COO^-$ stretching vibration of the $NCOO^-$ derivative at 1289 cm^{-1} [1]. The protonated amine NH_2^+ generated upon absorption of CO_2 created an absorbance band at 1475 cm^{-1}. This is likely to be the result of a chemical reaction between the secondary amino group and the CO_2 molecule. One amine molecule acts as the absorption site for CO_2, and the other as a proton acceptor. Also, the absorbance in the 1276−1294 cm^{-1} region is attributed to the formation of $OOC-PZ-COO^-$ [1]. The bicarbonate (HCO_3^-) and carbonate (CO_3^{2-}) species were identified as broad peaks at around 1375 cm^{-1} which are overlapped by 1360 and 1388 cm^{-1}. Figure 4h also shows that during the initial 5 min carbonation reaction, the peaks of carbamate at 1546, 1425, and 1289 cm^{-1} shifted to 1524, 1432, and 1276 and 1294 cm^{-1}, consistent with the literature [3]. The peak intensity of PZ carbamate (1524, 1432, 1276 and 1294 cm^{-1}), protonated PZ (1475 cm^{-1}), bicarbonate (1360 cm^{-1}) and carbonate (1388 cm^{-1}) decreased rapidly, indicating reaction between these species and calcium hydroxide. This agreed well with the sharp decrease of CO_2-loading, as seen in Figure 4c. As the carbonation reaction continued from 10 to 60 min, no further peak intensity change was observed. Moreover, the FTIR peaks of PZ at 60 min is very close to fresh PZ, indicating a very low lean loading and high regeneration efficiency. This is consistent with the results in Figure 4c.

For MDEA and AMP, carbamate is not formed or forms at negligible concentrations, and all the peaks can be assigned to amine, protonated amine, and bicarbonate. In Figure 4i, a distinct transmittance peak at a wavelength of 1645 cm^{-1} corresponds to N–H rocking for the fresh MDEA solution, while the peak at 1024 cm^{-1} was the characteristic peak of the C–O stretching mode, in agreement with current literature [2]. After CO_2 absorption, there was no signal to prove that carbamate was formed. The peak at 1645 cm^{-1} shifted to 1634 cm^{-1} due to the tertiary amino group, which acted as the proton acceptor in CO_2 absorption. A typical absorption peak at 1360 cm^{-1} corresponding to the $-CO_2^-$ symmetric stretching was assigned to bicarbonate [4]. Figure 4i also shows that in the initial 5 min of carbonation, the peak intensity of the carbonate (1388 cm^{-1}) and bicarbonate (1360 cm^{-1}) decreased, while the peak at 1634 cm^{-1} shifted back to 1645 cm^{-1}, indicating that carbonate/bicarbonate reacted with calcium ions, and MDEA was regenerated during the carbonation reactions. From 5 to 60 min, the peak intensity of bicarbonate also gradually decreased, which confirmed the gradually occurring carbonation reaction observed in Figure 4d.

Figure 4j shows that the distinct transmittance peak at 1645 cm^{-1} corresponds to N–H rocking in the fresh AMP solution, while the peak at 914 cm^{-1} reflects the characteristic peak of C–N–H out-of-plane wagging and $C–NH_2$ twisting [3]. There was a significant contribution from $–CH_2$, $–CH_3$, and C–C stretching of AMP absorb in the 1300 cm^{-1} region. This complexity and the overlapping of bands make it difficult to identify the individual vibrational modes. The main peaks at 1477 cm^{-1} and 1371 cm^{-1} are probably due to $–CH_3$ asymmetric and symmetric rocking. After the CO_2 absorption, the peaks corresponding to N–H rocking disappeared, and the peak at 1645 cm^{-1} shifted to 1634 cm^{-1} [1]. The bands at 1533 cm^{-1} and 1623 cm^{-1} are due to symmetric and asymmetric NH_3^+ scissoring. C–N and C–O stretching modes shifted from 1043 to 1074 cm^{-1} and from 1043 to 1050 cm^{-1}, respectively, as protonated AMP. The bicarbonate (HCO_3^-) and carbonate (CO_3^{2-}) species were identified by a broad peak at around 1350–1390 cm^{-1} which is overlapped by 1360 and 1388 cm^{-1}. Figure 4j also shows that in the initial 5 min of carbonation, the peak intensity of the carbonate (1388 cm^{-1}) and protonated AMP (1074 cm^{-1}) decreased rapidly, while the peak of AMP (1043 cm^{-1}) increased and the peak at 1634 cm^{-1} shifted back

to 1645 cm^{-1}, indicating that bicarbonate reacted, and the AMP was regenerated during the carbonation reactions. From 5 to 60 min, the peak intensity of bicarbonate and carbonate gradually decreased, which confirmed the gradually occurring carbonation reaction observed in Figure 4e.

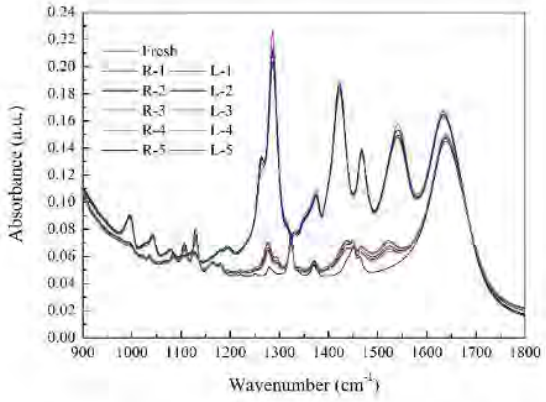

Figure S1 Infrared spectra of the liquid phases of 2 mol/L PZ solution in five cycles of CO_2 absorption–chemical regeneration at a 1.0 mol CaO/mol CO_2 CaO dosage

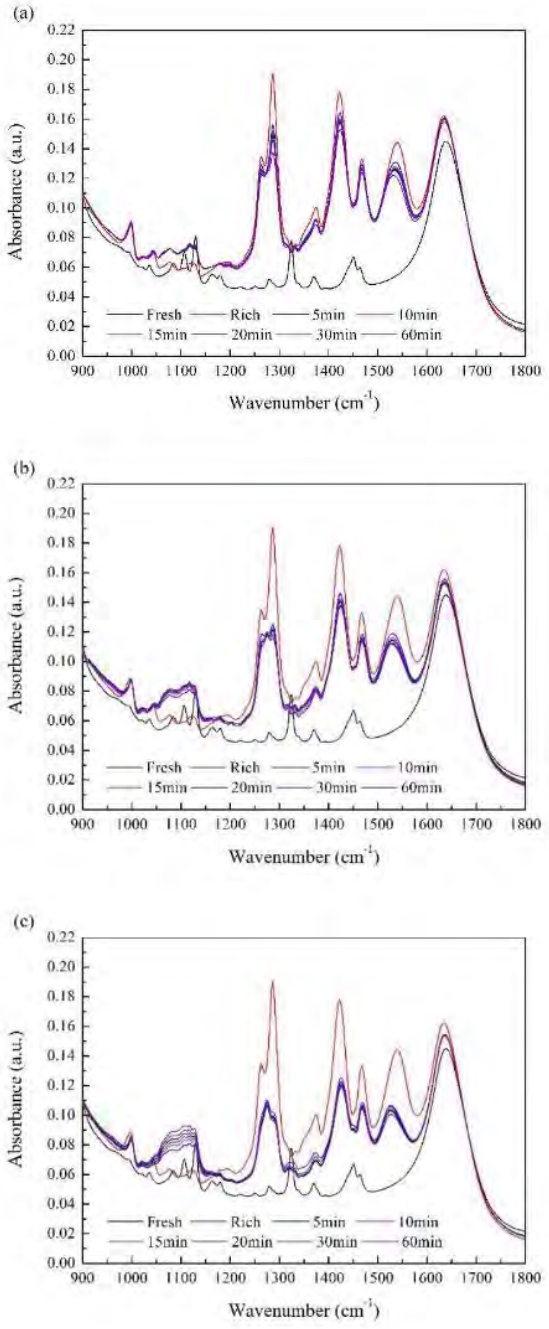
(a)
(b)
(c)
Absorbance (a.u.)
Wavenumber (cm-1)
Fresh
Rich
5min
10min
15min
20min
30min
60min

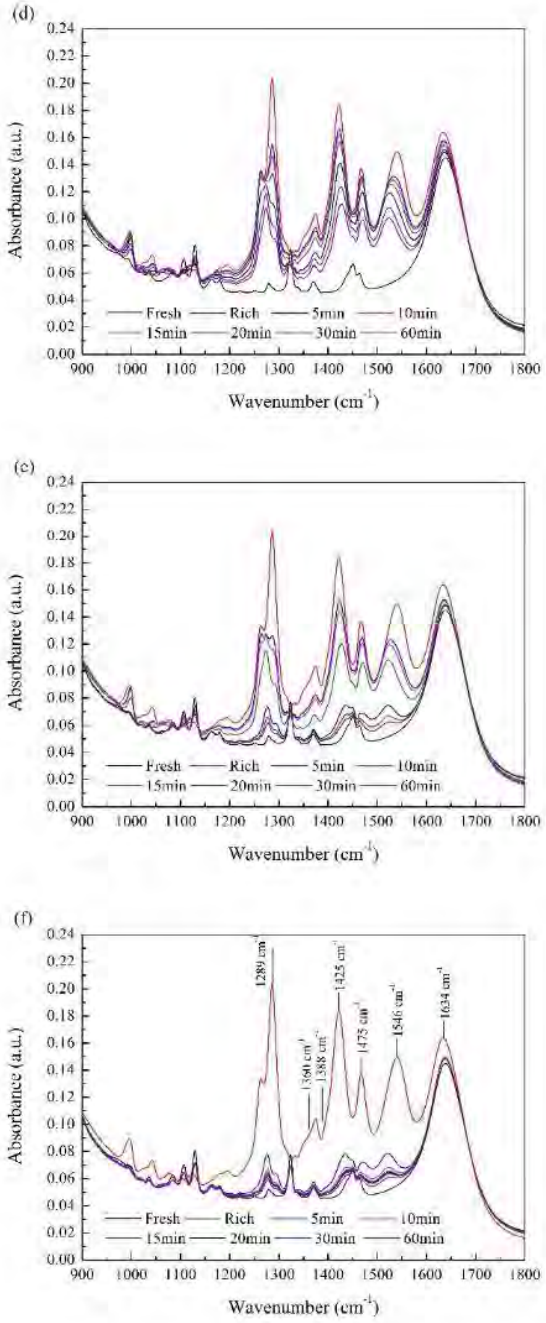

Figure S2 FT-IR spectra of the liquid phases of 50 mL of 2 mol/L PZ solutions in the carbonation reaction with 10 g (a), 20 g (b) and 30 g (c) fly ash dosages and 0.5 mol CaO/mol CO_2 (d), 0.75 mol CaO/mol CO_2 (e) and 1.0 mol CaO/mol CO_2 (f) CaO dosages. Note that the different absorbance bands have been assigned to corresponding vibrational modes to the most accurate extent possible, considering the overlapping of bands.

References

1. Richner, G. and G. Puxty, Assessing the chemical speciation during CO_2 absorption by aqueous amines using in situ FTIR. Industrial & Engineering Chemistry Research, 2012. 51(44): 14317–14324.
2. Jackson, P., et al., In situ Fourier transform-infrared (FT-IR) analysis of carbon dioxide absorption and desorption in amine solutions. Energy Procedia, 2009. 1(1): 985–994.
3. Robinson, K., A. McCluskey, and M.I. Attalla, An FTIR spectroscopic study on the effect of molecular structural variations on the CO_2 absorption characteristics of heterocyclic amines. Chemphyschem, 2011. 12(6): 1088–1099.
4. Robinson, K., A. McCluskey, and M.I. Attalla, An ATR-FTIR study on the effect of molecular structural variations on the CO_2 absorption characteristics of heterocyclic amines, part II. Chemphyschem, 2012. 13(9): 2331–2341.

Chemical Engineering Journal 352 (2018) 151–162

Contents lists available at ScienceDirect

Chemical Engineering Journal

journal homepage: www.elsevier.com/locate/cej

Integrated absorption–mineralisation for energy-efficient CO_2 sequestration: Reaction mechanism and feasibility of using fly ash as a feedstock

Long Ji[a,b,c], Hai Yu[b,*], Bing Yu[b], Kaiqi Jiang[b], Mihaela Grigore[d], Xiaolong Wang[e], Shuaifei Zhao[a], Kangkang Li[b,*]

[a] Department of Environmental Sciences, Macquarie University, Sydney, NSW 2109, Australia
[b] CSIRO Energy, Newcastle, NSW 2304, Australia
[c] School of Chemical & Environmental Engineering, China University of Mining & Technology (Beijing), Beijing 100083, China
[d] CSIRO Energy, North Ryde, NSW 2113, Australia
[e] Huaneng Clean Energy Research Institute, Beijing 102209, China

HIGHLIGHTS

- The application of fly ash in integrated CO_2 absorption and mineralisation for energy efficient CO_2 sequestration.
- Low energy penalty and cost.
- Detailed investigation of amine regeneration by mineralisation.

ARTICLE INFO

Keywords:
CO_2 capture
Chemical regeneration
MEA
Multicycle
Fly ash

ABSTRACT

The most critical challenge for the large-scale implementation of amine-based carbon dioxide (CO_2) capture is the high energy consumption of absorbent thermal regeneration. To reduce the energy requirement, absorbent thermal regeneration can be replaced by a chemical method that integrates amine scrubbing, chemical regeneration and CO_2 mineralisation in one process. However, the mechanisms of the process and the application of industrial waste as feedstocks have not been fully investigated. In the present work, we studied the integrated CO_2 absorption–mineralisation process using the benchmark solvent monoethanolamine (MEA) as an amine absorbent and fly ash as a chemical regeneration agent. We investigated the mechanism involved in the mineralisation in detail and studied the performance of MEA in regeneration by mineralisation of calcium oxide (CaO) at various CO_2-loadings. The performance stability of MEA was verified in multicycle CO_2 absorption–mineralisation experiments. We also investigated the technical feasibility of using fly ash as a feedstock for absorbent regeneration. Our results show that MEA can be regenerated after a carbonation reaction with both calcium oxide and fly ash at 40 °C, and that the CO_2 absorbed by MEA is precipitated as calcium carbonate. Compared with traditional thermal regeneration-based CO_2 capture, the integrated CO_2 absorption–mineralisation process displays a similar cyclic CO_2-loading (0.21 mol/mol) but has great advantages in energy reduction and capital cost savings due to the smaller energy requirement of amine regeneration and the limitation of CO_2 compression and pipeline transport. This technology has great potential for industrial application, particularly with CaO-containing wastes such as fly ash and carbide slag.

1. Introduction

Carbon dioxide (CO_2) emissions resulting from human activity are widely accepted as the major greenhouse gas contributing to global warming [1]. Despite fossil-fuelled power plants being the greatest contributor (~37%) of global CO_2 emissions, the use of fossil fuels will continue to power the world's economic growth in the foreseeable future [2]. Post-combustion CO_2 capture (PCC) technology is a promising strategy to directly reduce CO_2 emissions from coal and gas-fired power plants and mitigate global climate change in the short to intermediate term [1]. A variety of PCC technologies have been developed, including amine scrubbing [3], membrane separation [4–8], solid adsorption [9] and mineralisation [10–13]. Of these, amine scrubbing, used for decades in the gas processing industry to absorb CO_2, is the

* Corresponding authors.
E-mail addresses: hai.yu@csiro.au (H. Yu), kangkang.li@csiro.au (K. Li).

https://doi.org/10.1016/j.cej.2018.07.014
Received 21 March 2018; Received in revised form 22 June 2018; Accepted 1 July 2018
Available online 02 July 2018
1385-8947/

Ji, L., Yu, H., Yu, B., Jiang, K., Grigore, M., Wang, X., Zhao, S., & Li, K. (2018). Integrated absorption–mineralisation for energy-efficient CO_2 sequestration: reaction mechanism and feasibility of using fly ash as a feedstock. Chemical Engineering Journal, 352, 151-162. https://doi.org/10.1016/j.cej.2018.07.014

most mature technology available for large-scale CO_2 capture. Monoethanolamine (MEA) is commonly considered as a benchmark amine absorbent for CO_2 capture, due to its commercial availability, relatively low cost, fast absorption rate and extensive experience in industrial applications [14,15]. However, its large energy penalty and high capital cost make it economically unviable. For instance, integrating the state-of-the-art MEA capture process into a coal-fired power plant would reduce power generation efficiency by 25–40% and raise the cost of electricity by 70–100% [16].

Extensive research has been conducted to reduce the energy consumption of solvent regeneration by improving solvent performance and implementing process improvements. For instance, amine regeneration duty consists of three components: the heat of CO_2 desorption, sensible heat and latent heat. The heat of CO_2 desorption can be reduced by using an advanced absorbent formulation [2,17]. A widely developed absorbent formula combines primary or secondary amines that have fast absorption rates with cyclic, tertiary or sterically hindered amines that have high CO_2 absorption capacity and low heat of CO_2 desorption [18,19]. Sensible heat and latent heat can be reduced by process improvements, such as absorber inter-cooling, rich-split and stripper inter-heating [16,20,21]. Process modifications can reduce the overall energy consumption of the MEA process by 8–20% compared to the conventional configuration [16]. Although the energy consumption of PCC has been largely reduced by advanced absorbent formulations and process configuration modifications, the energy consumption from thermal regeneration, which accounts for greater than 50% of total PCC energy consumption [16], is still too high for large-scale application. In addition, amine volatilisation and degradation are still environmental concerns, and equipment corrodes as a result of the high regeneration temperature. CO_2 transportation and subsequent geological storage also require further energy and capital costs. To deal with these problems, an alternative CO_2 capture technology is required to reduce the energy consumption of traditional thermal regeneration. CO_2 mineralisation is an attractive technology that provides leakage-free CO_2 sequestration and does not require post-storage monitoring [13]. The basic idea of CO_2 mineral carbonation is to mimic the process of natural rock weathering, where carbonic acid from the dissolution of CO_2 in rainwater is neutralised with alkaline metal minerals to form stable carbonate minerals [11]. The carbonation reactions can occur at moderate temperatures and release significant amounts of heat. Natural silicates (serpentine, olivine and wollastonite) can be used as feedstocks for CO_2 mineralisation, as can alkaline industrial wastes such as fly ash, carbide slag and steel slag [22–30]. These raw materials have low costs, high reactivity, and are readily available near CO_2 emission sources without further pre-treatment. However, CO_2 mineralisation is confronted by several challenges, the most critical being slow reaction kinetics.

Inspired by the fast CO_2 absorption of aqueous amines and low energy consumption of CO_2 mineralisation, one promising scenario makes use of the dual benefits of the two processes to achieve energy-efficient CO_2 sequestration. Fig. 1 shows the concept of the integrated CO_2 absorption–mineralisation (IAM) process. CO_2 is first captured by an amine absolvent in a CO_2 absorber, resulting in a CO_2-rich solution. The solution is then transferred to a carbonation reactor for amine regeneration and CO_2 sequestration by alkaline oxide or alkaline oxide-rich industrial wastes. The regenerated solvent is sent back to the top of the absorber for continuous CO_2 absorption. In this cyclic process, CO_2 is sequestrated in the form of calcium carbonate ($CaCO_3$), while the amine is chemically regenerated through pH swing, instead of the temperature swing used in the conventional amine scrubbing process. As a new developed process, the technical feasibility and the reaction mechanism of IAM should be investigated. The mechanism of CO_2 absorption by MEA solution was well studied and can be simply described by the reaction: $2MEA + H_2O + CO_2(aq) \leftrightarrow MEAH^+ + MEACOO^-$, while the thermal regeneration was the backward reaction. However, the mechanisms of MEA regeneration by mineralisation is unclear, which involves the reactions between CaO and the species of CO_2-

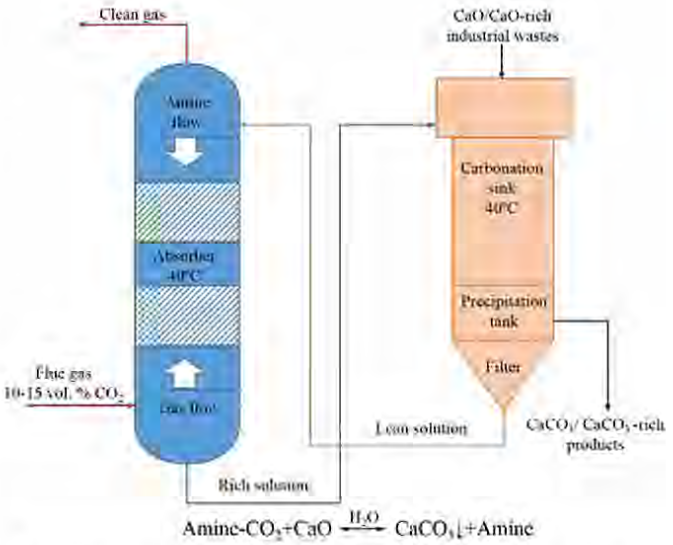

Fig. 1. Concept of the integrated CO_2 absorption–mineralisation process.

loaded MEA solutions including $MEAH+$, $MEACOO^-$, HCO_3^-, and CO_3^{2-}. Arti et al. [31] investigated the technical feasibility of amine regeneration by introducing calcium chloride ($CaCl_2$) into CO_2-loaded amine solutions, including MEA, diethanolamine (DEA), N-methyldiethanolamine (MDEA) and 2-amino-2-methy-1-propanol (AMP). The results indicated that the absorbed CO_2 in amine solutions was converted to solid $CaCO_3$ without additional energy input, but the amine absorbents were not regenerated after carbonation reaction, which makes the process non-recyclable and chemical consuming. Also, the reaction pathways between $CaCl_2$ and CO_2-loaded amines were not investigated in their study. Kang et al. [32] improved the process by introducing calcium oxide (CaO) instead of $CaCl_2$ into CO_2-loaded AMP solutions, in which CO_2 was released from AMP solutions to form $CaCO_3$ precipitate and AMP was recovered in the carbonation reaction without thermal energy consumption. The reaction pathways in the carbonation of CaO and CO_2-loaded AMP solution were well investigated in their study, and the reaction mechanism was directly evidenced by Carbon-13 nuclear magnetic resonance (^{13}C NMR) results. However, as a sterically hindered amine, the species of CO_2-loaded AMP solution were very different from other primary and secondary amines, which were much more complex. Thus, the mechanisms involved in the IAM, especially the reaction pathways between CO_2–amine mixtures and CaO, were not fully understood. The key performance of the whole IAM process — including amine regeneration efficiency, CO_2 cyclic loading and performance stability using industrial waste — has not been reported. Furthermore, the technical and economic feasibility of the IAM process using industrial wastes as feedstocks has not yet been investigated.

In the present study, the benchmark MEA absorbent was selected to investigate the technical performance and the reaction mechanisms of the IAM process. The CO_2 mineralisation feedstock material chosen were industrial wastes that contain alkaline oxide, such as fly ash, with the purpose of simultaneous disposal of CO_2 and wastes. Considering the highly heterogeneous nature and diverse components of the wastes, we first employed the reaction-active chemical CaO to gain insights into the carbonation mechanisms and fundamental reaction pathways. Since CaO provides two types of ions — calcium ions (Ca^{2+}) and hydroxide ions (OH^-) — into the MEA–CO_2–H_2O system, they have different action mechanisms in the reactions with the species in MEA solution. This makes it very difficult to monitor the behaviours of both ions at the same time. We also added sodium hydroxide (NaOH) and $CaCl_2$ separately into the CO_2-loaded MEA solution to clearly investigate the reaction mechanisms of Ca^{2+} and OH^- separately. The performance of MEA in the IAM process, including cyclic CO_2-loading and regeneration

efficiency, was systematically investigated at various CO_2-loadings and reaction times. The performance stability of MEA was also investigated in multicycle IAM experiments by adding CaO. Further experiments were conducted using fly ash as a feedstock to demonstrate the technical feasibility of IAM in practical applications. Finally, the comparison with the traditional thermal absorbent regeneration was conducted to determine the energy and cost savings of IAM. The novelty of the present work includes: (i) investigating the detailed mechanism of IAM, (ii) exploring absorbent performance stability in cyclic CO_2 absorption and mineralisation, and (iii) using fly ash for absorbent regeneration and CO_2 sequestration in one step.

2. Materials and methods

2.1. Materials

The reagents MEA (≥99%), $CaCl_2$ (≥96%), NaOH (≥98%), $CaCO_3$ (≥99%) and CaO (reagent grade) were purchased from Sigma-Aldrich without further purification. MEA solutions of different concentrations were prepared using deionised water and volumetric glassware. CO_2 (99.5% purity) and nitrogen gases (N_2, 99.99% purity) were purchased from BOC Gases Australia. The fly ash used in this study was collected from Huaneng Gaobeidian power plant in Beijing, which is based on Chinese black coal from Shenfu, Shanxi province. The chemical composition of the fly ash is given in Table 1. This raw material has been identified as a suitable fly ash for CO_2 mineralisation because of the high CaO fraction. More detailed information of the fly ash can be found in our previous studies [33,34].

2.2. CO_2 absorption–mineralisation experiment

A bubble column was used for CO_2 absorption to obtain CO_2-loaded solutions (Fig. 2a). Mixed gas with 9% CO_2 in N_2 was humidified and bubbled through 200 mL aqueous MEA solution (2 mol/L) in the bubble column at a flow rate of 1.7 L/min controlled by Bronkhornst mass-flow controllers. The temperature was maintained by a circulating water bath at 40 °C. The CO_2 concentration of the outlet gas was determined and recorded every 15 s using a Horiba VA-3000 gas analyser. CO_2 bubbling was stopped when the CO_2 inlet concentration equalled the outlet concentration, or a target CO_2-loading was achieved.

The CO_2-rich solution was then transferred into a three-necked flask system (Fig. 2b) with a certain amount of chemicals (CaO, NaOH or $CaCl_2$) or fly ash added for MEA regeneration and/or CO_2 mineralisation. The solid sample was mixed with the rich solution using a magnetic stirrer at 500 rpm. The flask remained constant at atmospheric pressure throughout the experiment, and the temperature was maintained at 40 °C using a water bath. During the reaction, slurry samples (10 mL) were extracted with a syringe at different reaction times. The extracted suspension was immediately filtered through a 0.2-μm nylon syringe filter. The filter cake was washed and then dried overnight in an oven at 40 °C, and then tested by acid titration to determine the amount of CO_2 carbonated in the solid powders.

To investigate the performance stability of MEA upon recycling, five cycles of CO_2 absorption and mineralisation experiments were conducted following the procedures shown in Fig. 3. Firstly, 200 mL CO_2-rich MEA solution (2 mol/L) was prepared following the above procedures and conditions. CaO was added to the rich solution at a 1.0 mol CaO/mol-CO_2 dosage for MEA regeneration and CO_2 sequestration. After a 15-min reaction, the suspension was immediately filtered through a 0.2-μm nylon filter to obtain a CO_2-lean solution. The lean solution was then reused for four successive cycles of CO_2 absorption and mineralisation experiments.

Table 1
Elemental quantification of fly ash determined by X-ray fluorescence spectroscopy.

Composition (wt. %)							
SiO_2	Al_2O_3	Fe_2O_3	CaO	MgO	Na_2O	K_2O	SO_3
42.80	19.15	9.06	16.41	1.23	1.68	1.50	1.9

2.3. Characterisation

The CO_2-loadings of liquid and solid samples were measured by acid titration [35]. This method involved acidifying a precisely measured quantity of liquid and solid samples by adding excess nitric acid (HNO_3, 1 mol/L) aqueous solution. The volume of CO_2 released from the sample was measured at constant atmospheric pressure using two burettes and was used to calculate the CO_2-loading of the solid and liquid samples. Reagent grade $CaCO_3$ was used to assess the accuracy of this analytical method. The average error was ± 3%, indicating that the method was valid for CO_2-loading measurements. The CO_2-loading of solid samples was defined as the molar amount of CO_2 captured per mole of calcium, while the CO_2-loading of the amine solution was defined as the molar amount of CO_2 captured per mole of amine absorbent. The regeneration efficiency was calculated by E1:

$$Regeneration efficiency\,(\%) = \frac{CO_2\,rich loading - CO_2\,lean loading}{CO_2\,rich loading} \times 100\% \quad \text{(E1)}$$

The overall gas phase mass transfer coefficient (K_G) of the CO_2-lean solution was measured using a wetted-wall column to assess the kinetic properties of the fresh and regenerated amine solutions. The measurement was operated at 40 °C using circulated water from a thermostatic bath. A stainless-steel column with effective height and external diameter of 8.21 cm and 1.27 cm, respectively, was used. The absorbent was pumped into the column at an appropriate flow rate that formed a stable, thin film on the surface of the steel tube. CO_2 absorption flux by diamines was measured by adjusting the CO_2 partial pressures (1, 3, 5 and 7 kPa) using mass-flow controllers. The CO_2 concentration of the outlet gas was measured using a Horiba VA-3000 IR gas analyser. A total gas flow rate of 3.0 L min^{-1} was employed for all measurements, and liquid flow rates were kept between 100 and 120 mL min^{-1} to form a thin, uniform film on the surface of the column. A plot of the CO_2 absorption flux as a function of applied CO_2 partial pressures yielded a straight line, the slope of which was equal to the K_G of CO_2 absorption [36].

Carbon-13 nuclear magnetic resonance (^{13}C NMR) was used to determine the chemical species of liquid samples to provide direct evident to the investigation of the reaction mechanisms involved in IAM process. The samples were collected into 5-mm NMR tubes. An external standard of dioxane-D_2O (50% v/v) containing sodium 3-(trimethysilyl) propinonate-2,2,3,3-d_4 (TMSPd) (1%, w/v) was added to each sample. The pH value of each sample solution was then measured using an Inlab NMR electrode connected to pH meter (Oakton pH110). The ^{13}C NMR spectra of the samples were analysed using a NMR spectrometer (Bruker Avance III 400) at 293 K. A minimum pulse delay time (D_1) of 70 s was applied in a total of 32 scans. Topspin version 3.5 was used to determine accurate peak area and analyse chemical shifts. The reference carbon signal of dioxan in the standard was calibrated with external tetramethylsilane (TMS) as 66.83 ppm.

Fourier-transform infra-red (FT-IR) spectroscopy (VERTEX 70, Bruker Co. Ltd.) was used to analyse the species changes in the amine solutions during regeneration, through which the reaction pathways of IAM process can be roughly investigated. The crystalline phases present in the solid samples were determined by X-ray diffraction (XRD) analysis to provide direct evidence to the $CaCO_3$ formation in the solid samples. The samples were run on an X-ray diffractometer (Empyrean PANalytical) using CuKα radiation at 40 kV and 40 mA. Step scans were conducted from 2 to 90° 2θ, with a step interval of 0.02° 2θ. Mineral

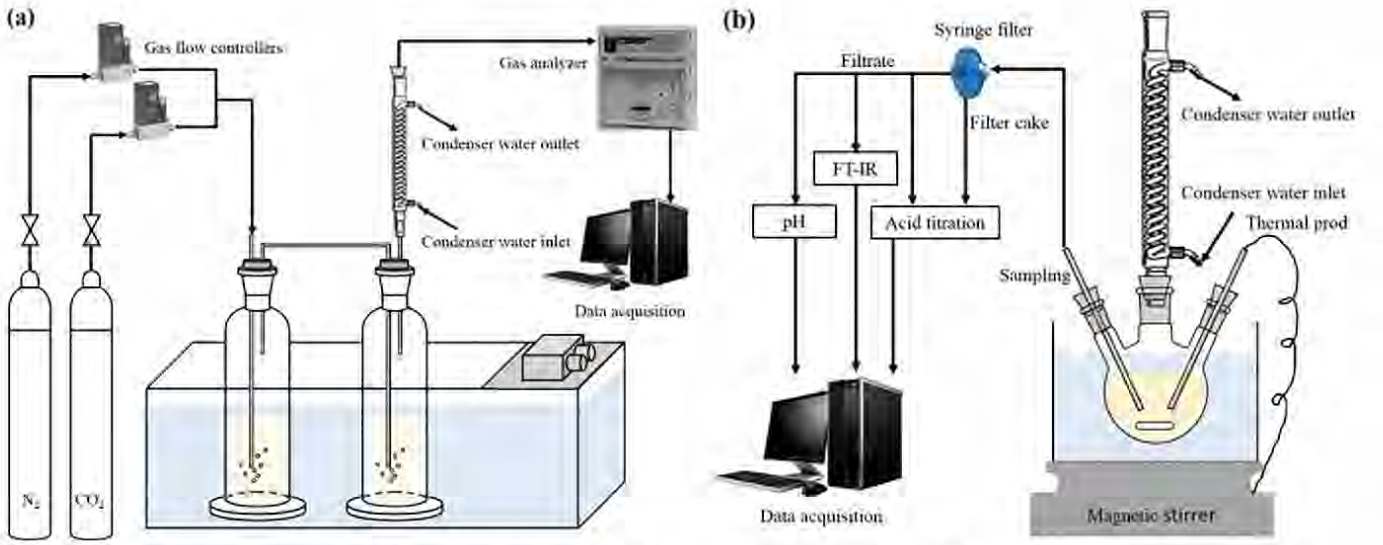

Fig. 2. Schematic diagram of (a) CO_2 absorption and (b) mineralisation experiments.

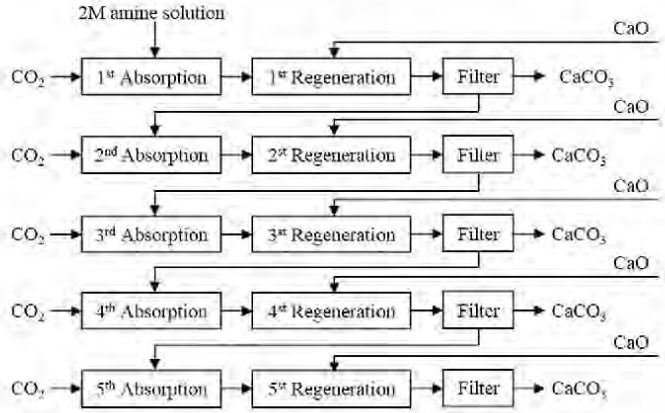

Fig. 3. Flow diagram of multicycle experiments.

phases were identified with the Bruker Eva software package.

2.4. Chemistry model

The process chemistry of CO_2 absorption and MEA regeneration by mineralisation can be described by reactions 1–10 (Table 2). The species distribution in CO_2-loaded MEA solutions as a function of NaOH dosage was calculated using a thermodynamic model performed in the software ReactLab-Equilibrium (www.jplusconsulting.com/products) and Matlab [37,38]. The thermodynamic model included all the reactions involved in CO_2 absorption and MEA regeneration by NaOH (reactions 1–6 and 9). The equilibrium constants of reactions 1–6 were obtained from the literature [37,39–41]. The model was developed based on the following assumptions: (i) all species' concentrations have the activity coefficient of 1, and are not influenced by the ionic strength; (ii) no precipitation occurs under the studied conditions, which was confirmed by our experiments; (iii) the system temperature is 25 °C.

Table 2
Possible reactions and corresponding equilibrium constants in the MEA–CO_2–H_2O system at 298.15 K.

Reaction No.	Reaction	Equilibrium constant, $\log_{10}K^a$
1	$CO_2(aq) + H_2O \overset{K_1}{\leftrightarrow} H_2CO_3$	−2.78
2	$CO_3^{2-} + H^+ \overset{K_2}{\leftrightarrow} HCO_3^-$	10.33
3	$HCO_3^- + H^+ \overset{K_3}{\leftrightarrow} H_2CO_3$	6.35
4	$OH^- + H^+ \overset{K_4}{\leftrightarrow} H_2O$	14
5	$MEA + H^+ \overset{K_5}{\leftrightarrow} MEAH^+$	9.44
6	$MEA + HCO_3^- \overset{K_6}{\leftrightarrow} MEACOO^-(+H_2O)$	1.76
7	$CaO(s) + H_2O \leftrightarrow Ca(OH)_2$	
8	$Ca(OH)_2 \leftrightarrow Ca^{2+} + 2OH^-$	
9	$MEAH^+ + OH^- \leftrightarrow MEA(+H_2O)$	
10	$Ca^{2+} + CO_3^{2-} \rightarrow CaCO_3$	

[a] Equilibrium constants for MEA–CO_2–H_2O are from the literature [37,39–41].

3. Results and discussion

3.1. Regeneration mechanism of MEA in mineralisation

3.1.1. Regeneration mechanism of MEA by calcium oxide

With the addition of CaO into the solution, the CO_2-loading of the MEA solution decreased and the solution pH increased (Fig. 4a). The hypothetical reaction mechanism is that the dissolved CaO provides calcium ions (Ca^{2+}) and hydroxide ions (OH^-) via reactions 7 and 8. The released OH^- reacts with protonated amine ($MEAH^+$) via reaction 9 to form MEA, thereby increasing the pH value in the solution and regenerating fresh amine. The increased pH value shifts reaction 6 backward to convert MEA carbamate ($MEACOO^-$) into bicarbonate ions (HCO_3^-) which is then converted into carbonate ions (CO_3^{2-}) via the backward reaction 2. The formation and precipitation of $CaCO_3$ occurs via reaction 10, which transfers CO_2 from liquid phase to solid phase and thus decreases the CO_2-loading of the MEA solution. MEA carbamate ($MEACOO^-$) can participate in this process by releasing HCO_3^- but cannot react with Ca^{2+} to form precipitation directly. This way, the absorbed CO_2 in the form of $MEACOO^-$ and HCO_3^- can be transferred from the liquid phase into the solid phase, resulting in absorbent regeneration and CO_2 sequestration.

The reaction pathways can be confirmed by the FT-IR results in Fig. 4b. When the MEA solution was loaded with CO_2, four new signals appeared resulting from the chemical reaction between the amino group and CO_2 molecule [17,42–44]. Newly formed peaks of COO^- asymmetric stretching at 1568 cm^{-1}, symmetric stretching at 1486 cm^{-1} and N–COO^- stretching vibration at 1322 cm^{-1} were assigned to $MEACOO^-$ [43,44]. A typical absorption peak at 1388 cm^{-1} corresponding to doubly degenerate stretching was assigned to CO_3^{2-}. The HCO_3^- peak was assigned to $-COO^-$ symmetric stretching at

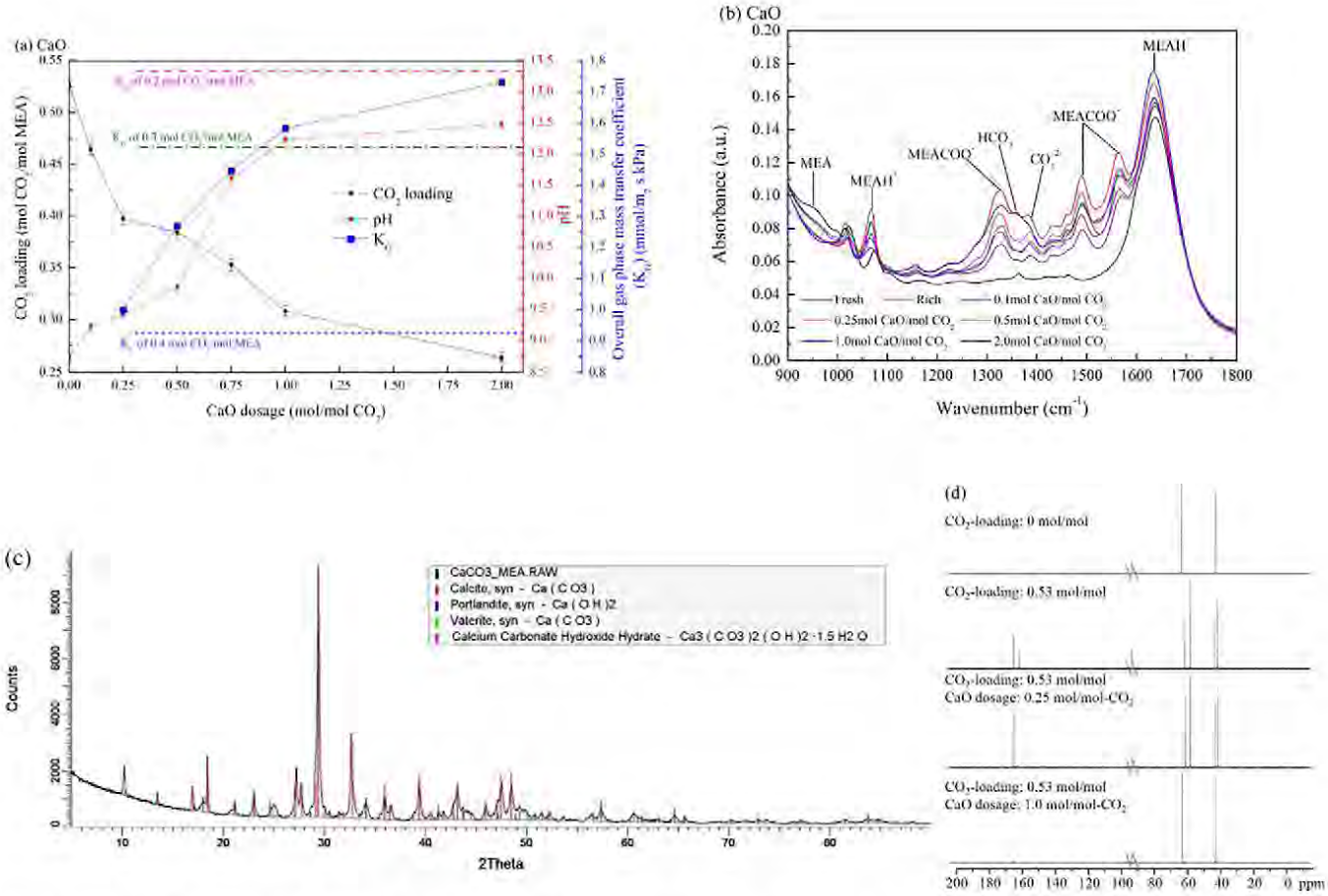

Fig. 4. (a) CO_2-loading, pH value and K_G of MEA solutions after 15 min reaction as a function of CaO dosages; (b) FT-IR spectra of MEA solutions; (c) XRD patterns of solid samples after reaction; (d) ^{13}C NMR spectra of MEA solutions.

1360 cm^{-1}, which overlapped with the carbonate peak [42]. The symmetric and asymmetric NH_3^+ scissoring at 1518 and 1634 cm^{-1} respectively, and C−N stretching shift from 1076 to 1069 cm^{-1} were assign to $MEAH^+$ [42].

After the carbonation reaction, the peak intensity of $MEACOO^-$ (1568, 1486, and 1322 cm^{-1}), CO_3^{2-} (1388 cm^{-1}) and HCO_3^- (1360 cm^{-1}) decreased rapidly, reflecting the reduced amount of these species in the solution. This is consistent with the decline in CO_2-loading of the solution shown in Fig. 4a. This result confirmed that $MEACOO^-$ and CO_3^{2-}/HCO_3^- were consumed in the carbonation reaction. The MEA peak at 955 cm^{-1} was enlarged after carbonation reaction, while the $MEAH^+$ peak at 1069 cm^{-1} decreased and the peak at 1634 cm^{-1} shifted back to 1645 cm^{-1}, confirming that MEA was regenerated after the carbonation reaction. The XRD data (Fig. 4c) of the solid sample after carbonation confirmed the precipitation of carbonates (calcite, vaterite and hydrated calcium carbonate) as major phases of the sample, thereby confirming that the absorbed CO_2 was converted into $CaCO_3$ after CaO addition. No calcium carbamate precipitate peak is observed in Fig. 4c, which provides evidence that the carbonation pathway goes through CO_3^{2-}/HCO_3^- instead of calcium carbamate.

Fig. 4a also shows that as CaO dosage increased, the CO_2-loading of the MEA solution decreased while the pH and K_G increased. This is because a larger CaO dosage provided more Ca^{2+} for $CaCO_3$ precipitation, which reduced the CO_2-loading of the MEA solution and provided more OH^- for MEA regeneration. The higher K_G value confirmed that the reactive of MEA with CO_2 was recovered due to the increased regeneration of MEA. Compared with the reference MEA solution with similar CO_2-loading, the CaO–regenerated MEA displayed a larger K_G value. This was attributed to the increase of OH^- released by excessive CaO. The excessive OH^- converted more $MEAH^+$ into fresh MEA. In this way, the amount of MEA available for CO_2 absorption in the recovered MEA solution was larger than that of the reference MEA, leading to faster CO_2 absorption kinetics.

The reaction mechanism was further confirmed by the ^{13}C NMR results in Fig. 4d. Compared with fresh MEA solution, new signals appeared at 164.5 and 160.2 ppm of CO_2-loaded MEA (0.53 mol/mol), which were assigned to $MEACOO^-$ and CO_3^{2-}/HCO_3^-, respectively [45]. After CaO was added to the MEA solution at a dosage of 0.25 mol/mol-CO_2, the CO_3^{2-}/HCO_3^- peak at 160.5 ppm disappeared, while the $MEACOO^-$ peak at 164.5 ppm increased slightly, confirming the decline of CO_2-loading observed in Fig. 4a. This result also indicates that CO_3^{2-}/HCO_3^- were converted into $MEACOO^-$ at a relatively low CaO dosage (less than1.0 mol/mol-CO_2). As the CaO dosage increased to 1.0 mol/mol-CO_2, the $MEACOO^-$ peak at 164.5 ppm significantly decreased, consistent with the CO_2-loading decline of the MEA solution shown in Fig. 4a.

3.1.2. Further investigation of the reaction mechanisms of hydroxide ions in MEA regeneration

To gain a deeper insight into the action mechanism of OH^-, we introduced NaOH into CO_2-loaded MEA solutions. Fig. 5a shows that with increasing NaOH dosage, no obvious CO_2-loading change occurs in the MEA solutions. The pH and K_G values increased with elevated NaOH dosage, due to the increase of OH^- and the regenerated MEA from $MEAH^+$ by OH^-. This phenomenon is consistent with the observation in Figs. 4a. 5b shows a significant increase of the CO_3^{2-} peak as NaOH dosage increased, confirming that the addition of NaOH shifts reaction 6 backward to produce more HCO_3^- and then more CO_3^{2-} via reaction 2. As expected, after NaOH was added into the solution, $MEAH^+$

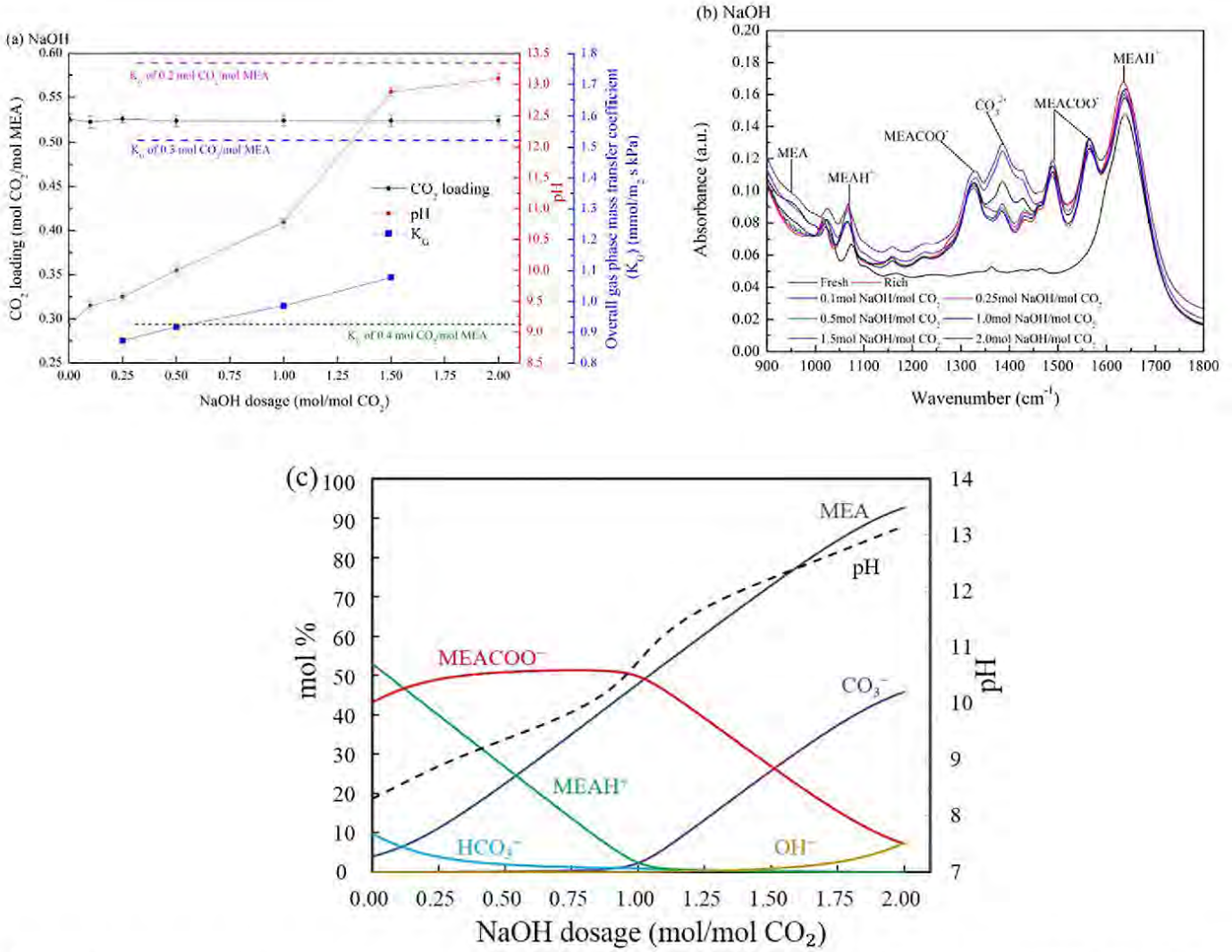

Fig. 5. (a) CO_2-loading, pH value and overall CO_2 mass transfer coefficient (K_G) of MEA solutions after 15 min reaction as a function of NaOH dosage; (b) FT-IR spectra of the MEA solutions; (c) calculated speciation profile of MEA solutions with 0.53 mol/mol CO_2-loading as a function of NaOH dosage.

declined. Surprisingly, no decrease in intensity of $MEAH^+$ was observed in the FT-IR spectra (Fig. 5b). This is because the typical $MEAH^+$ peak at 1518 cm^{-1} overlapped with the $MEACOO^-$ peaks at 1568 and 1486 cm^{-1}, which is a limitation of the FT-IR spectra study.

To further investigate the mechanism involved in the reactions between OH^- and other species, we used a thermodynamic model to theoretically analyse the speciation profile after NaOH was added into the solution. Fig. 5c shows the speciation in the MEA solution with 0.53 mol/mol CO_2-loading as a function of NaOH dosage. The pH value clearly rose with increasing NaOH dosage, while the trend of calculated pH agreed well with the measurements, as shown in Fig. 5a. When the NaOH dosage was less than 1.0 mol/mol-CO_2, MEA increased while $MEAH^+$ decreased as NaOH dosage increased, consistent with the previous conclusion that OH^- reacts with $MEAH^+$ to regenerate MEA. The increase of $MEACOO^-$ and decrease of HCO_3^- indicates the conversion of HCO_3^- into $MEACOO^-$ via the backward reaction of reaction 9 in the presence of OH^-. This is consistent with the $MEACOO^-$ increase observed by ^{13}C NMR, as shown in Fig. 4d. When the NaOH dosage was more than 1.0 mol/mol-CO_2, the pH and MEA kept increasing while $MEACOO^-$ decreased rapidly. The increase of CO_3^{2-} indicates that $MEACOO^-$ was converted into CO_3^{2-}, consistent with the enlarged CO_3^{2-} peak observed in Fig. 5b. At this stage, the regeneration of MEA results from the decomposition of $MEACOO^-$. Thus, adding NaOH to CO_2-loaded MEA solutions cannot achieve CO_2 sequestration, but can regenerate MEA.

3.1.3. *Further investigation of the reaction mechanisms of calcium ions in MEA regeneration*

To further investigate the role of Ca^{2+} in the carbonation reaction, experiments were conducted by introducing $CaCl_2$ into CO_2-loaded MEA solutions. Fig. 6a shows that the pH value and CO_2-loading of the MEA solution decreased rapidly with the addition of $CaCl_2$, because Ca^{2+} reacted with CO_3^{2-} in the solution and precipitated as $CaCO_3$ via reaction 10. The consumption of CO_3^{2-} decreased the pH of the solution, which promoted the decomposition of $MEACOO^-$ to release CO_2 and thereby led to a further decrease in CO_2-loading. The decreased CO_2-loading was confirmed by the FT-IR spectra (Fig. 6b), in which the peak intensity of $MEACOO^-$ (1568, 1486, and 1322 cm^{-1}), CO_3^{2-} (1388 cm^{-1}) and HCO_3^- (1360 cm^{-1}) decreased rapidly with increasing $CaCl_2$ dosage, representing the reduced amount of these species in the solution. The decreased pH also indicates the increase of protonated MEA. When $CaCl_2$ dosage was less than 0.75 mol/mol-CO_2, the $MEACOO^-$ peaks at 1568 and 1486 cm^{-1} were still large and overlapped with the $MEAH^+$ peak at 1518 cm^{-1}. As $CaCl_2$ dosage increased, the $MEACOO^-$ peaks at 1568 and 1486 cm^{-1} decreased, which made the $MEAH^+$ peak at 1530 cm^{-1} clearer in the FT-IR spectra curve of 1.0 and 2.0 mol /mol-CO_2 $CaCl_2$ dosage. Thus, dosing $CaCl_2$ into CO_2-loaded MEA solutions cannot regenerate MEA but can desorb CO_2.

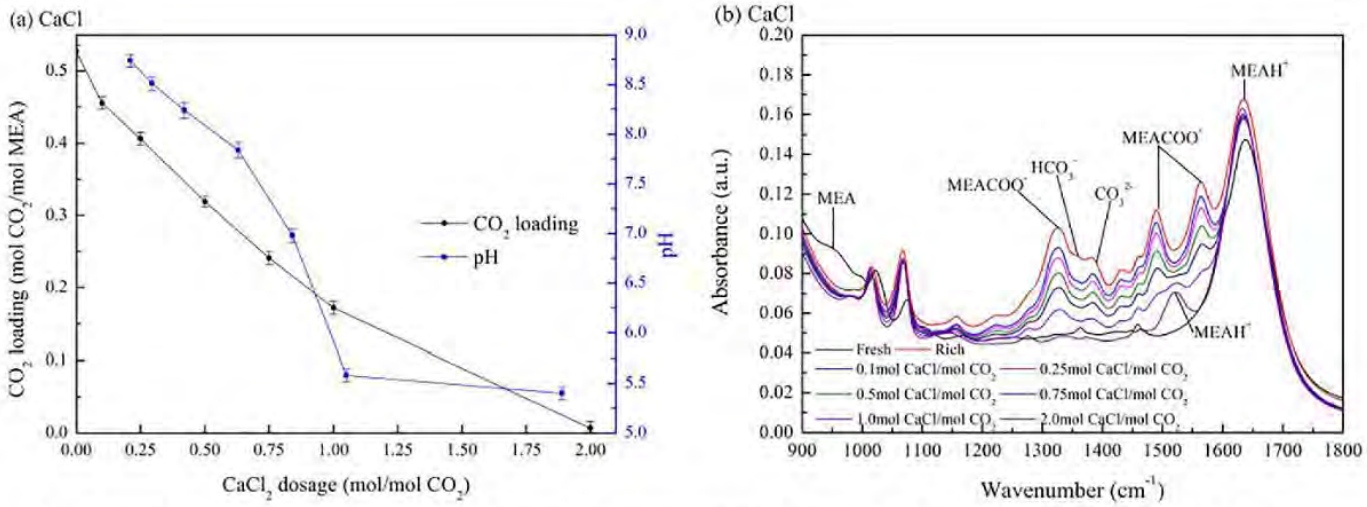

Fig. 6. (a) CO_2-loading and pH value of MEA solutions after 15 min reaction as a function of $CaCl_2$ dosages; (b) FT-IR spectra of MEA solutions.

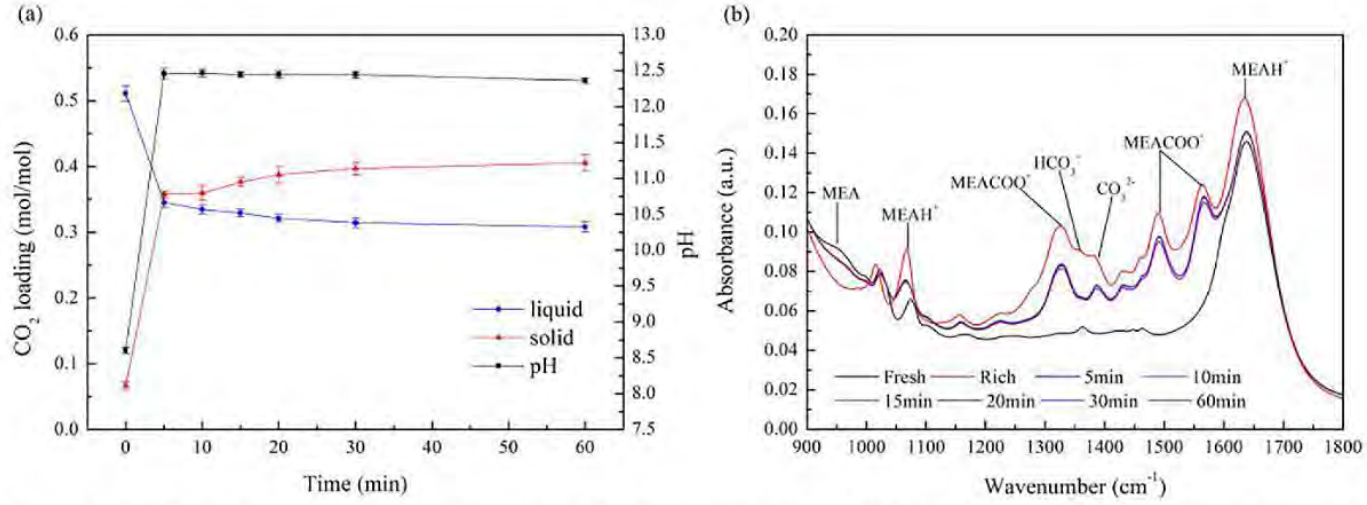

Fig. 7. Time profile of (a) pH value and CO_2-loading of liquid and solid phases of MEA solutions with 1.0 mol/mol-CO_2 CaO dosage; (b) FT-IR spectra of MEA solutions.

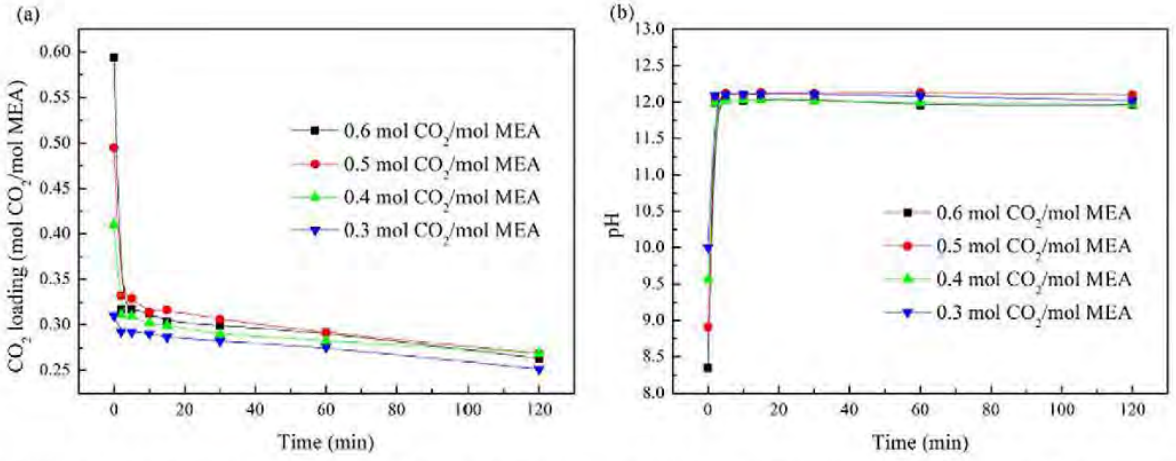

Fig. 8. Time profile of (a) CO_2-loading and (b) pH value of MEA solutions with different CO_2-loadings and CaO dosage of 1.0 mol/mol-CO_2.

3.2. The amine regeneration performance of calcium oxide-based IAM with different reaction time and CO_2-loading

3.2.1. Reaction time

Fig. 7a shows that as the CaO was added into the solution, the CO_2-loading of the MEA solution decreased rapidly in the first 5 min of the regeneration reaction, while the CO_2-loading of the solid phase increased together with the solution pH. This result can be confirmed by the FT-IR peaks in Fig. 7b, where a rapid decrease in peak intensity of $MEACOO^-$, CO_3^{2-}/HCO_3^- and $MEAH^+$ were observed during the

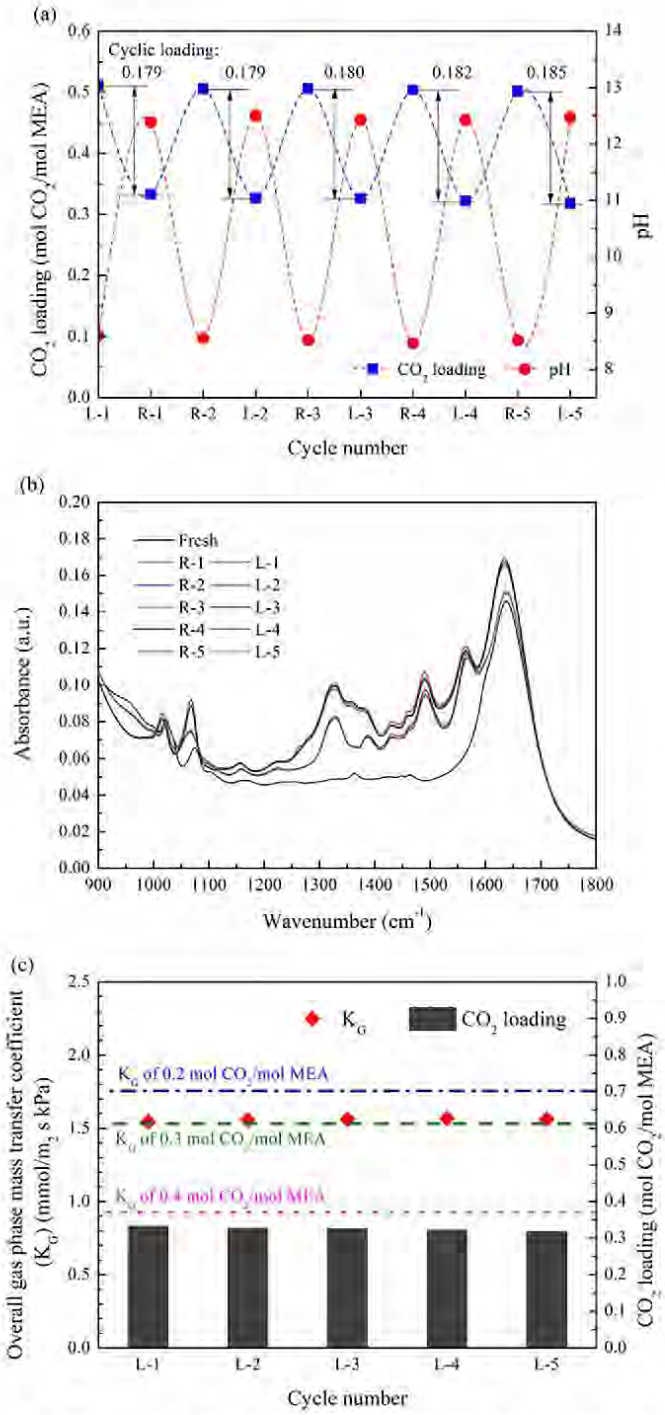

Fig. 9. Five cycles of the integrated CO_2 absorption–mineralisation (IAM) process showing (a) CO_2-loading and pH value of 2 mol/L MEA solution with a CaO dosage of 1.0 mol/mol-CO_2 (R-i: rich solution of cycle i; L-i: lean solution of cycle i); (b) K_G of 2 mol/L MEA lean solution; (c) FT-IR spectra of the liquid phases of 2 mol/L MEA solution.

initial 5 min of the carbonation reaction. After 5 min, a slight decrease of CO_2-loading in the solution and an increase of CO_2-loading in the solid phase were observed, while the pH value stabilised at 12.4 (Fig. 7a). The FT-IR in Fig. 7b confirmed this result with a limited peak intensity change from 5 to 60 min, though the peak intensity of $MEACOO^-$ was still larger than that of fresh MEA. This is due to the slow dissolution of CaO and precipitation of $CaCO_3$. A 40% MEA regeneration efficiency with 0.20 mol/mol cyclic loading was achieved in a 15–min carbonation reaction. This regeneration performance is similar to CSIRO pilot plant trials of the MEA process (~0.2 CO_2-loading) [21]. However, chemical regeneration can save a great amount of energy, as no heat consumption is involved.

3.2.2. CO_2-loading

Chemical regeneration experiments were performed by dosing CaO (1.0 mol/mol-CO_2) into MEA solutions of various CO_2-loadings. Fig. 8 shows the CO_2-loading and pH value of MEA solutions as a function of reaction time. CO_2-loading decreased rapidly in the initial 5 min, dropping to a value of around 0.30 mol/mol. After this time, the CO_2-loading of MEA solutions decreased very slightly, consistent with the trend observed in Fig. 7a. These results indicate that different CO_2-rich loading produced similar CO_2-lean loadings, and that higher CO_2-rich loadings led to larger cyclic CO_2-loadings.

3.2.3. Multicycle IAM

In the continuous IAM process, the absorbent is meant to be operated steadily at a high absorption rate, cyclic CO_2-loading and regeneration efficiency. When the regeneration process by carbonation takes place quickly, it shortens the reaction time. We performed multicycle experiments with 2 mol/L MEA to investigate the sustainability of the IAM process — particularly for technical performance aspects, such as amine reactivity with CO_2 and CO_2 absorption capability (Fig. 9).

Fig. 9a presents the pH value and CO_2-loadings of MEA solutions in five cycles of absorption–regeneration. MEA-based IAM has stable performance, showing no obvious decline in cyclic loading and regeneration efficiency over the five cycles, an average cyclic loading of 0.18 mol/mol and a regeneration efficiency of 37%. The average pH of the five lean solutions was 12.3, which is very close to that of fresh MEA solution. The successive regeneration cycles confirm the stability of MEA's CO_2 absorption capacity. FT-IR spectra (Fig. 9b) confirms that CO_2 was effectively removed from the amine solutions as $CaCO_3$ precipitate, and that MEA can be chemically regenerated. The stability of CO_2 absorption performance is also reflected by the CO_2 absorption kinetics, with the K_G being stable over the five successive cycles of absorption–regeneration (Fig. 9c).

3.3. Fly ash-based IAM

When fly ash was added into the solution, the CO_2-loading of the MEA solution decreased together with a rise of solution pH and K_G (Fig. 10a). This result was confirmed by the FT-IR spectroscopy of liquid samples in Fig. 10b: the more fly ash dosed into the MEA solution, the closer the FT-IR curve came to that of fresh MEA solution. When the fly ash dosage (grams of fly ash added per litre of CO_2-rich amine solution) was 500 g/L, the CO_2-loading of MEA solution decreased from 0.53 to 0.33 mol/mol after the carbonation reaction. This provided a cyclic loading of 0.20 mol/mol, which is similar to that of the CaO scenario shown in Fig. 9a. A larger fly ash dosage led to higher MEA regeneration efficiency. XRD analysis of the fresh fly ash (Fig. 11a) shows that the crystalline calcium-bearing phases present in the samples included lime (CaO), portlandite ($Ca(OH)_2$), calcite ($CaCO_3$), calcium sulfate ($CaSO_4$), basanite ($CaSO_4{\cdot}0.5H_2O$), gypsum ($CaSO_4{\cdot}2H_2O$) and srebrodolskite ($Ca_2Fe_2O_5$). After carbonation, the concentration of $CaCO_3$ increased significantly in the solid sample, as indicated by the dramatic rise in intensity of the $CaCO_3$ peak in the XRD pattern (Fig. 11b). The increase in the concentration of $CaCO_3$ was due to the carbonation of CaO/$Ca(OH)_2$ and calcium sulfates. Only small amounts of $Ca(OH)_2$ were present in the sample, which may be due to excess calcium available in the fly ash. Srebrodolskite is the only calcium-bearing phase that did not appear to take part in the carbonation reaction, as it was still present in the solid sample after carbonation. However, the XRD data confirmed that most of the crystalline calcium-bearing phases reacted with carbon dioxide to produce calcium carbonate. These results clearly prove that fly ash can effectively sequester CO_2 and regenerate MEA in IAM and indicate that the chemical

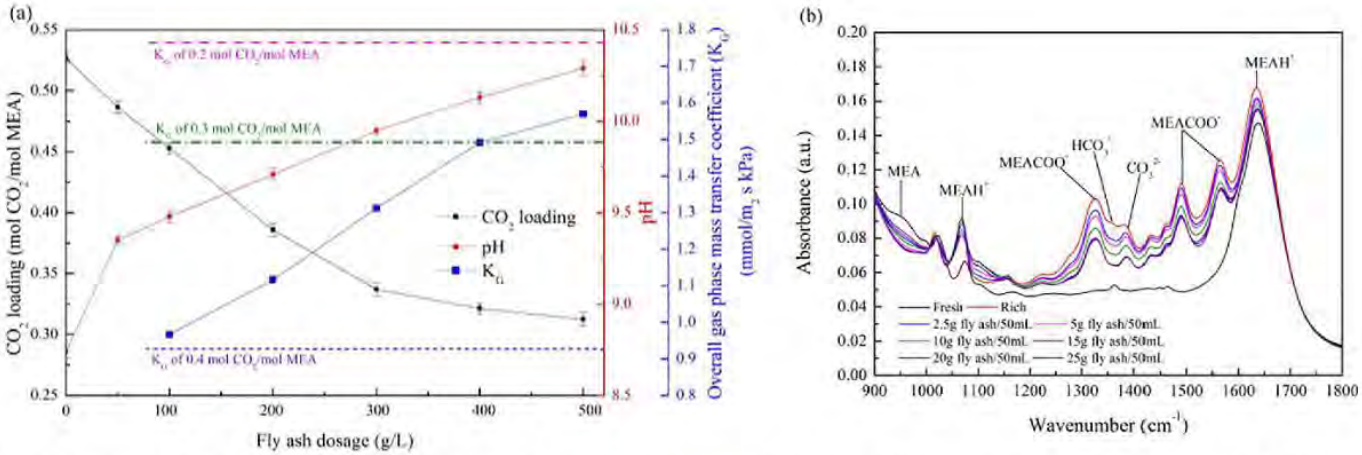

Fig. 10. (a) CO_2-loading, pH value and K_G of 2 M MEA solutions as a function of dosages of fly ash; (b) FT-IR spectra of the liquid phases of 2 mol/L MEA solutions with different CO_2-loadings in carbonation reactions with different dosages of fly ash.

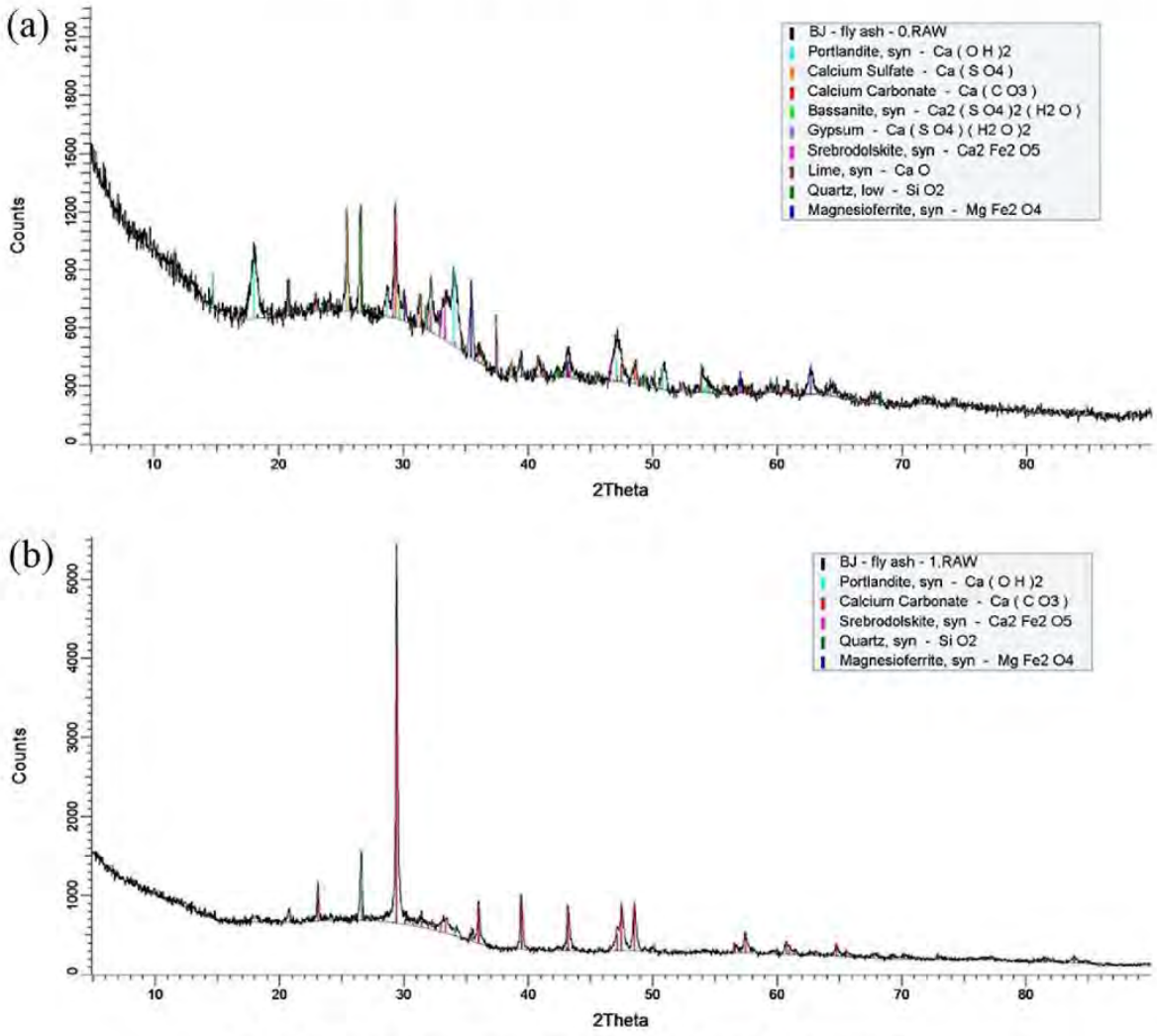

Fig. 11. X-ray diffraction patterns of (a) fresh fly ash and (b) carbonated ash.

regeneration of amines using fly ash is a promising way to effectively reduce the energy penalty of amine regeneration.

3.4. Possible energy and cost reduction of IAM compared to thermal MEA regeneration

Table 3 compares the regeneration energy performance of IAM process and the traditional thermal regeneration process. To have a fair comparison, the conditions for the traditional amine process are similar to the experimental conditions in IAM process, described in Section 2.2. A rigorous rate-based model that has been validated by our pilot plant results, was used to simulate the conventional MEA process [21,48]. This ensures the results reliability of the MEA process. It was simulated that the amine regeneration temperature in traditional MEA process,

Table 3
Comparison of chemical regeneration and conventional MEA process.

CO_2 capture technology	Chemical regeneration(CaO)	Chemical regeneration(fly ash)	Conventional amine scrubbing[a]
	Experimental/simulation conditions		
Solvent concentration, mol/L	2	2	2
Flue gas CO_2, kPa	9	9	9
Absorption temperature, °C	40	40	40
Regeneration pressure, atm	1	1	2
Temperature approach of heat exchanger, K	–	–	10
	Experimental/simulation results		
CO_2-loading after absorption, mol/mol	0.51	0.53	0.51
CO_2-loading after regeneration, mol/mol	0.30	0.32	0.30
Cyclic CO_2-loading, mol/mol	0.20	0.20	0.21
Regeneration temperature, °C	40	40	116
Regeneration duty, MJ/kg CO_2	0	0	4.7
Product	$CaCO_3$	Fly ash rich with $CaCO_3$	CO_2

[a] Results obtained from Aspen Plus process simulation [21,48].

Table 4
Possible energy cost reduction for the IAM process.

Pretreatment and absorption units	Energy consumption (kW)	Desorption and compression units	Energy consumption (kW)	Possible energy saving in IAM process	Energy consumption saving (kW)
Blower	3586	Stripper reboilerb	25,422	Stripper reboiler	25,422
Pumps	2032	Compressors	12,889	Compressors	12,889
		Pumps	63	–	–
Subtotal	5618	Subtotal	38,374	Subtotal	38,311
Annual energy costa (1000 AU$)	20,914	Annual energy cost (1000 AU$)	142,865	Annual energy cost (1000 AU $)	142,632

[a]Energy cost is calculated based on an Australian electricity price of 50 cents/kWh.
[b]Reboiler energy is based on a reboiler duty of 4.0 MJ/kg CO_2.

Table 5
Possible equipment cost[a] reduction for the IAM process.

Pretreatment and absorption units	Equipment costs (1000 AU$)	Desorption and compression units	Equipment costs (1000 AU$)	Items not required.	Equipment cost saving (1000 AU$)
Blower	1018	CO_2 stripper	2849	Reboiler	3989
Direct contact cooler column	3603	Stripper packing	1835	Condenser	382
DCC packing	2360	Reboiler	3989	Main heat exchanger	1882
DCC pump	135	Condenser	382	Condenser pump	44
DCC cooler	253	Main heat exchanger	1882	Stripper reflux drum	58
Storage tank	117	Lean solvent cooler	654	Solvent stripper reclaimer	227
CO_2 absorber column	10,498	Condenser pump	44	Solvent reclaimer cooler	226
Absorber packing	7667	Stripper reflux drum	58	CO_2 compressor	30,115
Rich solvent pump	199	Lean solvent pump	199	–	–
Solvent storage tank	429	Solvent stripper reclaimer	227	–	–
Solvent filtration	1085	Solvent reclaimer cooler	226	–	–
Washing column	3562	–	–	–	–
Washing column packing	2582	–	–	–	–
Others	165	–	–	–	–
Subtotal	33,673	Subtotal	42,460	Subtotal	36,923

[a] Equipment cost is based on 2013 Q1 Australian dollars.

was ~120 °C, with the subsequent regeneration duty of 4.7 MJ/kg-CO_2. The steam extraction from the power station for amine thermal regeneration would decrease the thermal efficiency by 25–40% and raise the cost of electricity in coal-fired power stations by 70–100% [16]. In contrast, the IAM process was conducted at low regeneration temperature of 40 °C, which is the same as the absorption temperature. The heat requirement of amine regeneration is expected to be negligible since the regeneration of MEA is driven by the pH swing (rather than thermal swing). The heat released in mineral carbonation reaction could potentially be reused. Considering that stripper reboiler duty and CO_2 compression duty are the two largest power consumers, accounting for ~55% and ~30% of the total energy consumption of a coal-fired power station [21], respectively, and chemical regeneration could significantly reduce the energy consumption compared with conventional amine scrubbing. Although the IAM consumes the alkaline chemicals for absorbent regeneration, the IAM process can make the use of CaO-containing fly ash wastes as the feedstock, which has the potential to reduce the raw material cost significantly.

Based on our previous techno-economic evaluation of MEA process [16], the energy consumption accounts for 55.4% of the CO_2-avoided cost (exclusive CO_2 transport and storage). As shown in Table 4, 87% of the energy is consumed for CO_2 desorption and compression [16]. Since the IAM process does not require thermal regeneration and CO_2 compression, the energy reduction in IAM process is anticipated to reduce the CO_2-avoided cost by 48% (55.4%*0.87 = 48%).

In addition to energy consumption, capital investment is another

major contributor, representing 25.3% of the CO_2-avoided cost [16]. Table 5 provides the breakdown of equipment cost for the MEA process and the associated equipment cost reduction in the IAM process. Provided that the cost of the reactor used for mineralisation is equivalent to that of the stripper (including column and packing material) in the MEA process. The equipment used for CO_2 desorption and compression, such as reboiler, condenser, main heat exchanger, reclaimer, compressors etc. would not be needed for the IAM process. Less equipment required for the IAM process would reduce the total equipment costs by 48% which leads to the capture cost reduction of 12% (25.3%∗0.48 = 12%). The overall cost reduction from capital and energy in the IAM process is around 60% compared to the conventional MEA process. The actual savings will be even higher considering the IAM process does not require CO_2 transport and underground storage and can be carried out independently, i.e. having a high operational flexibility and minimal cost needed for plant integration.

Therefore, IAM has significant advantages over conventional amine scrubbing, as it greatly reduces energy consumption, energy and capital cost. Without the thermal regeneration, the potential environmental issues resulting from amine volatilisation and degradation at high regeneration temperatures would also be avoided. The resultant products from the carbonated fly ash also benefit subsequent uses in aggregate, concrete and geopolymer [46,47], which is expected to further reduce the cost of CO_2 sequestration.

4. Conclusion

This study explored the mechanism and confirmed the technical feasibility of the integrated process of MEA-based CO_2 absorption and fly ash-based mineralisation. The process converts aqueous CO_2 from amine solutions into calcium carbonate precipitates to simultaneously regenerate solvent and sequester CO_2. The released OH^- from CaO increases the pH value in the MEA solution when $MEACOO^-$ is converted into HCO_3^- and then CO_3^{2-}. OH^- also reacts with $MEAH^+$ to form fresh MEA. Ca^{2+} from CaO reacts with CO_3^{2-} to formed $CaCO_3$, thereby sequestering CO_2. In our study, MEA had 0.20 mol/mol cyclic loading and 40% regeneration efficiency after a 15 min carbonation reaction. Five successive experiments confirmed the stability of IAM with respect to cyclic loading, regeneration efficiency and CO_2 absorption kinetics. The industrial waste of fly ash had 0.20 mol/mol cyclic loading, which is very close to that of the MEA-based scrubbing process by thermal regeneration.

Compared with conventional amine processes, IAM can greatly reduce the energy penalty of amine-based CO_2 capture and has the potential to significantly reduce costs. However, a more detailed study is required to investigate potential problems. For example, various amines should be analysed to find a more suitable absorbent for IAM. The technology is also likely to require a new amine-CO_2 contactor instead of a packing column, because the carbonation of the calcium ions in lean solutions may block the traditional packing column. In addition, the leaching behaviours of the metals from fly ash and their effect on amine degradation should be studied in the future.

Acknowledgments

Long Ji is grateful to Macquarie University for the Cotutelle-iMQRES scholarship, to China University of Mining & Technology (Beijing) for funding from the 'Creating Outstanding Innovative Talent Project', to CSIRO Energy for the opportunity to work in their laboratories and access their resources, to Dr Monica Rossignoli from School of Environmental and Life Sciences Faculty of Science of University of Newcastle for the NMR analysis. The views expressed herein are not necessarily the views of the Commonwealth, and the Commonwealth does not accept responsibility for any information or advice contained herein.

References

[1] M.E. Boot-Handford, et al., Carbon capture and storage update, Energy Environ. Sci. 7 (1) (2014) 130.
[2] B. Yu, et al., Insights into the chemical mechanism for CO_2(aq) and H^+ in aqueous diamine solutions – An experimental stopped-flow kinetic and $^1H/^{13}C$ NMR study of aqueous solutions of N, N-Dimethylethylenediamine for postcombustion CO_2 capture, Environ. Sci. Technol. 52 (2) (2018) 916–926.
[3] G.T. Rochelle, Amine scrubbing for CO_2 capture, Science 325 (2009) 1652–1654.
[4] S. Zhao, et al., Status and progress of membrane contactors in post-combustion carbon capture: a state-of-the-art review of new developments, J. Membr. Sci. 511 (2016) 180–206.
[5] S. Yan, et al., Biogas upgrading by CO_2 removal with a highly selective natural amino acid salt in gas–liquid membrane contactor, Chem. Eng. Process. Process Intensif. 85 (2014) 125–135.
[6] S. Yan, et al., Innovative use of membrane contactor as condenser for heat recovery in carbon capture, Environ. Sci. Technol. 49 (2015) 2532–2540.
[7] S. Zhao, et al., Membrane evaporation of amine solution for energy saving in post-combustion carbon capture: Performance evaluation, J. Membr. Sci. 473 (2015) 274–282.
[8] S. Zhao, et al., Membrane evaporation of amine solution for energy saving in post-combustion carbon capture: wetting and condensation, Sep. Purif. Technol. 146 (2015) 60–67.
[9] A.E. Creamer, B. Gao, Carbon-based adsorbents for postcombustion CO_2 capture: a critical review, Environ. Sci. Technol. 50 (14) (2016) 7276–7289.
[10] E.R. Bobicki, et al., Carbon capture and storage using alkaline industrial wastes, Prog. Energy Combust. Sci. 38 (2) (2012) 302–320.
[11] T. Wang, et al., Accelerated mineral carbonation curing of cement paste for CO_2 sequestration and enhanced properties of blended calcium silicate, Chem. Eng. J. 323 (2017) 320–329.
[12] X. Wang, M.M. Maroto-Valer, Integration of CO_2 capture and mineral carbonation by using recyclable ammonium salts, ChemSusChem 4 (9) (2011) 1291–1300.
[13] J.-H. Wee, A review on carbon dioxide capture and storage technology using coal fly ash, Appl. Energy 106 (2013) 143–151.
[14] P. Muchan, et al., Screening tests of aqueous alkanolamine solutions based on primary, secondary, and tertiary structure for blended aqueous amine solution selection in post combustion CO_2 capture, Chem. Eng. Sci. 170 (2017) 574–582.
[15] J. Narku-Tetteh, et al., Selection of components for formulation of amine blends for post combustion CO_2 capture based on the side chain structure of primary, secondary and tertiary amines, Chem. Eng. Sci. 170 (2017) 542–560.
[16] K. Li, et al., Systematic study of aqueous monoethanolamine (MEA)-based CO_2 capture process: techno-economic assessment of the MEA process and its improvements, Appl. Energy 165 (2016) 648–659.
[17] B. Yu, et al., Characterisation and kinetic study of carbon dioxide absorption by an aqueous diamine solution, Appl. Energy 208 (2017) 1308–1317.
[18] W. Conway, et al., Toward rational design of amine solutions for PCC applications: The kinetics of the reaction of CO_2(aq) with cyclic and secondary amines in aqueous solution, Environ. Sci. Technol. 46 (13) (2012) 7422–7429.
[19] W. Conway, et al., Toward the understanding of chemical absorption processes for post-combustion capture of carbon dioxide: electronic and steric considerations from the kinetics of reactions of CO_2(aq) with sterically hindered amines, Environ. Sci. Technol. 47 (2) (2013) 1163–1169.
[20] K. Jiang, et al., Advancement of ammonia based post-combustion CO_2 capture using the advanced flash stripper process, Appl. Energy 202 (2017) 496–506.
[21] K. Li, et al., Systematic study of aqueous monoethanolamine-based CO_2 capture process: model development and process improvement, Energy Sci. Eng. 4 (1) (2016) 23–39.
[22] S. Teir, et al., Production of precipitated calcium carbonate from calcium silicates and carbon dioxide, Energy Convers. Manage. 46 (18–19) (2005) 2954–2979.
[23] G. Gadikota, et al., Experimental design and data analysis for accurate estimation of reaction kinetics and conversion for carbon mineralization, Ind. Eng. Chem. Res. 53 (16) (2014) 6664–6676.
[24] H. Zhao, et al., Tuning the dissolution kinetics of wollastonite via chelating agents for CO_2 sequestration with integrated synthesis of precipitated calcium carbonates, PCCP 15 (36) (2013) 15185–15192.
[25] W.J. Huijgen, et al., Mechanisms of aqueous wollastonite carbonation as a possible CO2 sequestration process, Chem. Eng. Sci. 61 (13) (2006) 4242–4251.
[26] S.J. Gerdemann, et al., Ex situ aqueous mineral carbonation, Environ. Sci. Technol. 41 (2007) 2587–2593.
[27] A.-H.A. Park, et al., CO_2 mineral sequestration: physically activated dissolution of serpentine and pH swing process, Chem. Eng. Sci. 59 (22–23) (2004) 5241–5247.
[28] G. Gadikota, et al., Chemical and morphological changes during olivine carbonation for CO2 storage in the presence of NaCl and $NaHCO_3$, PCCP 16 (10) (2014) 4679–4693.
[29] A. Sanna, et al., Post-processing pathways in carbon capture and storage by mineral carbonation (CCSM) towards the introduction of carbon neutral materials, Energy Environ. Sci. 5 (2012) 7781–7796.
[30] G. Gadikota, et al., Morphological changes during enhanced carbonation of asbestos containing material and its comparison to magnesium silicate minerals, J. Hazard. Mater. 264 (2014) 42–52.
[31] M. Arti, et al., Single process for CO_2 capture and mineralization in various alkanolamines using calcium chloride, Energy Fuels 31 (1) (2017) 763–769.
[32] J.M. Kang, et al., Energy-efficient chemical regeneration of AMP using calcium hydroxide for operating carbon dioxide capture process, Chem. Eng. J. 335 (2018) 338–344.

[33] L. Ji, et al., CO_2 sequestration by direct mineralisation using fly ash from Chinese Shenfu coal, Fuel Process. Technol. 156 (2017) 429–437.
[34] L. Ji, et al., Insights into carbonation kinetics of fly ash from Victorian lignite for CO_2 sequestration, Energy Fuels 8 (2018).
[35] S. Yan, et al., Regeneration of CO_2 from CO_2-rich alkanolamines solution by using reduced thickness and vacuum technology: Regeneration feasibility and characteristic of thin-layer solvent, Chem. Eng. Process. Process Intensif. 48 (1) (2009) 515–523.
[36] H. Yu, et al., Promoted CO_2 absorption in aqueous ammonia, Greenhouse Gases Sci. Technol. 2 (3) (2012) 200–208.
[37] W. Conway, et al., Comprehensive kinetic and thermodynamic study of the reactions of CO_2(aq) and HCO_3^- with monoethanolamine (MEA) in aqueous solution, J. Phys. Chem. A 115 (50) (2011) 14340–14349.
[38] C.-H. Cheng, et al., Amine-based post-combustion CO_2 capture mediated by metal ions: Advancement of CO_2 desorption using copper ions, Appl. Energy 211 (2018) 1030–1038.
[39] X. Wang, et al., Kinetics of the reversible reaction of CO_2(aq) with ammonia in aqueous solution, J. Phys. Chem. A 115 (24) (2011) 6405–6412.
[40] X. Wang, et al., Comprehensive study of the hydration and dehydration reactions of carbon dioxide in aqueous solution, J. Phys. Chem. A 114 (2010) 1734–1740.
[41] N. McCann, et al., Kinetics and mechanism of carbamate formation from CO_2(aq), carbonate species, and monoethanolamine in aqueous solution, J. Phys. Chem. A 113 (2009) 5022–5029.
[42] G. Richner, G. Puxty, Assessing the chemical speciation during CO_2 absorption by aqueous amines using in situ FTIR, Ind. Eng. Chem. Res. 51 (44) (2012) 14317–14324.
[43] K. Robinson, A. McCluskey, M.I. Attalla, An FTIR spectroscopic study on the effect of molecular structural variations on the CO_2 absorption characteristics of heterocyclic amines, Chemphyschem 12 (6) (2011) 1088–1099.
[44] K. Robinson, A. McCluskey, M.I. Attalla, An ATR-FTIR study on the effect of molecular structural variations on the CO_2 absorption characteristics of heterocyclic amines, part II, Chemphyschem 13 (9) (2012) 2331–2341.
[45] B. Lv, et al., Mechanisms of CO_2 capture into monoethanolamine solution with different CO_2 loading during the absorption/desorption processes, Environ. Sci. Technol. 49 (17) (2015) 10728–10735.
[46] S.-Y. Pan, et al., Integrated and innovative steel slag utilization for iron reclamation, green material production and CO_2 fixation via accelerated carbonation, J. Cleaner Prod. 137 (2016) 617–631.
[47] S.-Y. Pan, et al., Integrated CO_2 fixation, waste stabilization, and product utilization via high-gravity carbonation process exemplified by circular fluidized bed fly ash, ACS Sust. Chem. Eng. 4 (6) (2016) 3045–3052.
[48] K. Li, et al., Techno-economic assessment of stripping modifications in an ammonia-based post-combustion capture process, Int. J. Greenhouse Gas Control 53 (2016) 319–327.

Chapter 8 Discussion

Five coal fly ashes were selected for carbonation studies in **Chapter 3**. Experiments were performed in a batch reactor at 40 and 140 °C with 20 bar initial CO_2 pressure, 200 g/L solid to liquid ratio, 450 rpm stirring rate to compare the carbonation capacities and efficiencies of the selected ashes, and the effects of temperature and fly ash properties on carbonation reactions. Particle size distributions, and elemental and mineralogical compositions of the selected ashes were measured to determine the fly ash properties affecting carbonation efficiencies and capacities, and investigate the process chemistry. The results show that the D_{90} of BJ, YA, LY, WH and HW ashes were 7.9, 24.1, 31.9, 9.9 and 14.6 μm, respectively, indicating that the particle diameters of these ashes were very fine. A previous study indicated that grinding can be avoided, and the sample particle size had very limited effect on carbonation reactions when the particle size of the feedstock was < 100 μm [1]. HW ash displayed the highest carbonation capacity at 40 and 140 °C, being 103 and 102 g-CO_2/kg-FA, respectively, followed by YA, BJ, WH and LY ashes. The carbonation capacities and efficiencies of different ashes were significantly affected by their mineralogical properties. X-ray diffractometry indicated that the reactants were lime, portlandite and brownmillerite for BJ ash, srebrodolskite, gypsum, basanite, brucite and periclase for HW ash, and diopside, spinel, srebrodolskite and periclase for YA ash. The highest carbonation capacity of HW ash was due to its largest fraction of Ca/Mg-bearing phases available for carbonation. But the carbonation efficiency of HW was low (about 24 %) at 40 °C, which indicated that most of the Ca-/Mg-bearing phases cannot react with CO_2. Increasing the reaction temperature to 140 ℃ did not promote the carbonation efficiency. The reason might be that un-reacted phases were stable in this temperature range (40-140 °C). Although the carbonation capacity of BJ ash was much smaller than HW ash, being 35.9 and 43.2 g-CO_2/kg-FA at 40 and 140 °C respectively, BJ ash displayed the highest carbonation efficiency, of 36.8 % and 44.4 % at 40 and 140 °C, respectively. Given that the reactants of BJ ash were mainly lime and portlandite while the reacted phases of HW ash included both Ca-bearing phases (srebrodolskite, gypsum and basanite) and Mg-bearing phases (brucite and periclase), the Ca-bearing phases might be more reactive with CO_2. Lime and portlandite phases of BJ ash were almost completely converted to calcite after carbonation. YA ash behaved differently to BJ and WH ash: the YA ash exhibited a significant increase of carbonation capacity from 33.3 to 93.1 g-CO_2/kg-FA when the temperature was elevated from 40 to 140 °C, probably because the elevated temperature made more phases reactive with CO_2. ΔG of Ca/Mg-oxide/hydroxides with CO_2 confirmed that Mg oxide/hydroxide displayed lower reactivity in carbonation reactions than Ca hydroxide. YA presented a low weight fraction of Ca-bearing phases

but a high weight fraction of Mg-bearing phases. This explains the obviously improved carbonation capacity of YA ash at 140 °C. Compared to the above three ashes, LY and WH ash displayed much lower carbonation capacities at the same conditions, which was attributed to the small fraction of CaO/MgO phases identified in their fresh samples.

To further investigate the effects of temperature on carbonation capacities and efficiencies of different ashes. BJ, YA and HW ashes were then selected for experiments in a wide temperature range (40−220 °C). The three ashes exhibited the same trend of the carbonation rate decreasing as reaction time elapsed. The carbonation capacity/efficiency increased rapidly in the first 20 min and reached a maximum value after 120 min. More than 80 % of the maximum carbonation efficiency was achieved in 20 min. This is attributed to the exhaustion of the reactant on the surface of the ash particles, and the formation of a precipitate layer at the early stage of carbonation, which hindered diffusion of the reactant inside the particles. This explanation can be confirmed by analyses which showed that the reacted particles displayed larger particle sizes and lower porosities and pore areas than the fresh samples due to the new precipitates not only depositing on the active surface, but also filling the pores of the fly ash particles, which was responsible for the reduced kinetics with time. Also, particle sizes of carbonated samples were strongly affected by carbonation reactions and were related to carbonation efficiencies. Compared to YA and HW ashes, BJ ash displayed faster carbonation kinetics because the reactant phases of BJ ash were mainly Ca-bearing phases which have higher reactivity with CO_2 than Mg-bearing phases. The three fly ashes displayed different trends of carbonation efficiency within the temperature range (40−220 °C). Specifically, the carbonation efficiency of BJ ash within 120 min at different temperature decreased in the order: 220 °C > 180 °C > 140 °C > 40 °C > 60 °C > 100 °C > 80 °C. When the temperature increased from 40 to 220 °C, carbonation efficiency decreased first and then increased, due to the complex effects of temperature on carbonation. Elevated temperatures can increase reaction rates by improving mass transfer rates in liquid phase, promoting thermal motion of molecules and increasing their average kinetic energy which helped speed up carbonation. Raising reaction temperature also reduced the solubility of carbon dioxide in the solution and the precipitation of the carbonate product. Thus, the kinetic results of BJ ash indicated that the reduced CO_2 solubility had a larger effect on carbonation resulting in a low carbonation efficiency in the temperature range 40 to 80 °C, while the enhanced mass transfer rate at elevated temperatures might have a larger effect in the temperature range 80 to 220 °C. Similar to BJ ash, the carbonation efficiency of HW ash decreased first from 40 to 80 °C and then obviously increased when the temperature increased from 80 to 220 °C. However, the carbonation efficiency increase of HW ash is much larger than

BJ ash when temperature was elevated from 80 to 220 °C. In addition, the carbonation efficiency of YA ash decreased from 40 to 60 °C and then increased thereafter which is different from BJ and HW ashes. Considering the same operating parameters used in the carbonation experiments, the different carbonation efficiency trends of the three ashes within the temperature range used, results from their different mineralogical properties. The main reacted minerals of BJ ash, Ca-bearing minerals, have very low ΔG which means high reactivity with CO_2, and thus leads to its fast kinetics and large carbonation efficiency in low temperature. For YA ash, it was difficult for srebrodolskite, spinel and diopside phases to react with CO_2 at low temperature due to their low reactivity.

In Chapter 4, the effects of operating conditions (temperature, solid to liquid ratio, gas flow rate, initial CO_2 pressure and additives) on carbonation efficiency of BJ ash and reaction mechanisms involved were systematically investigated to find the optimized conditions. The experimental results at moderate temperatures (60, 70, 80 and 90 °C) and ambient pressure show that carbonation rates decreased as the reaction time elapsed. In the first 30 min, carbonation efficiency increased rapidly and reached a maximum value after 90 min. X-ray diffractometry showed that after 90 min, there was no lime or portlandite detected in the carbonated ashes, which means that the dissolution of lime and portlandite occurred very fast and was not the rate limiting step for carbonation. The X-ray diffractometry also showed anhydrite, brownmillerite and an amorphous phase partially reacted with CO_2 to form calcite during the carbonation reaction. As mentioned in Chapter 3, the reactivity of anhydrite, brownmillerite and an amorphous phase with CO_2 were much lower than lime and portlandite, thus the limited carbonation efficiency was due to the consumption of reactive calcium available. The solid to liquid ratio and gas flow rate had very limited effects on carbonation efficiencies. To further increase carbonation efficiency, it is necessary to raise the carbonation temperature to activate the unreactive Ca-bearing phases and produce more Ca^{2+} and to increase the concentration of CO_3^{2-} to precipitate $CaCO_3$. However, the elevated temperatures hindered the carbonation reaction by reducing the solubility of CO_2 in the liquid phase and the solubility of $Ca(OH)_2$. Elevated initial CO_2 pressure and additives such $NaHCO_3$ or Na_2CO_3 were thus used to maintain the CO_2 or CO_3^{2-} concentration in the liquid phase while increasing the temperature. The carbonation efficiency increased with temperature at 10 bar and 20 bar initial CO_2 pressure respectively, and the carbonation efficiency at 20 bar was higher than that at 10 bar under the same temperature. According to Henry's law, CO_2 pressure plays a critical role in the mass transfer of CO_2 molecules from gas into water. At high pressures, the amount of CO_2 molecules dissolved into the water increases, leading to more carbonate ions available for carbonation. Although increasing temperature decreases CO_2 solubility in water, carbonation efficiency can be improved through the

combined effects of increased temperature and initial CO_2 pressure. Carbonation efficiency in the presence of Na_2CO_3 was much higher than in its absence. X-ray diffractometry confirmed that the increased carbonation efficiency is mainly contributed by the conversion of calcium from the amorphous phase of BJ ash. Elevated temperatures can effectively make more unreactive calcium available for carbonation, and a high concentration of calcium and carbonate ions benefits the precipitation of calcium carbonate. The carbonation efficiency can therefore be significantly improved by the combination of increased temperature and Na_2CO_3.

In **Chapter 5**, experiments were conducted in a vessel reactor at low temperatures (40, 50, 60, and 70 °C), stirring rates (900, 1050, 1200 and 1350 rpm) and CO_2 pressures (3, 4, 5, 6 and 7 bar) to investigate the carbonation kinetics of HW ash and to identify the rate-limiting steps of carbonation. The results show that both the carbonation rate and the maximum carbonation efficiency could be improved by optimizing parameters and by the introduction of $NaHCO_3$. The complex effects of the operating parameters on the carbonation rate and the maximum carbonation efficiency of HW ash were investigated. The carbonation efficiency within 2 h at different temperatures increased in the following order: 60 °C > 70 °C > 50 °C > 40 °C. But the carbonation efficiency after 2 h displayed a reverse trend that the carbonation efficiency decreased with the elevated temperature from 40 °C to 70 °C. This is due to the complex effects of temperature on carbonation reactions. The elevated temperature increased reaction rate by improving the mass transfer rate, promoting the thermal motion of molecules and increasing their average kinetic energy which helped speed up the carbonation reaction. Raising the reaction temperature also reduced the solubility of carbon dioxide in the solution. The equilibrium concentration of dissolved CO_2 in solution follows Henry's law:

$[H_2CO_3] = P_{CO_2}/\mathrm{K}_H$ (equation 12 in Chapter 5)

The concentration of the CO_3^{2-} in the solution can be evaluated by:

$\log[CO_3^{2-}] = \log \mathrm{K_{a2}K_{a1}P_{CO_2}}/\mathrm{K_H} + 2\mathrm{pH}$ (equation 13 in Chapter 5)

Given that K_{a1}, K_{a2}, K_H and pH values were functions of temperature, and increased with elevated temperatures, the overall impact of elevated temperatures was to increase the concentrations of carbonate ions in the solution slightly, which benefited the carbonation reaction. This result is consistent with findings in the literature. On the other hand, elevated temperatures also influenced

the precipitation of the product. The precipitation of the $CaCO_3$ and $MgCO_3$ products was related to the solubility product constant of Ca/Mg-carbonate, K_{sp}:

$K_{sp} = [Ca^{2+}/Mg^{2+}] \times [CO_3^{2-}]$ (equation 14 in Chapter 5)

where $[Ca^{2+}/Mg^{2+}]$ is the concentration of calcium or magnesium ions, and $[CO_3^{2-}]$ is the concentration of carbonate ions. The elevated temperature can lower the K_{sp} of Ca/Mg-calcite, which promotes the precipitation of Ca/Mg-carbonate. The solubility of the Ca/Mg-carbonate product also decreased with the increase in temperature. More newly formed precipitates might deposit on the surface of the fly ash particles at higher temperatures than that at lower temperatures, which would hinder the reaction of the reactant inside the particles. This explains the lower maximum carbonation efficiency at 70 °C than at 40 °C. Thus, it can be concluded that the enhanced mass transfer rate at elevated temperatures might have a dominating effect on the carbonation reaction in the first 2 h of the carbonation reaction, while the fast precipitation of the Ca/Mg-carbonate product at elevated temperatures lowered the carbonation rate thereafter. Due to the rapid carbonation reaction at elevated temperatures, the fly ash particles were quickly covered by the rapidly formed product layer, which resulted in a low maximum carbonation efficiency at elevated temperatures.

As the initial CO_2 pressure increased from 3 to 7 bar, both the carbonation rate and the maximum carbonation efficiency increased, indicating the significant impact of CO_2 pressure on the carbonation reaction. Similar results were observed by Ukwattage et al. [3], in which fly ash was subjected to aqueous carbonation, with the CO_2 pressure ranging from 20 to 60 bar. It is well known that increased CO_2 pressure lowers the pH value, and this would help to leach calcium and magnesium from the fly ash particles. According to Henry's law (equation 12 in Chapter 5), increasing CO_2 pressure also increases the CO_2 solubility in the solution, and thus increases the carbonate ions available for the carbonation reaction. Since elevating the CO_2 pressure was highly energy intensive, 0.5 mol/L $NaHCO_3$ was introduced into the solution to accelerate carbonation. The introduction of $NaHCO_3$ increases the concentration of the carbonate ion (CO_3^{2-}) in the aqueous system. Addition of $NaHCO_3$ can significantly increase carbonation efficiency at 40, 50 and 60 °C. Compared with carbonation without additive, the maximum carbonation efficiency in the presence of 0.5 mol/L $NaHCO_3$ was improved from 27.7 % to 33.4 %, with the CO_2 sequestration capacity improved from 71.0 g-CO_2/kg-FA to 85.6 g-CO_2/kg-FA under the same operating conditions.

The kinetic data can be well fitted by the surface coverage model with $R^2 \geq 0.98$, indicating that the carbonation of fly ash can be physically expressed by this model. The model assumed that the precipitates formed in a carbonation reaction would coat the active site of the surface of the reactant particles, which would hinder the reactant inside the particles from diffusion and reaction. The maximum carbonation efficiency of fly ash could also be well predicted by the model. In addition, the assumed mechanisms of the carbonation reaction were validated by particle size, surface area and porosity changes of the fly ash particles after carbonation reactions. The particle size results show a strong relationship between the particle size change and the carbonation efficiency achieved. The increased particle size after carbonation reactions was attributed to the newly formed precipitates that covered the fly ash particles. The increase in the average pore size of the particles indicates that the precipitates formed in the carbonation reaction probably filled the small pores. Observations using a scanning electron microscope equipped with energy-dispersive X-ray spectrometer before and after carbonation also confirmed that the newly formed precipitates were not only deposited on the active surface, but also filled the pores of the fly ash particles.

Although parameter optimization can enhance carbonation reactions between fly ash and CO_2, the 1.5 h carbonation duration is still not suitable for the large-scale application of CO_2 mineralisation by fly ash. To deal with this problem, a novel process ─ integrated CO_2 absorption−mineralisation (IAM) ─ that integrates amine scrubbing, CO_2 mineralisation and amine regeneration in a single process was developed in **Chapter 6**. The technical feasibility of IAM and the associated mechanisms were investigated by adding CaO or fly ash into CO_2-loaded amine solutions, including five commonly used amines: MEA, DEA, MDEA, PZ and AMP. The stability of cyclic capacity and kinetics of the optimised amine was verified in multicycle experiments. The technical feasibility of IAM in practical applications using fly ash as a feedstock for absorbent regeneration was also investigated. The CO_2 absorption and mineralisation experiments were performed in a bubble column and a stirred reactor respectively. Acid titration was used to measure the CO_2-loading of solid and liquid samples. FT-IR spectroscopy was used to analyse the species changes in the amine solutions during regeneration. The crystalline phases present in fresh and carbonated fly ash samples were determined by X-ray diffractometry. The results indicate that CO_2 absorbed by the five amine solutions was sequestered into carbonate precipitates at a moderate temperature (40ºC) and the amine absorbents were regenerated after carbonation reactions within 15 min. PZ exhibited the largest cyclic loading (0.72 mol/mol) and regeneration efficiency (91%) among the five amines. PZ also achieved stable cyclic loading, regeneration efficiency and kinetic performance over five cycles of IAM experiments. When the industrial waste, fly ash was used, PZ

displayed a cyclic loading of 4.2 mol/mol, lower than that of CaO but still 1.1 times higher than that of the thermal regeneration-based process. Compared with traditional thermal regeneration-based CO_2 capture, the IAM process has great advantages in energy reduction and capital savings due to a larger cyclic CO_2 capacity, a requirement for less energy for amine regeneration and no need for CO_2 compression and pipeline transport.

Although the technical feasibility of IAM was confirmed in the experiments using five different amines and fly ash, the detailed reaction mechanisms were still unclear. Thus, the benchmark solvent MEA was selected to deeply investigate the reaction mechanisms of IAM in **Chapter 7**. Since CaO provides two types of ions (Ca^{2+} and OH^-) into the MEA−CO_2−H_2O system, they have different action mechanisms in the reactions with the species in MEA solution. This makes it very difficult to monitor the behaviour of both ions at the same time. To address this issue, NaOH and $CaCl_2$ was separately added into CO_2-loaded MEA solutions to clearly investigate the action mechanism of Ca^{2+} and OH^-. The performance of MEA in the IAM process, including cyclic CO_2-loading and regeneration efficiency, was systematically investigated at various CO_2-loadings and reaction times. The performance stability of MEA was verified in multicycle CO_2 absorption−mineralisation experiments. The technical feasibility of using fly ash as a feedstock for absorbent regeneration was also investigated. The results show that MEA can be regenerated after a carbonation reaction with both calcium oxide and fly ash at 40 °C, and that the CO_2 absorbed by MEA is precipitated as calcium carbonate. The released OH^- from CaO increases the pH value in the MEA solution when $MEACOO^-$ was converted into HCO_3^- and then CO_3^{2-}. OH^- also reacts with $MEAH^+$ to form fresh MEA. Ca^{2+} from CaO reacts with CO_3^{2-} to formed $CaCO_3$, thereby sequestering CO_2. In our study, MEA had 0.20 mol/mol cyclic loading and 40 % regeneration efficiency after a 15 min carbonation reaction. Five successive experiments confirmed the stability of IAM with respect to cyclic loading, regeneration efficiency and CO_2 absorption kinetics. The industrial waste of fly ash had 0.20 mol/mol cyclic loading, which is similar to that of the MEA-based scrubbing process using thermal regeneration.

Compared with the traditional thermal regeneration-based CO_2 capture, IAM has great advantages in energy reduction and capital saving due to larger cyclic CO_2 capacity, less energy requirement of amine regeneration and no need for CO_2 compression and pipeline transport. This technology has great potential for industrial application, particularly with CaO-containing wastes, such as fly ash and carbide slag. However, further detailed study is required to investigate potential problems. For example, various amines should be analysed to find a more suitable absorbent for IAM. The technology is also likely to require a new amine-CO_2 contactor instead of a packing column,

because the carbonation of the calcium ions in lean solutions may block the traditional packing column. In addition, the leaching behaviour of the metals from fly ash and their effect on amine degradation should be studied in detail.

References

1. Sanna, A.; Uibu, M.; Caramanna, G.; Kuusik, R.; Maroto-Valer, M. M., A review of mineral carbonation technologies to sequester CO_2. Chemical Society reviews, 2014, 43 (23): 8049-8080.
2. Pan, S.-Y.; Chiang, P.-C.; Chen, Y.-H.; Tan, C.-S.; Chang, E. E., Kinetics of carbonation reaction of basic oxygen furnace slags in a rotating packed bed using the surface coverage model: Maximization of carbonation conversion. Applied Energy, 2014. 113(0): 267-276.
3. Ukwattage, N. L.; Ranjith, P. G.; Yellishetty, M.; Bui, H. H.; Xu, T., A laboratory-scale study of the aqueous mineral carbonation of coal fly ash for CO_2 sequestration. Journal of Cleaner Production, 2014. 103: 665-674.

Chapter 9 Conclusions and future work

9.1 Conclusions

This research provides insights to the mechanisms involved in coal fly ash-based CO_2 mineralisation and develops a parameter optimization approach, additives and innovative IAM process to enhance carbonation reactions.

The rate of mineral carbonation decreases, and carbonation efficiency increases with reaction time. In the early stage, carbonation efficiency increases rapidly, and becomes stable thereafter. The kinetics of mineral carbonation fits to a surface coverage model. Carbonation reactions occur on the surface of fly ash particles and are controlled by both reaction and diffusion. Active surface sites of coal fly ash would be gradually covered by newly formed precipitates (calcite, aragonite and magnesite) during carbonation reaction. Once reaction products form a layer covering the surface of fly ash particles, the diffusion of reactants would be hindered, and this layer would become the rate-limiting step for carbonation. The formation of this coating hinders the fly ash particles from further carbonation and helps to define the maximum carbonation efficiency. Also, the porous structure of the fly ash particles would be filled by reaction product during carbonation, which would further reduce surface area and reactant diffusion.

The mineral compositions of coal fly ash have significant effects on carbonation performance. Reactants can be Ca/Mg-bearing minerals or amorphous phases rich in Ca/Mg, such as lime and portlandite in BJ ash, periclase and srebrodolskite in YA ash, and periclase and brucite in HW ash. These minerals are present in different amounts in different coal fly ashes, creating differing reactivities in carbonation reactions. For example, BJ, YA and HW ashes displayed much higher CO_2 sequestration capacity than LY and WH ashes due to the low fraction of reactive Ca/Mg-bearing minerals in the latter two ashes. BJ ash displayed faster carbonation reaction kinetics because the reactant phases of BJ ash were mainly Ca-bearing phases which have higher reactivity with CO_2 than Mg-bearing phases. Also, calcium in brownmillerite and amorphous phase(s) partially react with CO_2, but the reactivity of the Ca-bearing amorphous phase is much lower than that of lime and portlandite. Large CO_2 sequestration capacity and fast kinetics can be achieved by selecting suitable coal fly ash as the feedstock.

Carbonation performance can also be improved by parameter optimization and introduction of additives. Specifically, the carbonation efficiency of carbonation reactions increases as the stirring rate increases to about 1050 rpm. A further increase in stirring rate leads to a reduction in

carbonation efficiency. Both carbonation rate and maximum carbonation efficiency increase with elevated initial CO_2 pressure. Operating temperature has complex effects on carbonation reactions. Elevated temperature increases the reaction rate by improving the mass transfer rate, promoting the thermal motion of molecules and increasing their average kinetic energy which helps increase the speed of the carbonation reaction. Raising the reaction temperature also reduces the solubility of CO_2 in the solution. The introduction of additives such as Na_2CO_3 can significantly promote carbonation efficiency by increasing the CO_2 concentration in the solution. However, reaction kinetics were still too slow for further application.

The IAM process developed in this research can solve this problem, integrating amine scrubbing, CO_2 mineralisation and amine regeneration in a single process. The CO_2 concentration in the absorbents can be very high, normally 0.5 mol-CO_2/mol-absorbent. After carbonation reaction, the absorbents can be regenerated and recycled for another round of CO_2 capture. The regeneration performance of five commonly used amines (MEA, DEA, MDEA, AMP and PZ) by CaO and fly ash has been confirmed. Another advantage of IAM is that, compared with the traditional thermal regeneration-based CO_2 capture, IAM has better energy reduction and capital saving due to larger cyclic CO_2 capacity, less energy requirement of amine regeneration and no need to compress and transport CO_2.

9.2 Future work

Despite the contributions of this research make towards the carbonation mechanisms and carbonation enhancement approaches, much more work is needed to gain further development of CO_2 sequestration by mineralisation in the future.

(1) The chemical compositions of fly ash particles with different size should be analysed, as well as the carbonation capacities and efficiencies of these particles.

(2) A wider range of fly ash samples should be collected and analysed. The key findings of relationships between carbonation capacities and mineralogical properties in this research can be used to assess the application potential of the target samples in CO_2 sequestration.

(3) The application of carbonated samples should be further investigated. The carbonated ash has great potential to be used as construction materials, such as cement, concrete, aggregate, and geopolymer materials. The changes in physico-chemical properties of carbonated fly ash may be be beneficial to sequential uses in cement and concrete. After the carbonation reaction, the potential for heavy metal leaching and uncontrollable expansion should be eliminated. Also, the carbonated

ash has a larger surface area. The larger surface area means greater mechanical strength of cement. In addition, the formation of the fine $CaCO_3$ precipitates can provide a favourable surface for nucleation and growth of hydration products in cement/concrete, which is beneficial to the strength development of blended cement.

(4) Further research is required to identify potential problems in IAM. For example, a wider range of amines should be considered and tested to determine whether there are more suitable absorbents for IAM. The technology is also likely to require a new amine-CO_2 contactor instead of a packed column, because the carbonation of the calcium ions in lean solutions may block the traditional packed column. The leaching behaviour of metal ions from fly ash, and their effects on amine degradation, should also be studied in detail.